Computational Particle Mechanics
https://doi.org/10.1007/s40571-018-0200-0

3D numerical simulations of granular materials using DEM models considering rolling phenomena

Alex Alves Bandeira[1] · **Tarek Ismail Zohdi**[2]

Received: 14 December 2017 / Revised: 7 June 2018 / Accepted: 18 June 2018

Abstract
This work presents a review of the formulation for computer simulation based on the discrete element method to analyze granular materials and a validation of the method using different types of tridimensional examples. The individual particulate dynamics under the combined action of particle collisions, particle–surface contact and adhesive interactions is simulated and aggregated to obtain global system behavior. The formulations to compute the forces and momentums developed at the particles are explained in details. The environment and gravity forces are considered as well as the contact forces that occur due the contact between particles and walls, like normal contact forces, frictional contact forces, damping and adhesive bond. The rolling phenomenon is also taken into account and is presented using a standard formulation. A numerical algorithm adapted from Zohdi is also presented. A few tridimensional examples of classical physics are selected to validate the formulations and the numerical program developed and to provide an illustration of the applicability of the numerical integration scheme. For this purpose, each analytical formulation is demonstrated to compare and analyze the numerical results with the analytical one. At the end of this article, a few tridimensional examples of granular materials are simulated. This article contributes to the study of granular materials including the rotation phenomenon using particle methods.

Keywords Particle method · DEM · Explicit solution · Rolling · Granular materials

1 Introduction

The Discrete Element Method (DEM), also called distinct element method, is any of a family of numerical methods for computing the motion and effect of a large number of small particles. As one of the several applications, DEM is a method capable of simulating the mechanical behavior of granular materials, this being the focus of the present work. The method is based on interactions between particles and walls, i.e., as the elements move through time and space, contact may happen between them.

✉ Alex Alves Bandeira
alexbandeira@ufba.br

Tarek Ismail Zohdi
zohdi@me.berkeley.edu

[1] Structural Engineering Program, Construction and Structures Department, Polytechnic School, Federal University of Bahia – UFBA, Salvador, Bahia 40210-630, Brazil

[2] Computational Materials Research Laboratory, Department of Mechanical Engineering, University of California, Berkeley, 6117 Etcheverry Hall, Berkeley, CA 94720-1740, USA

The introduction will be presented in two subsections. One regarding the evolution of the DEM method and the other with the specific objectives of the present work.

1.1 DEM method evolution

The DEM, also known as Particle Method, was created by Peter Cundall for simulating the movement of blocky rocks systems (see [1]) and adapted for granular materials in collaboration with Strack (see [2]), as a model for the study of the mechanical behavior of rocks, based on the work of previous researches like [3]. In 1958 Deresiewicz idealized an analytic model to represent the behavior of the spheres of different sizes inside a volume, see [3]. The works of Wakabayashi in 1950 and Dantu in 1957 enabled the direct determination of the contact between particles, see [4, 5]. In 1969 Josselin de Jong described the stress distribution between the particles, improving the contact force determination and the resulting displacements and rotations, for each individual particle, see [6]. In 1973 Serrano e Rodriguez-Ortiz developed the first bidimensional numerical model for the arrangement of particles, more flexible in applications than the analytic model

Published online: 02 July 2018

presented by Deresiewicz, see [7] (apud [2]). These authors show the different configurations of loads, sizes and physical properties of the particles, making possible the calculation of the contact forces and the subsequent displacements.

Although there are various approaches to the method, Soft-Sphere Discrete Element Method (SSDEM) and Hard-Sphere Discrete Element Method (HSDEM) are two of these that are briefly explained. They were selected for their relevance in the modeling of granular particle dynamics.

The Hard-Sphere Discrete Element Method (HSDEM) predicts grain collisions in advance, treating these as instantaneous, and occurring at a single point of contact. The contact happens at the surface of the particles. This method is ideal for highly kinetically active systems, where the time that a particle takes to cover a distance is considerably larger than the time of a collision. This theory presents good results for dilute/ballistic regimes, but for situations where the deformations of the grains have to be accounted for, this method is not such a good choice (see [8, 9]). The authors in [8] presented the implementation of the Hard-Sphere Discrete Element Method (HSDEM) in this code, along with a discussion of the primitives (walls) that can be used to represent various kinds of boundary conditions (crater floors, geometry of sampling tools, experimental conditions, etc.). Other works on HSDEM are presented by Hong and McLennan in [10], Huilin et al. in [11], Kosinski and Hoffmann in [12] and Mitarai and Nakanishi in [13].

The modeling of physical phenomena where the deformation of the grains needs to be considered is usually handled by the Soft Sphere Discrete Element Method or, as it is commonly referred, Molecular Dynamics (MD). Each particle interacts with the other via a soft potential, therefore its name. This method doesn't predict the contacts in advance, and so, requires smaller integration interval times, increasing the computational simulation time. This computational burden may be relieved by parallel implementation (see [8, 9]). The authors in [8] affirm that the implementation of SSDEM allows for the modeling of the different contact forces between particles in granular material, such as various kinds of friction, including rolling and twisting friction, and the normal and tangential deformation of colliding particles. Other works regarding SSDEM are presented by Cleary and Sawley in [14], Tsuji et al. in [15], Sànchez in [16] and Tancredi et al. in [17].

Other different approaches have been used to perform modeling of granular materials, see for example [18].

Since then, a great amount of advances regarding the method have been developed in the literature, being possible to highlight the following works presented by Vu-Quoc et al. in [19], Martin and Bouvard in [20], Oñate et al. in [21], Zohdi and Wriggers in [22] and Zohdi in [23].

Also, based on the formulation of the particle method, a great amount of advances have been developed in studies of granular materials, such as presented by Ghaboussi and Barbosa in [24], Donzé in [25], De Saxce et al. in [26], Kruggel-Emden et al. in [27], Obermayr et al. in [28], El Shamy and Aldebhamid in [29] and Casas et al. in [30]; among other works in the study of soil mechanics.

Capable of representing the most diverse geometries and physical phenomena, the Discrete Element Method (DEM) is, however, relatively computationally intensive, which limits either the length of a simulation or the number of particles. This problem can be avoided by using parallel processing capabilities to scale up the number of particles or the length of the simulation. See [31] for more details.

An alternative to treating all particles separately is to average the physics across many particles and thereby treat the material as a continuum. In the case of solid-like granular behavior, the continuum approach usually treats the material as elastic or elasto-plastic and models it with the finite element method or a mesh-free method, as developed by Elaskar et al. in [32]. In the case of liquid-like or gas-like granular flow, the continuum approach may treat the material as a fluid and use computational fluid dynamics, see [33].

1.2 Proposed research

Having presented a brief introduction of the method and previous works on the field, the basic aim of this paper is to present a complete review of the particle method and to apply it to the study of granular materials. With this purpose, tridimensional examples are presented to validate the method and analyze the performance of the algorithms presented in this article. The numerical results of selected particles are presented in the Appendices.

The particles used in this work to simulate granular materials are modeled by rigid spheres by using the model proposed by Hertz. Several mechanical forces are taken into account in the dynamic equilibrium equation. The effect of rotation on the movement of particles is also considered. The friction force is calculated by Coulomb's law and this is used to calculate the spin effect. The purpose of the paper is to demonstrate that these formulations are perfectly suited for the analysis of granular materials. Classical analytical examples are described in the literature to verify the efficiency of the algorithm and formulations presented. The convergence criterion is applied to the particle displacements, but also extended to velocities and angular velocities. The convergence is obtained when these three quantities reach the established tolerance. Finally, more elaborate three-dimensional examples are shown to verify the efficiency of the algorithm and the formulations presented in this research. Another study on rotation in granular materials was proposed by Campello in [34]. In his work, the formulation of Euler Rodrigues was used. Here, a simpler Coulomb's law will be applied. Also, a

comparison between explicit and implicit integration method is presented.

2 Rolling phenomena on a particle

In this section, the rolling phenomena on a particle will be presented. Initially, a brief review of rolling phenomena is summarized taking into account the contribution of the translation and rotation in motion. The fundamental relation between force and acceleration is given by Newton's second law of motion and is defined in vector form as

$$m_i \ddot{\boldsymbol{r}}_i = m_i \dot{\boldsymbol{v}}_i = \mathbf{F}_i^{tot}\left(\boldsymbol{r}_1, \boldsymbol{r}_2, \ldots, \boldsymbol{r}_{N_p}\right), \tag{1}$$

where m_i represents the mass, $\boldsymbol{r}_i$ is the position vector, $\boldsymbol{v}_i$ and $\dot{\boldsymbol{v}}_i$ are the velocity and acceleration of the center of mass of the ith particle, respectively, and $\mathbf{F}_i^{tot}$ represents all forces acting on particle i. These forces will be presented in Sect. 3.

The linear moment ($\boldsymbol{G}_i$) is obtained from Eq. (1) by integrating over the time. So,

$$\begin{aligned}&\int_{t_1}^{t_2} \mathbf{F}_i^{tot}\left(\boldsymbol{r}_1, \boldsymbol{r}_2, \ldots, \boldsymbol{r}_{N_p}\right) dt \\ &= \int_{t_1}^{t_2} m_i d\boldsymbol{v}_i \\ &\Rightarrow \boldsymbol{G}_i(t_1) + \int_{t_1}^{t_2} \mathbf{F}_i^{tot}\left(\boldsymbol{r}_1, \boldsymbol{r}_2, \ldots, \boldsymbol{r}_{N_p}\right) dt = \boldsymbol{G}_i(t_2),\end{aligned} \tag{2}$$

where

$$\begin{aligned}\boldsymbol{G}_i(t_1) &= (m_i \boldsymbol{v}_i)|_{t_1} \\ \boldsymbol{G}_i(t_2) &= (m_i \boldsymbol{v}_i)|_{t_2}.\end{aligned} \tag{3}$$

Clearly, if $\mathbf{F}_i^{tot} = 0$, then $\boldsymbol{G}_i(t_1) = \boldsymbol{G}_i(t_2)$ and the linear momentum is said to be conserved.

An important quantity of interest is the velocity on the surface of the particles denoted by $\boldsymbol{v}_i^P$, which have a potential contact point with other particles or surfaces, represented by the point P in Fig. 1, and is defined by

$$\boldsymbol{v}_i^P = \boldsymbol{v}_i + \boldsymbol{v}_i^r = \boldsymbol{v}_i + \boldsymbol{\omega}_i \times \boldsymbol{r}_{i\to c}, \tag{4}$$

where $\boldsymbol{r}_{i\to c}$ is the vector that connects the center of particle to the contacting point with another particle or wall, $\boldsymbol{\omega}_i$ is the angular velocity and $\boldsymbol{v}_i^r = \boldsymbol{\omega}_i \times \boldsymbol{r}_{i\to c}$ is the velocity at particle's surface generated by the rotation. See Fig. 1 for a geometrical representation.

A related quantity is the angular momentum ($\boldsymbol{H}_i$). About the origin

$$\boldsymbol{H}_i \overset{\text{def}}{=} \boldsymbol{r}_i \times \boldsymbol{G}_i = \boldsymbol{r}_i \times m\boldsymbol{v}_i. \tag{5}$$

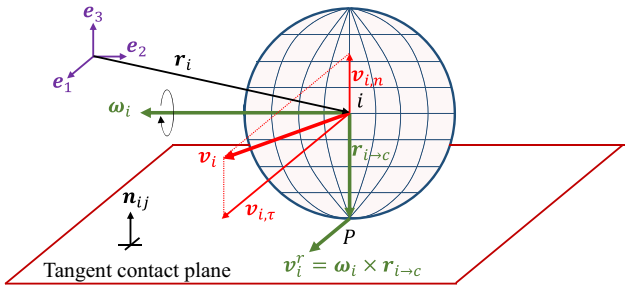

Fig. 1 Geometrical representation of rotation contribution

Deriving the Eq. (5) as a function of time, results in

$$\frac{d\boldsymbol{H}_i}{dt} = \frac{d}{dt}(\boldsymbol{r}_i \times m\boldsymbol{v}_i) \Rightarrow \dot{\boldsymbol{H}}_i = \frac{d\boldsymbol{r}_i}{dt} \times m\boldsymbol{v}_i + \boldsymbol{r}_i \times m\frac{d\boldsymbol{v}_i}{dt}. \tag{6}$$

Note that $\frac{d\boldsymbol{r}_i}{dt} \times \boldsymbol{v}_i = \boldsymbol{v}_i \times \boldsymbol{v}_i = 0$ and replacing in (6), it leads to

$$\dot{\boldsymbol{H}}_i = \boldsymbol{r}_i \times \mathbf{F}_i^{tot}. \tag{7}$$

The total moments $\boldsymbol{M}_i^{tot}$ generated by interaction forces, such as contact forces, rolling resistance, etc., is defined by

$$\boldsymbol{M}_i^{tot} = \boldsymbol{r}_i \times \mathbf{F}_i^{tot}. \tag{8}$$

So, the Eq. (7) can be rewritten as

$$\dot{\boldsymbol{H}}_i = \boldsymbol{M}_i^{tot}. \tag{9}$$

The Eq. (5) can also be written as

$$\begin{aligned}\boldsymbol{H}_i = m\left(\boldsymbol{r}_{i\to c} \times \boldsymbol{v}_i^r\right) &= m(\boldsymbol{r}_{i\to c} \times \boldsymbol{\omega}_i \times \boldsymbol{r}_{i\to c}) \\ &= m\left\|\boldsymbol{r}_{i\to c}^2\right\| \cdot \boldsymbol{\omega}_i = \bar{I}_{i,s} \cdot \boldsymbol{\omega}_i,\end{aligned} \tag{10}$$

where $\bar{I}_{i,s}$ is the inertial momentum. For spheres,

$$\bar{I}_{i,s} = \frac{2}{5} m_i R_i^2, \tag{11}$$

where R_i is the radius of the sphere. So, the Eq. (9) leads to

$$\dot{\boldsymbol{H}}_i = \frac{d}{dt}\left(\bar{I}_{i,s} \cdot \boldsymbol{\omega}_i\right) = \boldsymbol{M}_i^{tot}. \tag{12}$$

3 Active forces on a particle

In this section the acting forces on a particle are presented. The resultant force acting on a particle is composed by several contributions, as the normal contact force, the frictional contact force based on a Coulomb's friction law, the damping force, the particle-to-wall contact force, the adhesive bonding

force, the environmental force and the gravity force. These forces are very important to describe the particle's motion along the analysis time. All of them will be explained in details along this section.

The kinematics of the particle is presented by Zohdi in [35]. However, a short presentation is done including the contribution of the rolling effect. Basically, a group of non-intersecting particles ($i = 1, 2, \ldots, N_p$) is considered, where N_p is the number of particles. The objects in the system are assumed sufficiently large (in a sphere form) and consequently, the effects of their rotation relative to their center of mass are very important for their general movement and need to be considered.

According to the Euler's laws, at every time instant t, the following equations of motion for the ith particle in system must hold:

$$\begin{aligned} m_i \ddot{\boldsymbol{r}}_i &= \mathbf{F}_i^{tot}\left(\boldsymbol{r}_1, \boldsymbol{r}_2, \ldots, \boldsymbol{r}_{N_p}\right) \\ &= \mathbf{F}_i^{con} + \mathbf{F}_i^{fric} + \mathbf{F}_i^{wall} + \mathbf{F}_i^{bond} + \mathbf{F}_i^{damp} + \mathbf{F}_i^{env} + \mathbf{F}_i^{grav} \\ \bar{I}_{i,s} \cdot \boldsymbol{\omega}_i &= \boldsymbol{M}_i^{tot} = \sum_{j=1}^{N_{ci}} \boldsymbol{r}_{i\to c} \times \mathbf{F}_{ij}^{fric} \end{aligned} \tag{13}$$

which $\mathbf{F}_i^{tot}$ is decomposed into the sum of forces, where $\mathbf{F}_i^{con}$ are the normal contact forces inter particle generated by contact with other particles, $\mathbf{F}_i^{fric}$ are the sliding frictional forces, $\mathbf{F}_i^{wall}$ are the wall forces generated by contact with constraining surfaces (having contact, friction and damping), $\mathbf{F}_i^{bond}$ are the adhesive bonding forces with other particles and wall, $\mathbf{F}_i^{damp}$ are the damping forces arising from the surrounding interstitial environment that occurs from potentially viscous media, interstitial fluids or surfactants, $\mathbf{F}_i^{env}$ is the environment force coming into play as force opposing the motion of the particle due to the surrounding environment (i.e., damping from interstitial fluid or even smaller-scale particles or solvents) and $\mathbf{F}_i^{grav}$ is the gravity force. The second expression in Eq. (13) is needed for the description of the active forces.

3.1 Normal contact forces developed in a contact particle-to-particle

The particle-to-particle contact forces formulation was presented by Zohdi in [35, 36].

This formulation consists of determining the normal contact force contributions from the surrounding particles (N_{ci}) in contact, see Fig. 2. The particle-to-particle contact forces are defined by

$$\mathbf{F}_i^{con} = \sum_{j=1}^{N_{ci}} \mathbf{F}_{ij}^{con}, \tag{14}$$

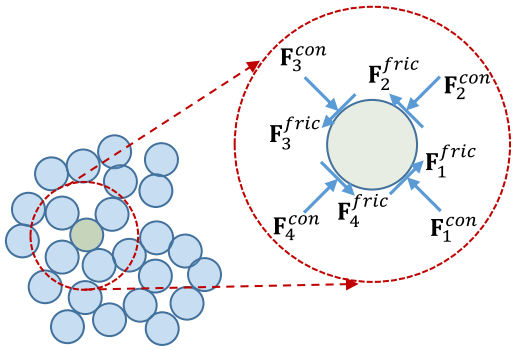

Fig. 2 Normal contact and friction forces induced by neighboring particles in contact (Reproduced with permission from [36])

based on separation distance between particles in contact. Generally,

$$\mathbf{F}_{ij}^{con} = \mathcal{F}\left(\left\|\boldsymbol{r}_i - \boldsymbol{r}_j\right\|, R_i, R_j, material\ parameters\right), \tag{15}$$

where R_i and R_j are the radii of particles i and j, respectively.

To obtain the expression (15) a simple relation is assumed, i.e., the contact force is proportional to the relative normalized proximity of particles i and j in contact, detected by the distance between centers being less than the sum of the radii. The geometric interpretation is shown in Fig. 3. Then,

$$If\left(\left\|\boldsymbol{r}_i - \boldsymbol{r}_j\right\| \le R_i + R_j\right) \Rightarrow activate\ contact. \tag{16}$$

The overlap is defined by

$$\delta_{ij} \overset{\text{def}}{=} \left|\left\|\boldsymbol{r}_i - \boldsymbol{r}_j\right\| - \left(R_i + R_j\right)\right|. \tag{17}$$

So, the Eq. (17) can also be written in the following manner

$$\begin{cases} If\ \left\|\boldsymbol{r}_i - \boldsymbol{r}_j\right\| - \left(R_i + R_j\right) \le 0 \Rightarrow \delta_{ij} \overset{\text{def}}{=} \left|\left\|\boldsymbol{r}_i - \boldsymbol{r}_j\right\| - \left(R_i + R_j\right)\right| \\ If\ \left\|\boldsymbol{r}_i - \boldsymbol{r}_j\right\| - \left(R_i + R_j\right) > 0 \Rightarrow \delta_{ij} = 0 \end{cases}. \tag{18}$$

The first expression in Eq. (18) corresponds to "activate contact" and the second one to "no contact".

Accordingly, consider the following general relationship

$$\mathbf{F}_{ij}^{con} \propto K_{p_{ij}} \left|\mathcal{E}_{ij}\right|^{P_p} A_{ij}^c \boldsymbol{n}_{ij}, \tag{19}$$

where $0 < K_{p_{ij}} < \infty$ is a particle-to-particle contact compliance constant, P_p is a material parameter, A_{ij}^c is a contact area parameter, $\mathcal{E}_{ij}$ is normalized/nondimensional (strain-like) deformation metric obtained by

$$\mathcal{E}_{ij} = \left|\frac{\left\|\boldsymbol{r}_i - \boldsymbol{r}_j\right\| - \left(R_i + R_j\right)}{\left(R_i + R_j\right)}\right| = \frac{\delta_{ij}}{\left(R_i + R_j\right)} \tag{20}$$

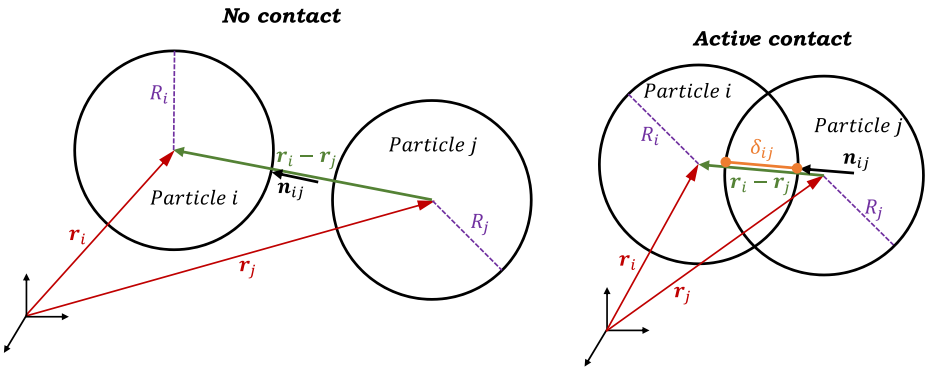

Fig. 3 Geometrical constrain

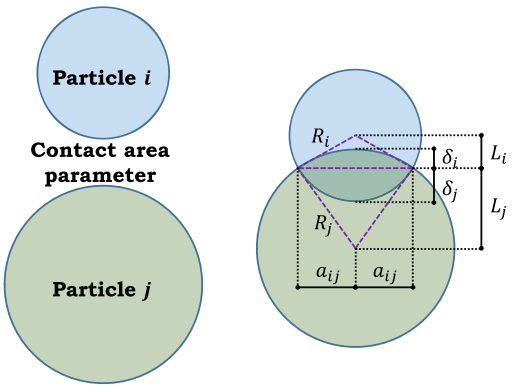

Fig. 4 An approximation of the contact area parameter for two particles in contact (adapted from [36])

and $\boldsymbol{n}_{ij}$ is the normalized normal contact vector defined by

$$\boldsymbol{n}_{ij} = \frac{\boldsymbol{r}_i - \boldsymbol{r}_j}{\|\boldsymbol{r}_i - \boldsymbol{r}_j\|} = -\frac{\boldsymbol{r}_j - \boldsymbol{r}_i}{\|\boldsymbol{r}_j - \boldsymbol{r}_j\|}. \tag{21}$$

It is important to mention the following relationship

$$\boldsymbol{n}_{ji} = \frac{\boldsymbol{r}_j - \boldsymbol{r}_j}{\|\boldsymbol{r}_j - \boldsymbol{r}_j\|} = -\frac{\boldsymbol{r}_i - \boldsymbol{r}_j}{\|\boldsymbol{r}_i - \boldsymbol{r}_j\|} = -\boldsymbol{n}_{ij}. \tag{22}$$

3.1.1 Contact area discretization

An approximation was suggested by Zohdi in [35] for the common contact radius a_{ij} and for the contact area A^c_{ij} defined by

$$A^c_{ij} = \pi a^2_{ij}, \tag{23}$$

see Fig. 4 for a geometrical representation.

The contact area A^c_{ij} can be calculated by solving these following equations

$$\begin{aligned} &a^2_{ij} + L^2_i = R^2_i \\ &a^2_{ij} + L^2_j = R^2_j \\ &L_i + L_j = \|\boldsymbol{r}_i - \boldsymbol{r}_j\|, \end{aligned} \tag{24}$$

where L_i is the distance from the center of particle i and the common contact interpenetration line and L_j is the distance from the center of particle j and the common contact interpenetration line, where the extent of interpenetration is δ_{ij} defined in Eq. (17). With Eq. (23) and first equation in (24), the above equations yield expression a_{ij}, which yields an expression for the contact area parameter

$$A^c_{ij} = \pi a^2_{ij} = \pi\left(R^2_i - L^2_i\right). \tag{25}$$

The value of L_i can be calculated using equations in (24). So, these expressions can be rewritten as:

$$\begin{aligned} &L_j = \|\boldsymbol{r}_i - \boldsymbol{r}_j\| - L_i \\ &L^2_j - L^2_i = R^2_j - R^2_i. \end{aligned} \tag{26}$$

Substituting the first equation in the second one

$$\left(\|\boldsymbol{r}_i - \boldsymbol{r}_j\| - L_i\right)^2 - L^2_i = R^2_j - R^2_i. \tag{27}$$

Simplifying

$$\left\|\boldsymbol{r}_i - \boldsymbol{r}^2_j\right\| + L^2_i - 2L_i\|\boldsymbol{r}_i - \boldsymbol{r}_j\| - L^2_i = R^2_j - R^2_i. \tag{28}$$

Again

$$\left\|\boldsymbol{r}_i - \boldsymbol{r}^2_j\right\| - 2L_i\|\boldsymbol{r}_i - \boldsymbol{r}_j\| = R^2_j - R^2_i. \tag{29}$$

Dividing (29) by $\|\boldsymbol{r}_i - \boldsymbol{r}_j\|$

$$\|\boldsymbol{r}_i - \boldsymbol{r}_j\| - 2L_i = \frac{R^2_j - R^2_i}{\|\boldsymbol{r}_i - \boldsymbol{r}_j\|}. \tag{30}$$

Then

$$L_i = \frac{1}{2}\left(\|\boldsymbol{r}_i - \boldsymbol{r}_j\| - \frac{R^2_j - R^2_i}{\|\boldsymbol{r}_i - \boldsymbol{r}_j\|}\right). \tag{31}$$

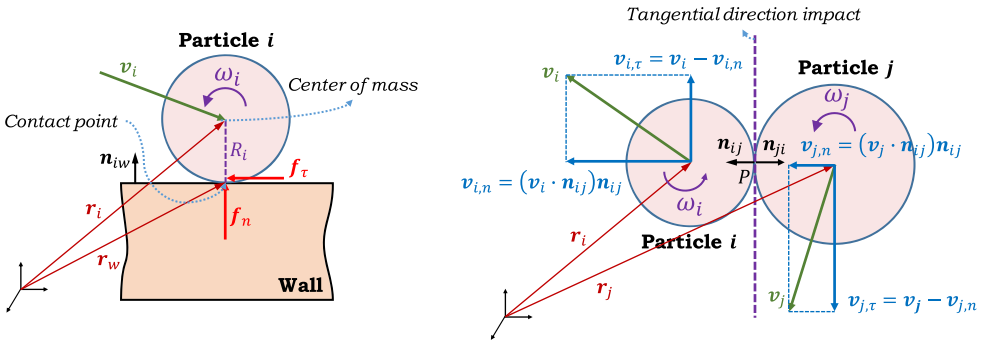

Fig. 5 Geometrical interpretation for contact particle-to-wall and particle-to-particle

3.1.2 Normal contact force based in Hertz theory of elastic contact

Alternative models for the normal contact pressure, defined in Eq. (15), have been presented in the literature. Especially the model proposed by Hertz, see [37] for details in its formulation:

$$\mathbf{F}_{ij}^{con} = \frac{4}{3}\left(R^*\right)^{1/2} E^* \delta_{ij}^{3/2} \boldsymbol{n}_{ij}, \tag{32}$$

which has the general form $\mathbf{F}_{ij}^{con} = K_{p_{ij}} \left|\delta_{ij}\right|^{P_p} \boldsymbol{n}_{ij}$, where

$$R^* = \frac{R_i R_j}{R_i + R_j} = \frac{1}{\frac{1}{R_i} + \frac{1}{R_j}} \tag{33}$$

and

$$E^* = \frac{E_i E_j}{E_j\left(1 - v_i^2\right) + E_i\left(1 - v_j^2\right)} = \frac{1}{\frac{\left(1-v_i^2\right)}{E_i} + \frac{\left(1-v_j^2\right)}{E_j}}. \tag{34}$$

In the above equations E_i and E_j are the Young's modulus of the particles i and j, respectively, and v_i and v_j are the Poisson coefficient of the particles i and j, respectively. Note that in the Hertz's formulation the contact area A_{ij}^c has already been incorporated in the relation above. The contact area A_{ij}^c of this model is equal to:

$$A_{ij}^c = \pi a_{ij}^2 = \pi R^* \delta_{ij}, \tag{35}$$

where $a_{ij} = \sqrt{R^* \delta_{ij}}$. For more details, see [37].

3.2 Frictional contact forces

A contact particle-to-wall or particle-to-particle can be geometrically represented as shown in Fig. 5. In this figure, $\boldsymbol{v}_i$ and $\boldsymbol{v}_j$ are the velocities of center of mass of the particles i and j, respectively, and $\boldsymbol{\omega}_i$ and $\boldsymbol{\omega}_j$ are the angular velocities of center of mass of the particles i and j, respectively.

Assuming that the particles are idealized rigid, i.e., any deformations arising from the contact are neither permanent nor significant when compared to the particle dimensions, the velocities at the contact point (P) for each spherical particle can thus now be written as:

$$\begin{aligned} \boldsymbol{v}_i^P &= \boldsymbol{v}_i + \boldsymbol{\omega}_i \times \left(R_i \boldsymbol{n}_{ji}\right) \\ \boldsymbol{v}_j^P &= \boldsymbol{v}_j + \boldsymbol{\omega}_j \times \left(R_j \boldsymbol{n}_{ij}\right). \end{aligned} \tag{36}$$

The particle-to-particle frictional contact forces are defined by:

$$\mathbf{F}_i^{fric} = \sum_{j=1}^{N_{ci}} \mathbf{F}_{ij}^{fric}. \tag{37}$$

The contact dissipation can be incorporated by tracking the relative velocity of the particles in contact. Observing the velocities in Fig. 5 is possible to determine the relative velocity as shown in Fig. 6.

In Fig. 6, $\boldsymbol{v}_i^P$ and $\boldsymbol{v}_j^P$ are the velocities at the contact point P of ith and jth particle, respectively. The relative velocity at the contact point can be determined as:

$$\boldsymbol{v}_{rel} = \boldsymbol{v}_j^P - \boldsymbol{v}_i^P. \tag{38}$$

The tangential velocity at the contact point in each particle is obtained by subtracting away the normal component of the velocity:

$$\begin{cases} \boldsymbol{v}_{i,\tau}^P = \boldsymbol{v}_i^P - \left(\boldsymbol{v}_i^P \cdot \boldsymbol{n}_{ij}\right)\boldsymbol{n}_{ij} \\ \boldsymbol{v}_{j,\tau}^P = \boldsymbol{v}_j^P - \left(\boldsymbol{v}_j^P \cdot \boldsymbol{n}_{ij}\right)\boldsymbol{n}_{ij} \end{cases}. \tag{39}$$

The tangential relative velocity at the contact point is calculated by:

$$\boldsymbol{v}_{rel,\tau} = \boldsymbol{v}_{rel} - \left(\boldsymbol{v}_{rel} \cdot \boldsymbol{n}_{ij}\right)\boldsymbol{n}_{ij} = \boldsymbol{v}_{j,\tau}^P - \boldsymbol{v}_{i,\tau}^P. \tag{40}$$

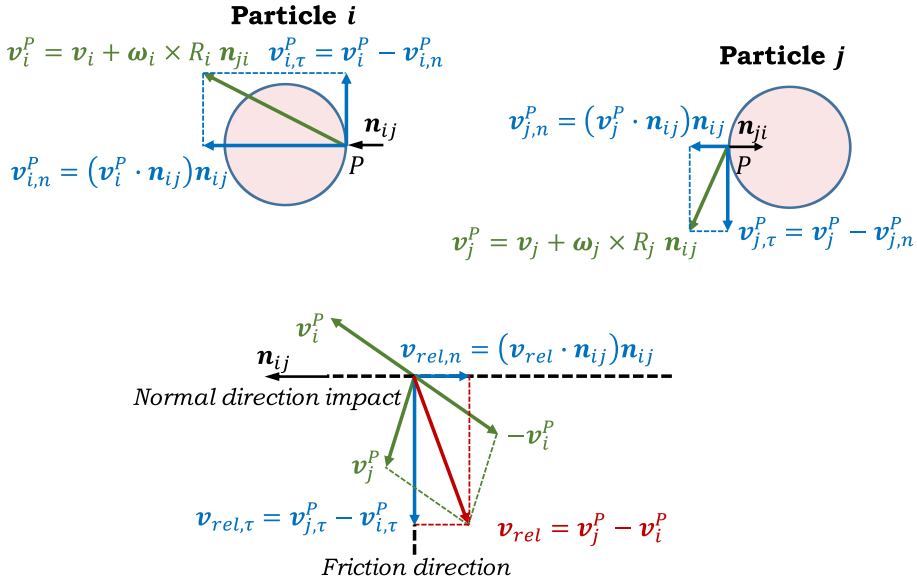

Fig. 6 Geometrical interpretation of velocities of the particles at the contact point P

Using the relative velocity at the contact point, the tangential slip direction can be characterized by a unit vector $\boldsymbol{\tau}_{ij}$ as follows:

$$\begin{aligned}\boldsymbol{\tau}_{ij} &= \frac{\boldsymbol{v}_{rel} - \left(\boldsymbol{v}_{rel}\cdot\boldsymbol{n}_{ij}\right)\boldsymbol{n}_{ij}}{\left\|\boldsymbol{v}_{rel} - \left(\boldsymbol{v}_{rel}\cdot\boldsymbol{n}_{ij}\right)\boldsymbol{n}_{ij}\right\|} \\ &= \frac{\boldsymbol{v}_{j,\tau}^P - \boldsymbol{v}_{i,\tau}^P}{\left\|\boldsymbol{v}_{j,\tau}^P - \boldsymbol{v}_{i,\tau}^P\right\|} \\ &= \frac{\boldsymbol{v}_{rel,\tau}}{\left\|\boldsymbol{v}_{rel,\tau}\right\|}. \end{aligned} \tag{41}$$

In frictional contact mechanics, two kinds of situation need to be taken into account. One is called "*stick case*" and other "*slip case*". Frictional stick is modeled via the following procedures. Initially the static friction threshold is checked by the following equation:

$$K^f \left\|\boldsymbol{v}_{j,\tau}^P - \boldsymbol{v}_{i,\tau}^P\right\| A_{ij}^c \Delta t, \tag{42}$$

against $\mu_s \left\|\mathbf{F}_{ij}^{con}\right\|$, where K^f is a tangential contact friction compliance constant, $\left\|\boldsymbol{v}_{j,\tau}^P - \boldsymbol{v}_{i,\tau}^P\right\|$ is the relative tangential velocity at the contact point, Δt is the time step used in the numerical discretization (to be presented later) and μ_s is the static friction coefficient. The stick case occurs when the Eq. (42) is less than $\mu_s \left\|\mathbf{F}_{ij}^{con}\right\|$, otherwise, the slip case occurs. The stick step can be considered a more rigorous and difficult step, because first no slip is assumed, generating the no-slip contact forces, by solving an entire multibody/multisurface contact problem.

So, the frictional contact force developed in each particle can be obtained in the following manner:

$$\begin{aligned} &IF && K^f \left\|\boldsymbol{v}_{j,\tau}^P - \boldsymbol{v}_{i,\tau}^P\right\| A_{ij}^c \Delta t < \mu_s \left\|\mathbf{F}_{ij}^{con}\right\| \\ &THEN && \mathbf{F}_{ij}^{fric} = K^f \left\|\boldsymbol{v}_{j,\tau}^P - \boldsymbol{v}_{i,\tau}^P\right\| A_{ij}^c \Delta t \boldsymbol{\tau}_{ij} && (\text{“}stickcase\text{”}) \\ &ELSEIF && \mathbf{F}_{ij}^{fric} = \mu_d \left\|\mathbf{F}_{ij}^{con}\right\| \boldsymbol{\tau}_{ij} && (\text{“}slipcase\text{”}), \end{aligned} \tag{43}$$

where $\boldsymbol{\tau}_{ij}$ is defined in (41) and μ_d is the dynamic friction coefficient.

3.3 Damping forces

Phenomenological particle contact dissipation can be incorporated by tracking the relative velocity of the particles in contact. The damping force is obtained by:

$$\mathbf{F}_i^{damp} = \sum_{j=1}^{N_{ci}} \mathbf{F}_{ij}^{damp}. \tag{44}$$

A simple model to calculate it is given by:

$$\mathbf{F}_{ij}^{damp} = c^d A_{ij}^c \left(\boldsymbol{v}_{j,n}^P - \boldsymbol{v}_{i,n}^P\right), \tag{45}$$

where c^d is a damping coefficient that represents the contact dissipation, $\boldsymbol{v}_{i,n}^P$ is the normal velocity at the contact point of the ith particle and $\boldsymbol{v}_{j,n}^P$ is the normal velocity at the contact point of the jth particle. It is important to mention that $\left(\boldsymbol{v}_{j,n}^P - \boldsymbol{v}_{i,n}^P\right)$ is the normal component of the relative velocity $\boldsymbol{v}_{rel}$, i.e.,

$$\boldsymbol{v}_{rel,n} = \left(\boldsymbol{v}_{rel}\cdot\boldsymbol{n}_{ij}\right)\boldsymbol{n}_{ij} = \left(\boldsymbol{v}_{j,n}^P - \boldsymbol{v}_{i,n}^P\right). \tag{46}$$

So, the Eq. (45) can be rewritten as:

$$\mathbf{F}_{ij}^{damp} = c^d A_{ij}^c \boldsymbol{v}_{rel,n}. \tag{47}$$

3.3.1 Damping force based in Hertz theory of elastic contact

The damping force can be also modeled via a standard Hertzian contact model for intersecting spheres (see [37]). This theory assumes that the contact area between the particles is small with respect to the dimensions of each particle and with respect to the relative radii of curvature of the surfaces. If the particle-to-particle contact force exists, the damping force is defined by:

$$\mathbf{F}_{ij}^{damp} = d\dot{\delta}_{ij}\boldsymbol{n}_{ij}, \tag{48}$$

where d is a damping parameter defined as:

$$d = 2\xi^*\sqrt{2E^*m^*}\left(R^*\delta_{ij}\right)^{1/4}\boldsymbol{n}_{ij} \tag{49}$$

and $\dot{\delta}_{ij}$ is the rate of change of overlap, defined by:

$$\dot{\delta}_{ij} = \left(\boldsymbol{v}_j^P - \boldsymbol{v}_i^P\right)\cdot\boldsymbol{n}_{ij} = \boldsymbol{v}_{rel}\cdot\boldsymbol{n}_{ij}. \tag{50}$$

In Eq. (49), ξ^* is a damping parameter that must be set, R^* is the effective radius defined in Eq. (33), E^* is Young's modulus of the interacting particles defined in Eq. (34) and m^* is the effective mass given by:

$$m^* = \frac{m_i m_j}{m_i + m_j} = \frac{1}{\frac{1}{m_i} + \frac{1}{m_j}}. \tag{51}$$

Note that the system can be qualified as follows: $\xi^* = 1$ critical damped, $\xi^* > 1$ is overdamped, $\xi^* < 1$ is less than critically damped and $\xi^* = 0$ is no damping force, as in an elastic collision. According to the literature review, especially the work presented by Zohdi in [35, 36], the damping coefficient (ξ^*) is taken as an arbitrary value ranging from zero to one, i.e. $0 \leq \xi^* \leq 1$. However, in this paper, it is assumed that there will be a deformation in the less rigid element, as a consequence of the contact between two bodies. Therefore, a weighted value of this coefficient is considered, such that:

$$\xi^* = \frac{E_i\xi_i + E_j\xi_j}{E_i + E_j}. \tag{52}$$

The Eq. (48) can be simplified as

$$\mathbf{F}_{ij}^{damp} = 2\xi^*\sqrt{2E^*m^*}\left(R^*\delta_{ij}\right)^{1/4}\left(\boldsymbol{v}_{rel}\cdot\boldsymbol{n}_{ij}\right)\boldsymbol{n}_{ij}. \tag{53}$$

Using the relationship $\boldsymbol{v}_{rel,n} = \left(\boldsymbol{v}_{rel}\cdot\boldsymbol{n}_{ij}\right)\boldsymbol{n}_{ij}$ in Eq. (53), results in

$$\mathbf{F}_{ij}^{damp} = 2\xi^*\sqrt{2E^*m^*}\left(R^*\delta_{ij}\right)^{1/4}\boldsymbol{v}_{rel,n}. \tag{54}$$

This expression has the same format given in Eq. (47).

3.4 Particle-to-wall contact

Particle-to-wall contact is handled in an identical manner to particle-to-particle contact, except that the wall displacement is considered given (externally controlled) and independent of the action with the particles. The amount of overlap of the particle with the wall position dictates the contact force intensity, see Fig. 7. In this paper, the walls are considered rigid, being discretized by triangular elements. The choice of triangular elements is to facilitate the modeling of irregular surfaces. A sophisticated search algorithm is used to determine the vector correspondent to the minimal distance between the particle and the wall. It is similar to the standard formulations of three-dimensional contact mechanics. These were intended to identify whether the contact was between node-to-surface, node-to-edge or node-to-node. In this work, as an analogy, the particle is considered as a slave node and the walls as the master contact surfaces. Due to the complexity of this algorithm and the fact that it is not the focus of this work, it will not be presented here. For more details regarding the contact between the slave node and the master contact surfaces see [38, 39].

Therefore, the particle-to-wall force is obtained by

$$\mathbf{F}_i^{wall} = \sum_{w=1}^{N_{wi}}\left(\mathbf{F}_{iw}^{wall,n} + \mathbf{F}_{iw}^{wall,f} + \mathbf{F}_{iw}^{damp}\right), \tag{55}$$

where N_{wi} is the number of surrounding walls in contact and $\mathbf{F}_{iw}^{wall,n}$, $\mathbf{F}_{iw}^{wall,f}$ and $\mathbf{F}_{iw}^{damp}$ are the normal, tangential and damping wall forces generated by contact with constraining surfaces, respectively.

Consider the following general relationship:

$$\mathbf{F}_{iw}^{wall,n} \propto K_{w_{iw}}|\mathcal{E}_{iw}|^{P_w}A_{iw}^c\boldsymbol{n}_{iw}, \tag{56}$$

where $0 < K_{w_{iw}} < \infty$ is a wall-to-particle compliance constant, P_w is a material constant,

$$\mathcal{E}_{iw} = \left|\frac{\|\boldsymbol{r}_i - \boldsymbol{r}_w\| - R_i}{R_i}\right| = \frac{\delta_{iw}}{R_i} \tag{57}$$

and $\boldsymbol{n}_{iw}$ is the normalized normal contact vector defined by:

$$\boldsymbol{n}_{iw} = \frac{\boldsymbol{r}_i - \boldsymbol{r}_w}{\|\boldsymbol{r}_i - \boldsymbol{r}_w\|} = -\frac{\boldsymbol{r}_j - \boldsymbol{r}_w}{\|\boldsymbol{r}_i - \boldsymbol{r}_w\|}. \tag{58}$$

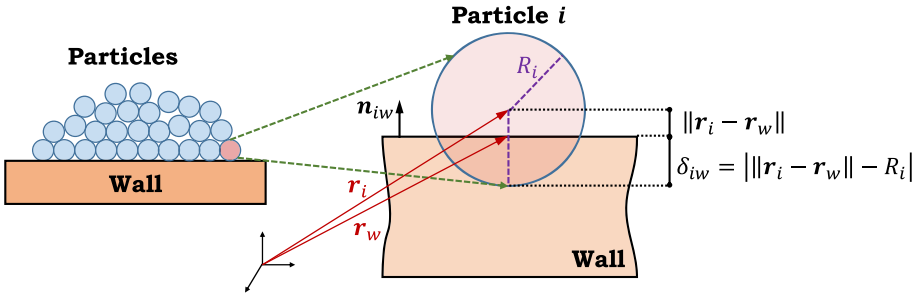

Fig. 7 Geometrical constrain

For the generated friction, a continuous sliding is assumed. So,

$$\begin{array}{lll} IF & K^f \left\| \boldsymbol{v}^P_{w,\tau} - \boldsymbol{v}^P_{i,\tau} \right\| A^c_{iw} \Delta t < \mu_s \left\| \mathbf{F}^{wall,n}_{iw} \right\| & \\ THEN & \mathbf{F}^{wall,f}_{iw} = K^f \left\| \boldsymbol{v}^P_{w,\tau} - \boldsymbol{v}^P_{i,\tau} \right\| A^c_{iw} \Delta t \boldsymbol{\tau}_{iw} & (\text{“}stickcase\text{”}) \\ ELSEIF & \mathbf{F}^{wall,f}_{iw} = \mu_d \left\| \mathbf{F}^{wall,n}_{iw} \right\| \boldsymbol{\tau}_{iw} & (\text{“}slipcase\text{”}), \end{array} \tag{59}$$

where

$$\boldsymbol{\tau}_{iw} = \frac{\boldsymbol{v}^P_{w,\tau} - \boldsymbol{v}^P_{i,\tau}}{\left\| \boldsymbol{v}^P_{w,\tau} - \boldsymbol{v}^P_{i,\tau} \right\|}. \tag{60}$$

The tangential velocity at the contact point is obtained through Eq. (39).

The damping force is calculated by

$$\mathbf{F}^{damp}_{iw} = c^d A^c_{iw} \boldsymbol{v}_{rel,n}. \tag{61}$$

3.4.1 Material parameters based in Hertz theory of elastic contact

The normal contact between a particle and a wall, based on Hertzian model, is given by:

$$\mathbf{F}^{wall,n}_{iw} = \frac{4}{3} \left(R^*\right)^{1/2} E^* \delta^{3/2}_{iw} \boldsymbol{n}_{ij}, \tag{62}$$

which has the general form $\mathbf{F}^{wall,n}_{iw} = K_{p_{iw}} |\delta_{iw}|^{P_p} \boldsymbol{n}_{iw}$ and the damping force is calculated by:

$$\mathbf{F}^{damp}_{ij} = 2\xi^* \sqrt{2E^* m^*} \left(R^* \delta_{iw}\right)^{1/4} \boldsymbol{v}_{rel,n}. \tag{63}$$

ξ^* is a damping parameter defined in Eq. (52) that must be set, R^* is the effective radius defined in Eq. (33), E^* is Young's modulus of the interacting particles defined in Eq. (34) and m^* is the effective mass defined in Eq. (51). Considering these relationships

$$R_w = R_j = \infty, \tag{64}$$

$$m_w = m_j = \infty, \tag{65}$$

these parameters can be rewritten as:

$$R^* = R_i \tag{66}$$

$$E^* = \frac{E_i E_w}{E_w\left(1 - \upsilon_i^2\right) + E_i\left(1 - \upsilon_w^2\right)} = \frac{1}{\frac{\left(1-\upsilon_i^2\right)}{E_i} + \frac{\left(1-\upsilon_w^2\right)}{E_w}}, \tag{67}$$

$$m^* = m_i \tag{68}$$

$$\xi^* = \frac{E_i \xi_i + E_w \xi_w}{E_i + E_w}. \tag{69}$$

3.5 Adhesive bonding forces

The adhesive bonding force is obtained by:

$$\mathbf{F}^{bond}_i = \sum_{j=1}^{N_{ci}} \left(\mathbf{F}^{bond,n}_{ij} + \mathbf{F}^{bond,r}_{ij} \right), \tag{70}$$

where $\mathbf{F}^{bond,n}_{ij}$ is the normal adhesive bonding force and $\mathbf{F}^{bond,r}_{ij}$ is the rotational adhesive bonding force.

The particle-to-particle adhesive bonding relation is considered based on exceeding critical interpenetration distance. A simple model can be defined as follows:

$$\begin{array}{lll} IF & \left\| \boldsymbol{r}_i - \boldsymbol{r}_j \right\| \leq R_i + R_j \ AND \ \left| \mathcal{E}_{ij} \right| \geq \mathcal{E}^* & \\ THEN & \mathbf{F}^{bond,n}_{ij} = K^{nb}_{ij} \left| \mathcal{E}_{ij} \right|^{P_p} A^c_{ij} \boldsymbol{n}_{ij} & , \\ ELSEIF & \mathbf{F}^{bond,n}_{ij} = 0 & \end{array} \tag{71}$$

where $0 \leq K^{nb}_{ij}$ is a bonding constant, $\mathcal{E}_{ij}$ is defined in (20), $\mathcal{E}^*$ is normalized deformation bonding and P_p is a material parameter. It is important to mention that if $\left\| \boldsymbol{r}_i - \boldsymbol{r}_j \right\| \leq R_i + R_j$, contact occurs between the particles. So, if the particles are in contact and $\left| \mathcal{E}_{ij} \right| \geq \mathcal{E}^*$, then an adhesive/attractive normal bond is activated between the particles, as defined in (43).

If the particles have an activated normal bond, then the particles automatically have a rotational bond equivalent in form to stick friction

$$\begin{array}{ll} IF & \left\|\boldsymbol{r}_i - \boldsymbol{r}_j\right\| \leq R_i + R_j \ AND \ \left|\mathcal{E}_{ij}\right| \geq \mathcal{E}^* \\ THEN & \mathbf{F}_{ij}^{bond,r} = K_{ij}^{rb}\left\|\boldsymbol{v}_{j,\tau}^P - \boldsymbol{v}_{i,\tau}^P\right\| A_{ij}^c \Delta t \boldsymbol{\tau}_{ij} \\ ELSEIF & \mathbf{F}_{ij}^{bond,r} = \mathbf{0} \end{array}, \quad (72)$$

where K_{ij}^{rb} is a rotational bonding constant.

3.6 Environmental force

The environment force comes into play as force opposing the motion of the particle due to the surrounding environment (i.e., damping from interstitial fluid or even smaller-scale particles or solvents between particles, such as binding enhancers, surfactants and lubricants). A simple model to account for this was defined by Reynolds (very low Reynolds number "Stokesian" model) in the following manner:

$$\mathbf{F}_i^{env} = 6\pi c^e R_i\left(\boldsymbol{v}^e - \boldsymbol{v}_i\right), \quad (73)$$

where c^e is the dynamic viscosity of the air and $\boldsymbol{v}^e$ is the local average velocity of the external interstitial medium, which one may assume to be $\boldsymbol{v}^e \approx \mathbf{0}$, for most applications of interest in this work. The mechanics of the interstitial fluid is unimportant in problems of interest here. However, for other applications such as high-speed flow, the motion of the fluid can be important, requiring more sophisticated drag laws. See [40, 41].

3.7 Gravity force

The other force that needs to be taken into account is the gravitational force, which acts in a downwards ($-z$ direction) and is given by:

$$\mathbf{F}_i^{grav} = -m_i g \hat{\boldsymbol{z}}, \quad (74)$$

where g is the gravity acceleration and $\hat{\boldsymbol{z}}$ is the unit vector in the z direction.

4 Time integration

In this section, the time integration scheme will be presented to solve the equations described in Sect. 2. First, the integration of the translational contribution will be explained and then, the same will be done for the integration of the rolling contribution. Subsequently, an iterative implicit solution method will be presented, as well as the time integration scheme for solution of the system's dynamics.

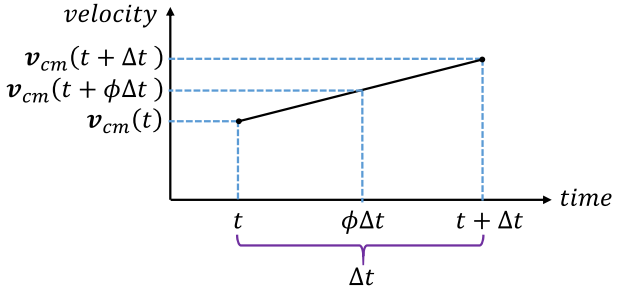

Fig. 8 Trapezoidal time-stepping rule for velocity

4.1 Integration of the translational contribution

Based on the second Newton's law, the translational component of the center of mass can be written as:

$$M\ddot{\boldsymbol{r}}_{cm} = M\dot{\boldsymbol{v}}_{cm} = \mathbf{F}^{tot}, \quad (75)$$

where M is the total system mass, $\boldsymbol{F}^{tot}$ is the overall external force acting on the system, $\boldsymbol{v}_{cm}$ is the center of mass velocity and $\boldsymbol{r}_{cm}$ is the position vector of the center of mass of the system, given by:

$$\boldsymbol{r}_{cm} \overset{\text{def}}{=} \frac{\sum_{i-1}^{N_{ci}} m_i \boldsymbol{r}_i}{\sum_{i-1}^{N_{ci}} m_i} = \frac{1}{M}\sum_{i-1}^{N_{ci}} m_i \boldsymbol{r}_i. \quad (76)$$

A trapezoidal time-stepping rule is used, see Fig. 8. Here, a short explanation will be presented, however, the complete formulation is described by Zohdi in [42].

Considering t the current time and Δt the time increment, at some intermediate moment in time, $t \leq t + \phi\Delta t \leq t + \Delta t$ with $0 < \phi \leq 1$, is possible to affirm:

$$\begin{aligned} \dot{\boldsymbol{v}}_{cm}(t+\phi\Delta t) &\approx \frac{\boldsymbol{v}_{cm}(t+\Delta t) - \boldsymbol{v}_{cm}(t)}{\Delta t} \\ &= \frac{1}{M}\boldsymbol{F}^{tot}(t+\phi\Delta t) \\ &\approx \frac{1}{M}\left[\phi\boldsymbol{F}^{tot}(t+\Delta t) + (1-\phi)\boldsymbol{F}^{tot}(t)\right], \end{aligned} \quad (77)$$

leading to

$$\begin{aligned} &\boldsymbol{v}_{cm}(t+\Delta t) \\ &\approx \boldsymbol{v}_{cm}(t) + \frac{\Delta t}{M}\left[\phi\mathbf{F}^{tot}(t+\Delta t) + (1-\phi)\mathbf{F}^{tot}(t)\right]. \end{aligned} \quad (78)$$

For the position vector

$$\begin{aligned} \dot{\boldsymbol{r}}_{cm}(t+\phi\Delta t) &\approx \frac{\boldsymbol{r}_{cm}(t+\Delta t) - \boldsymbol{r}_{cm}(t)}{\Delta t} \\ &\approx \boldsymbol{v}_{cm}(t+\phi\Delta t) \\ &\approx \phi\boldsymbol{v}_{cm}(t+\Delta t) + (1-\phi)\boldsymbol{v}_{cm}(t), \end{aligned} \quad (79)$$

leading to

$$\boldsymbol{r}_{cm}\left(t+\Delta t\right) \approx \boldsymbol{r}_{cm}\left(t\right)+\Delta t\left[\phi \boldsymbol{v}_{cm}\left(t+\Delta t\right)+\left(1-\phi\right)\boldsymbol{v}_{cm}\left(t\right)\right]. \tag{80}$$

This equation can be rewritten as:

$$\boldsymbol{r}_{cm}\left(t+\Delta t\right) \approx \boldsymbol{r}_{cm}\left(t\right)+\boldsymbol{v}_{cm}\left(t\right)\Delta t + \phi\left(\Delta t\right)^{2}\frac{\left[\boldsymbol{v}_{cm}\left(t+\Delta t\right)-\boldsymbol{v}_{cm}\left(t\right)\right]}{\Delta t}. \tag{81}$$

Finally, can be consolidated into:

$$\boldsymbol{r}_{cm}\left(t+\Delta t\right) = \boldsymbol{r}_{cm}\left(t\right)+\boldsymbol{v}_{cm}\left(t\right)\Delta t + \frac{\phi\left(\Delta t\right)^{2}}{M}\left[\phi \mathbf{F}^{tot}\left(t+\Delta t\right)+\left(1-\phi\right)\mathbf{F}^{tot}\left(t\right)\right]. \tag{82}$$

Other formulations to update the position vector and the velocity vector are presented by LeVeque in [43] These equations lead to a coupled system of equations, which are solved using an adaptive iterative scheme, building on approaches found in various form in [40, 44, 45].

4.2 Integration of the rolling phenomena

Solving the Eq. (12):

$$\int_{t_1}^{t_2} d\boldsymbol{\omega}_i = \int_{t_1}^{t_2} \frac{1}{\bar{I}_{i,s}}\boldsymbol{M}_i^{tot} dt \Rightarrow \boldsymbol{\omega}_i(t_2) = \boldsymbol{\omega}_i(t_1) + \frac{\Delta t}{\bar{I}_{i,s}}\boldsymbol{M}_i^{tot}. \tag{83}$$

Then, based in Eq. (83), the time discretization is done by the following equation:

$$\boldsymbol{\omega}_i\left(t+\Delta t\right) = \boldsymbol{\omega}_i\left(t\right) + \frac{\Delta t}{\bar{I}_{i,s}}\left\{\boldsymbol{M}_i^{tot}\left(t\right)+\left[\varnothing \boldsymbol{M}_i^{tot}\left(t+\Delta t\right)-\varnothing \boldsymbol{M}_i^{tot}\left(t\right)\right]\right\}, \tag{84}$$

where $\varnothing$ is a scalar value with range $0 < \phi \leq 1$. It is important to mention that when the parameter $\phi = 0$ the system is solved by explicit method and for $0 < \phi \leq 1$ the system is solved by implicit method. The Eq. (84) can be rewritten as

$$\boldsymbol{\omega}_i\left(t+\Delta t\right) = \boldsymbol{\omega}_i\left(t\right) + \frac{\Delta t}{\bar{I}_{i,s}}\left[\varnothing \boldsymbol{M}_i^{tot}\left(t+\Delta t\right)+\left(1-\varnothing\right)\boldsymbol{M}_i^{tot}\left(t\right)\right]. \tag{85}$$

The graphical interpretation of Eq. (84) is shown in Fig. 9.

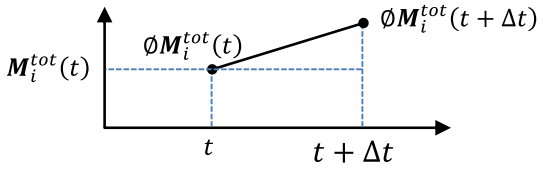

Fig. 9 Time discretization

Based on the expression (8) the moment $\boldsymbol{M}_i^{tot}$ can also be calculated by

$$\boldsymbol{M}_i^{tot} = \sum_{j=1}^{N_{ci}} \boldsymbol{r}_{i\rightarrow c} \times \mathbf{F}_{ij}^{fric}, \tag{86}$$

where $\mathbf{F}_{ij}^{fric}$ is the friction force between the particles i and j that will be presented in Sect. 3.2. This force is applied at the contact point P on the surface of particle i, see Fig. 1.

In this work the rolling is taken into account. Therefore, the friction force is modeled by assuming that sliding and rolling may occur between the contact pair, i.e., whether it is pure sliding, sliding with rolling or pure rolling. At the contact point P the friction occurs and its velocity must be computed by using Eq. (4).

The rotation vector $\boldsymbol{\theta}_i$ of a ith particle is obtained by

$$\begin{aligned} \boldsymbol{\omega}_i &= \frac{d\boldsymbol{\theta}_i}{dt} \\ &\Rightarrow \int_{t_1}^{t_2} d\boldsymbol{\theta}_i \\ &= \int_{t_1}^{t_2} \boldsymbol{\omega}_i dt \\ &\Rightarrow \boldsymbol{\theta}_i\left(t_2\right) \\ &= \boldsymbol{\theta}_i\left(t_1\right) + \boldsymbol{\omega}_i \Delta t. \end{aligned} \tag{87}$$

The time discretization is done by the following equation:

$$\boldsymbol{\theta}_i(t+\Delta t) = \boldsymbol{\theta}_i(t) + \Delta t\{\varnothing \boldsymbol{\omega}_i(t+\Delta t) + (1-\varnothing)\boldsymbol{\omega}_i(t)\}. \tag{88}$$

Finally, for a point P' belonged to a particle in the initial configuration placed $\boldsymbol{r}_{i\rightarrow c}^{P'}\Big|_{t=0}$ from its center, its current position is defined by:

$$\boldsymbol{r}_i^{P'}(t+\Delta t) = \boldsymbol{r}_i(t+\Delta t) + \boldsymbol{r}_{i\rightarrow c}^{P'}\Big|_{t=0} \times \boldsymbol{\theta}_i(t+\Delta t). \tag{89}$$

It is important to mention that, in this work, spheres are used to model particles. Therefore, the contact point can be easily found.

4.3 Iterative implicit solution method

Following the basic framework developed by Zohdi in [46, 47], the Eq. (82) can be rewritten in a slightly more streamlined for particle i

$$\boldsymbol{r}_i^{L+1} = \boldsymbol{r}_i^{L} + \boldsymbol{v}_i^{L}\Delta t + \frac{\phi(\Delta t)^2}{m_i}\Big[\phi \mathbf{F}_i^{tot,L+1} + (1-\phi)\mathbf{F}_i^{tot,L}\Big], \tag{90}$$

the same for Eq. (78)

$$\boldsymbol{v}_i^{L+1} = \boldsymbol{v}_i^{L} + \frac{\Delta t}{m_i}\Big[\phi \mathbf{F}_i^{tot,L+1} + (1-\phi)\mathbf{F}_i^{tot,L}\Big], \tag{91}$$

and the same for Eq. (85)

$$\boldsymbol{\omega}_i^{L+1} = \boldsymbol{\omega}_i^{L} + \frac{\Delta t}{\bar{I}_{i,s}}\Big[\varnothing \boldsymbol{M}_i^{tot,L+1} + (1-\varnothing)\boldsymbol{M}_i^{tot,L}\Big], \tag{92}$$

where superscript L and $L+1$ indicates the indices of the current and the future time-step in the discretization respectively. Basically, the superscript L is a time interval counter. This is a generalized one-step scheme, with $\phi \in (0, 1]$, and $\phi = 0$ is the explicit Euler integration scheme, while $\phi = 1$ is the fully implicit Euler integration scheme. The implicit implementation of the position, velocity and angular velocity updates, as is evident from Eqs. (78), (82) and (85), requires an iterative solution for $\boldsymbol{r}_i^{L+1}$, $\boldsymbol{v}_i^{L+1}$ and $\boldsymbol{\omega}_i^{L+1}$.

The set of equations represented by (90) to (92) can be solved recursively by recasting the relation as

$$\boldsymbol{r}_i^{L+1,K} = \boldsymbol{r}_i^{L} + \boldsymbol{v}_i^{L}\Delta t + \frac{\phi\,(\Delta t)^2}{m_i}\left[\phi \mathbf{F}_i^{tot,L+1,K-1} + (1-\phi)\,\mathbf{F}_i^{tot,L}\right], \tag{93}$$

$$\boldsymbol{v}_i^{L+1,K} = \boldsymbol{v}_i^{L} + \frac{\Delta t}{m_i}\left[\phi \mathbf{F}_i^{tot,L+1,K-1} + (1-\phi)\,\mathbf{F}_i^{tot,L}\right], \tag{94}$$

$$\boldsymbol{\omega}_i^{L+1,K} = \boldsymbol{\omega}_i^{L} + \frac{\Delta t}{\bar{I}_{i,s}}\left[\varnothing \boldsymbol{M}_i^{tot,L+1,K-1} + (1-\varnothing)\,\boldsymbol{M}_i^{tot,L}\right], \tag{95}$$

where $K = 1, 2, 3\ldots$ is the index of iteration with in time-step $L+1$. These equations can also be represented in the following form

$$\boldsymbol{r}_i^{L+1,K} = \mathcal{G}_r\left(\boldsymbol{r}_i^{L+1,K-1}\right) + \mathcal{R}_{i,r}, \tag{96}$$

$$\boldsymbol{v}_i^{L+1,K} = \mathcal{G}_v\left(\boldsymbol{v}_i^{L+1,K-1}\right) + \mathcal{R}_{i,v}, \tag{97}$$

$$\boldsymbol{\omega}_i^{L+1,K} = \mathcal{G}_\omega\left(\boldsymbol{\omega}_i^{L+1,K-1}\right) + \mathcal{R}_{i,\omega}, \tag{98}$$

where

$$\mathbf{F}_i^{tot,L+1,K-1} \stackrel{\text{def}}{=} \mathbf{F}_i^{tot,L+1,K-1}\left(\boldsymbol{r}_1^{L+1,K-1}, \boldsymbol{r}_2^{L+1,K-1}, \ldots, \boldsymbol{r}_{N_p}^{L+1,K-1}\right), \tag{99}$$

$$\mathbf{F}_i^{tot,L} \stackrel{\text{def}}{=} \mathbf{F}_i^{tot,L}\left(\boldsymbol{r}_1^{L}, \boldsymbol{r}_2^{L}, \ldots, \boldsymbol{r}_{N_p}^{L}\right), \tag{100}$$

$$\boldsymbol{M}_i^{tot,L+1,K-1} \stackrel{\text{def}}{=} \boldsymbol{M}_i^{tot,L+1,K-1}\left(\boldsymbol{r}_1^{L+1,K-1}, \boldsymbol{r}_2^{L+1,K-1}, \ldots, \boldsymbol{r}_{N_p}^{L+1,K-1}\right), \tag{101}$$

$$\boldsymbol{M}_i^{tot,L} \stackrel{\text{def}}{=} \boldsymbol{M}_i^{tot,L}\left(\boldsymbol{r}_1^{L}, \boldsymbol{r}_2^{L}, \ldots, \boldsymbol{r}_{N_p}^{L}\right), \tag{102}$$

$$\mathcal{G}_r\left(\boldsymbol{r}_i^{L+1,K-1}\right) = \frac{(\phi\Delta t)^2}{m_i}\mathbf{F}_i^{tot,L+1,K-1}, \tag{103}$$

$$\mathcal{R}_{i,r} = \boldsymbol{r}_i^{L} + \boldsymbol{v}_i^{L}\Delta t + \frac{\phi(\Delta t)^2}{m_i}(1-\phi)\mathbf{F}_i^{tot,L}, \tag{104}$$

$$\mathcal{G}_v\left(\boldsymbol{v}_i^{L+1,K-1}\right) = \frac{\phi\Delta t}{m_i}\mathbf{F}_i^{tot,L+1,K-1}, \tag{105}$$

$$\mathcal{R}_{i,v} = \boldsymbol{v}_i^{L} + \frac{\Delta t}{m_i}(1-\phi)\mathbf{F}_i^{tot,L}, \tag{106}$$

$$\mathcal{G}_\omega\left(\boldsymbol{\omega}_i^{L+1,K-1}\right) = \frac{\phi\Delta t}{\bar{I}_{i,s}}\boldsymbol{M}_i^{tot,L+1,K-1}, \tag{107}$$

$$\mathcal{R}_{i,\omega} = \boldsymbol{\omega}_i^{L} + \frac{\Delta t}{\bar{I}_{i,s}}(1-\phi)\boldsymbol{M}_i^{tot,L}. \tag{108}$$

The terms $\mathcal{R}_{i,r}$, $\mathcal{R}_{i,v}$ and $\mathcal{R}_{i,\omega}$ are remainder terms that do not depend on the solution. The convergence of such a scheme is dependent on the behavior of $\mathcal{G}_r$, $\mathcal{G}_v$ and $\mathcal{G}_\omega$. The form of the error function is presented below

$$\boldsymbol{\varpi}_{i,r}^{L+1,K} \stackrel{\text{def}}{=} \boldsymbol{r}_i^{L+1,K} - \boldsymbol{r}_i^{L+1} \tag{109}$$

$$\boldsymbol{\varpi}_{i,v}^{L+1,K} \stackrel{\text{def}}{=} \boldsymbol{v}_i^{L+1,K} - \boldsymbol{v}_i^{L+1}. \tag{110}$$

$$\boldsymbol{\varpi}_{i,\omega}^{L+1,K} \stackrel{\text{def}}{=} \boldsymbol{\omega}_i^{L+1,K} - \boldsymbol{\omega}_i^{L+1}. \tag{111}$$

Based on the formulations presented by Zohdi in [36], a sufficient condition for convergence is the existence of a contraction mapping

$$\begin{aligned}\left\|\boldsymbol{r}_i^{L+1,K} - \boldsymbol{r}_i^{L+1}\right\| &= \left\|\mathcal{G}_r\left(\boldsymbol{r}_i^{L+1,K-1}\right) - \mathcal{G}_r\left(\boldsymbol{r}_i^{L+1}\right)\right\| \\ &\leq \eta_r^{L+1,K}\left\|\boldsymbol{r}_i^{L+1,K-1} - \boldsymbol{r}_i^{L+1}\right\|\end{aligned} \tag{112}$$

$$\begin{aligned}\left\|\boldsymbol{v}_i^{L+1,K} - \boldsymbol{v}_i^{L+1}\right\| &= \left\|\mathcal{G}_v\left(\boldsymbol{v}_i^{L+1,K-1}\right) - \mathcal{G}_v\left(\boldsymbol{v}_i^{L+1}\right)\right\| \\ &\leq \eta_v^{L+1,K}\left\|\boldsymbol{v}_i^{L+1,K-1} - \boldsymbol{v}_i^{L+1}\right\|,\end{aligned} \tag{113}$$

$$\begin{aligned}\left\|\boldsymbol{\omega}_i^{L+1,K} - \boldsymbol{\omega}_i^{L+1}\right\| &= \left\|\mathcal{G}_\omega\left(\boldsymbol{\omega}_i^{L+1,K-1}\right) - \mathcal{G}_\omega\left(\boldsymbol{\omega}_i^{L+1}\right)\right\| \\ &\leq \eta_\omega^{L+1,K}\left\|\boldsymbol{\omega}_i^{L+1,K-1} - \boldsymbol{\omega}_i^{L+1}\right\|,\end{aligned} \tag{114}$$

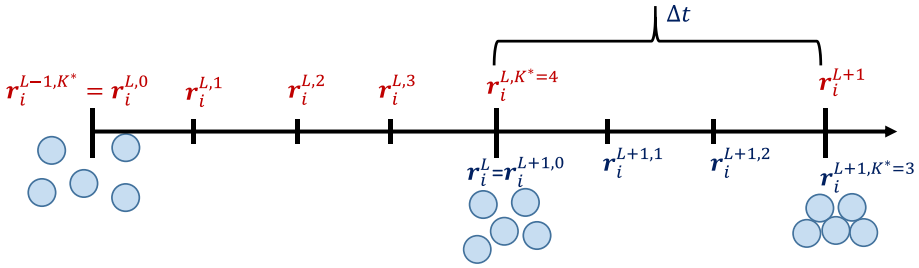

Fig. 10 Iterations within the time step

where $0 \leq \eta_r^{L+1,K} < 1$, $0 \leq \eta_v^{L+1,K} < 1$ and $0 \leq \eta_\omega^{L+1,K} < 1$ for each iteration K. Then $\boldsymbol{\varpi}_{i,r}^{L+1,K} \to 0$, $\boldsymbol{\varpi}_{i,v}^{L+1,K} \to 0$ and $\boldsymbol{\varpi}_{i,\omega}^{L+1,K} \to 0$ for any arbitrary starting value $\boldsymbol{r}_i^{L+1,K=0}$, $\boldsymbol{v}_i^{L+1,K=0}$ and $\boldsymbol{\omega}_i^{L+1,K=0}$, as $K \to \infty$, which is a contraction condition that is sufficient, but not necessary, for convergence. The convergence of Eq. (93) is scaled by $\eta_r \propto \frac{(\phi \Delta t)^2}{m_i}$ (see Eq. (103)), the convergence of Eq. (94) is scaled by $\eta_v \propto \frac{\phi \Delta t}{m_i}$ (see Eq. (105)) and the convergence of Eq. (95) is scaled by $\eta_\omega \propto \frac{\phi \Delta t}{\bar{I}_{i,s}}$ (see Eq. (107)). Therefore, the contraction constant of $\mathcal{G}_r$ and $\mathcal{G}_v$ is directly dependent on the magnitude of the interaction forces ($\|\mathbf{F}_i\|$), inversely proportional to the masses m_i and directly proportional to Δt. The contraction constant of $\mathcal{G}_\omega$ is directly dependent on the magnitude of the interaction moments ($\|\boldsymbol{M}_i\|$), inversely proportional to the moment of mass $\bar{I}_{i,s}$ and directly proportional to Δt. Thus, decreasing the time-step size improves the convergence.

An approach to maximize the time-step sizes to decrease overall computing time and keep the numerical solution's accuracy was proposed by Zohdi in [46]. This proposal takes into account only the position vector's errors. Here, the velocity vector's errors are also considered. Basically, these following expressions are assumed:

$$\eta_r^{L+1,K} \approx S_r (\Delta t)^2 \tag{115}$$

$$\eta_v^{L+1,K} \approx S_v \Delta t, \tag{116}$$

$$\eta_\omega^{L+1,K} \approx S_\omega \Delta t, \tag{117}$$

where S_r, S_v and S_ω are constants. The error resulted within an iteration is according to

$$\left[S_r (\Delta t_r)^2\right]^K \boldsymbol{\varpi}_{i,r}^{L+1,0} = \boldsymbol{\varpi}_{i,r}^{L+1,K} \tag{118}$$

$$(S_v \Delta t_v)^K \boldsymbol{\varpi}_{i,v}^{L+1,0} = \boldsymbol{\varpi}_{i,v}^{L+1,K}. \tag{119}$$

$$(S_\omega \Delta t_\omega)^K \boldsymbol{\varpi}_{i,\omega}^{L+1,0} = \boldsymbol{\varpi}_{i,\omega}^{L+1,K}. \tag{120}$$

where $\boldsymbol{\varpi}_{i,r}^{L+1,0} = \boldsymbol{r}_i^{L+1,K=1} - \boldsymbol{r}_i^{L}$, $\boldsymbol{\varpi}_{i,v}^{L+1,0} = \boldsymbol{v}_i^{L+1,K=1} - \boldsymbol{v}_i^{L}$ and $\boldsymbol{\varpi}_{i,\omega}^{L+1,0} = \boldsymbol{\omega}_i^{L+1,K=1} - \boldsymbol{\omega}_i^{L}$. These above equations can be rewritten as

$$\Delta t_r = \frac{1}{S_r^{\frac{1}{2}}} \left(\frac{\boldsymbol{\varpi}_{i,r}^{L+1,K}}{\boldsymbol{\varpi}_{i,r}^{L+1,0}} \right)^{\frac{1}{2K}}, \tag{121}$$

$$\Delta t_v = \frac{1}{S_v} \left(\frac{\boldsymbol{\varpi}_{i,v}^{L+1,K}}{\boldsymbol{\varpi}_{i,v}^{L+1,0}} \right)^{\frac{1}{K}}, \tag{122}$$

$$\Delta t_\omega = \frac{1}{S_\omega} \left(\frac{\boldsymbol{\varpi}_{i,\omega}^{L+1,K}}{\boldsymbol{\varpi}_{i,\omega}^{L+1,0}} \right)^{\frac{1}{K}}. \tag{123}$$

According to Zohdi in [36], at the end of the time-step iteration, $\boldsymbol{\varpi}_{i,r}^{L+1,K} = TOL_r$, $\boldsymbol{\varpi}_{i,v}^{L+1,K} = TOL_v$ and $\boldsymbol{\varpi}_{i,\omega}^{L+1,K} = TOL_\omega$, where TOL_r, TOL_v and TOL_ω are tolerances for the position and velocity vectors, respectively. So, assuming that S_r, S_v and S_ω are constants, a new smaller step size can be defined as

$$\Delta t_{tol} = \Delta t \cdot min \left\{ \underbrace{\left[\frac{\left(\frac{TOL_r}{\boldsymbol{\varpi}_{i,r}^{L+1,0}} \right)^{\frac{1}{2K_d}}}{\left(\frac{\boldsymbol{\varpi}_{i,r}^{L+1,K}}{\boldsymbol{\varpi}_{i,r}^{L+1,0}} \right)^{\frac{1}{2K}}} \right]}_{=^{\text{def}} \Lambda_{K,r}} ; \underbrace{\left[\frac{\left(\frac{TOL_v}{\boldsymbol{\varpi}_{i,v}^{L+1,0}} \right)^{\frac{1}{2K_d}}}{\left(\frac{\boldsymbol{\varpi}_{i,v}^{L+1,K}}{\boldsymbol{\varpi}_{i,v}^{L+1,0}} \right)^{\frac{1}{2K}}} \right]}_{=^{\text{def}} \Lambda_{K,v}} ; \underbrace{\left[\frac{\left(\frac{TOL_\omega}{\boldsymbol{\varpi}_{i,\omega}^{L+1,0}} \right)^{\frac{1}{2K_d}}}{\left(\frac{\boldsymbol{\varpi}_{i,\omega}^{L+1,K}}{\boldsymbol{\varpi}_{i,\omega}^{L+1,0}} \right)^{\frac{1}{2K}}} \right]}_{=^{\text{def}} \Lambda_{K,\omega}} \right\}$$

$$= \Delta t \cdot \underbrace{min(\Lambda_{K,r}; \Lambda_{K,v}; \Lambda_{K,\omega})}_{\Lambda_K} = \Delta t \cdot \Lambda_K, \tag{124}$$

where K_d is the number of desired iterations. According to Zohdi in [36], the expression in (124) can also be used for time-step enlargement, if convergence is met in less than K_d iterations, usually chosen to be between 5 to 10 iterations.

A geometrical interpretation about the iteration within the time step (parameter K) is shown in Fig. 10.

4.4 Time integration scheme for solution of the system's dynamics

The numerical solution scheme is shown on Table 1. This numerical algorithm is adapted from [35, 36]. Here the rolling phenomenon is taken into account.

Table 1 Algorithm: Numerical solution scheme

Iterative implicit solution method		
Step 1	Start a global fixed iteration and set the iteration counter $K = 0$. Store the variables: $\boldsymbol{r}_i^L\left(\boldsymbol{r}_i^{L+1,0}\right)$, $\boldsymbol{v}_i^L\left(\boldsymbol{v}_i^{L+1,0}\right)$, $\boldsymbol{\theta}_i^L\left(\boldsymbol{\theta}_i^{L+1,0}\right)$ and $\boldsymbol{\omega}_i^L\left(\boldsymbol{\omega}_i^{L+1,0}\right)$. Compute the total force: $\mathbf{F}_i^{tot,L}\left(\boldsymbol{r}_i^L, \boldsymbol{v}_i^L, \boldsymbol{\omega}_i^L\right)$. Compute the total momentum: $\boldsymbol{M}_i^{tot,L}\left(\boldsymbol{r}_i^L, \boldsymbol{v}_i^L, \boldsymbol{\omega}_i^L\right)$ Update the iteration counter $K = K + 1$.	
Step 2	Make a loop from $i = 1$ to $i = N_p$ and compute for each particle i: Resultant load vectors $\mathbf{F}_i^{tot,L+1,K-1}\left(\boldsymbol{r}_i^{L+1,K-1}, \boldsymbol{v}_i^{L+1,K-1}, \boldsymbol{\omega}_i^{L+1,K-1}\right)$, Resultant momentum vector $\mathbf{M}_i^{tot,L+1,K-1}\left(\boldsymbol{r}_i^{L+1,K-1}, \boldsymbol{v}_i^{L+1,K-1}, \boldsymbol{\omega}_i^{L+1,K-1}\right)$, Position vector $\boldsymbol{r}_i^{L+1,K} = \mathcal{G}_r\left(\boldsymbol{r}_i^{L+1,K-1}\right) + \mathcal{R}_{i,r} = \boldsymbol{r}_i^L + \boldsymbol{v}_i^L \Delta t + \frac{\phi(\Delta t)^2}{m_i}\left[\phi \mathbf{F}_i^{tot,L+1,K-1} + (1-\phi)\mathbf{F}_i^{tot,L}\right]$, Velocity vector $\boldsymbol{v}_i^{L+1,K} = \mathcal{G}_v\left(\boldsymbol{v}_i^{L+1,K-1}\right) + \mathcal{R}_{i,v} = \boldsymbol{v}_i^L + \frac{\Delta t}{m_i}\left[\phi \mathbf{F}_i^{tot,L+1,K-1} + (1-\phi)\mathbf{F}_i^{tot,L}\right]$, Angular velocity vector: $\boldsymbol{\omega}_i^{L+1,K} = \boldsymbol{\omega}_i^L + \frac{\Delta t}{\bar{I}_{i,s}}\left[\varnothing \boldsymbol{M}_i^{tot,L+1,K-1} + (1-\varnothing)\boldsymbol{M}_i^{tot,L}\right]$, Rotation vector: $\boldsymbol{\theta}_i^{L+1,K} = \boldsymbol{\theta}_i^L + \Delta t\left[\varnothing \boldsymbol{\omega}_i^{L+1,K-1} + (1-\varnothing)\boldsymbol{\omega}_i^L\right]$.	
Step 3	Measure normalized error quantities: $\boldsymbol{\varpi}_{K,r} \overset{\text{def}}{=} \frac{\sum_{i=1}^{N_p}\left\|\boldsymbol{r}_i^{L+1,K} - \boldsymbol{r}_i^{L+1,K-1}\right\|}{\sum_{i=1}^{N_p}\left\|\boldsymbol{r}_i^{L+1,K} - \boldsymbol{r}_i^{L}\right\|}$ $\boldsymbol{\varpi}_{K,v} \overset{\text{def}}{=} \frac{\sum_{i=1}^{N_p}\left\|\boldsymbol{v}_i^{L+1,K} - \boldsymbol{v}_i^{L+1,K-1}\right\|}{\sum_{i=1}^{N_p}\left\|\boldsymbol{v}_i^{L+1,K} - \boldsymbol{v}_i^{L}\right\|}$ $\boldsymbol{\varpi}_{K,\omega} \overset{\text{def}}{=} \frac{\sum_{i=1}^{N_p}\left\|\boldsymbol{\omega}_i^{L+1,K} - \boldsymbol{\omega}_i^{L+1,K-1}\right\|}{\sum_{i=1}^{N_p}\left\|\boldsymbol{\omega}_i^{L+1,K} - \boldsymbol{\omega}_i^{L}\right\|}$ $Z_{k,r} \overset{\text{def}}{=} \frac{\boldsymbol{\varpi}_{K,r}}{TOL_r}$ $Z_{k,v} \overset{\text{def}}{=} \frac{\boldsymbol{\varpi}_{K,v}}{TOL_v}$ $Z_{k,\omega} \overset{\text{def}}{=} \frac{\boldsymbol{\varpi}_{K,\omega}}{TOL_\omega}$ $\Lambda_{K,r} \overset{\text{def}}{=} \frac{\left(\frac{TOL_r}{\boldsymbol{\varpi}_{0,r}}\right)^{\frac{1}{2K_d}}}{\left(\frac{\boldsymbol{\varpi}_{K,r}}{\boldsymbol{\varpi}_{0,r}}\right)^{\frac{1}{2K}}}$ $\Lambda_{K,v} \overset{\text{def}}{=} \frac{\left(\frac{TOL_v}{\boldsymbol{\varpi}_{0,v}}\right)^{\frac{1}{2K_d}}}{\left(\frac{\boldsymbol{\varpi}_{K,v}}{\boldsymbol{\varpi}_{0,v}}\right)^{\frac{1}{2K}}}$ $\Lambda_{K,\omega} \overset{\text{def}}{=} \frac{\left(\frac{TOL_\omega}{\boldsymbol{\varpi}_{0,\omega}}\right)^{\frac{1}{2K_d}}}{\left(\frac{\boldsymbol{\varpi}_{K,\omega}}{\boldsymbol{\varpi}_{0,\omega}}\right)^{\frac{1}{2K}}}$	
Step 4	IF	$\left(Z_{k,r} \leq 1\ AND\ Z_{k,v} \leq 1\ AND\ Z_{k,\omega} \leq 1\right)\ AND\ K \leq K_d$
	THEN	Increment time: $t = t + \Delta t$, Construct the next time step: $(\Delta t)^{new} = \Lambda_K (\Delta t)^{old}$, where $\Lambda_K = min\left[\Lambda_{K,r}, \Lambda_{K,v}, \Lambda_{K,\omega}\right]$, Select the minimum size: $\Delta t = min\left[(\Delta t)^{lim}, (\Delta t)^{new}\right]$, Go to step 1
	ELSE	go to step 5
Step 5	IF	$\left(Z_{k,r} > 1\ OR\ Z_{k,v} > 1\ OR\ Z_{k,\omega} > 1\right)\ AND\ K < K_d$
	THEN	Update the iteration counter: $K = K + 1$, Go to step 2
	ELSE	go to step 6
Step 6	IF	$\left(Z_{k,r} > 1\ OR\ Z_{k,v} > 1\ OR\ Z_{k,\omega} > 1\right)\ AND\ K = K_d$
	THEN	Construct a next time step: $(\Delta t)^{new} = \Lambda_K (\Delta t)^{old}$, where $\Lambda_K = min\left[\Lambda_{K,r}, \Lambda_{K,v}, \Lambda_{K,\omega}\right]$, Select the minimum size: $\Delta t = min\left[(\Delta t)^{lim}, (\Delta t)^{new}\right]$, Restart at time t: Set $\boldsymbol{r}_i^{L+1,0} = \boldsymbol{r}_i^L$, $\boldsymbol{v}_i^{L+1,0} = \boldsymbol{v}_i^L$ and $\boldsymbol{\omega}_i^{L+1,0} = \boldsymbol{\omega}_i^L$, Go to step 1
	ELSE	Set a larger number for the variable K_d, Restart at time t: Set $\boldsymbol{r}_i^{L+1,0} = \boldsymbol{r}_i^L$, $\boldsymbol{v}_i^{L+1,0} = \boldsymbol{v}_i^L$ and $\boldsymbol{\omega}_i^{L+1,0} = \boldsymbol{\omega}_i^L$, Go to step 1

5 Contact search procedures

The efficiency of a program is measured directly by its computational cost. Therefore, it is fundamental that every calculation program has in its code an optimization algorithm that can solve any model, requiring the least calculation time possible. In particle method, the process that has a greater computational cost is the detection of the contact between particles. This occurs because it is necessary to check for contact of each particle against all the other particles and walls in the system, making the modeling of large scale problems difficult. Problems simulated by the discrete element method usually involve a large number of particles in possible contact. For each time increment, usually very small,

one must check all these contact possibilities and calculate the respective forces involved in this phenomenon, which requires a high computational cost. The imminent problem is the spent time on this search. To minimize, as much as possible, the analysis time in multi-scale problems, it is necessary to develop an efficient contact search algorithm. Basically, in this work, the solution found was to divide the tridimensional domain in several subspaces. Each particle will be addressed to a corresponding subspace based on its current position. In this way, for the currently analyzed particle, only the particles belonging to its subdomain and the adjacent ones will be selected to make the contact verification. Thus, the contact search for each individual particle involves a significantly reduced number of particles to be considered. This reduction decreases decisively the analysis time.

A method for contact detection developed and used in this research is based on the following considerations: (1) a volume defined by a hexahedron will be created to limit the possible coordinates for the particles and walls during the analysis, i.e., the analysis only proceeds if all particles and walls have their coordinates located inside the admissible zone. This domain corresponds to a viable zone and it will be divided into squares (2D) or cubes (3D) with size equal to the diameter of the smallest particle, as shown in Fig. 11; (2) the maximum number of particles allowed per cube shall be established; and (3) a vector called $volume\_matrix$ will be generated with dimension equal to the total number of cubes necessary to make up the domain times the number of particles allowed by each cube (this vector will store the quantity and identity of the particles contained in each cube). The condition for a particle to belong to a cube is that the particle's center is located inside it. Subsequently, starting from the coordinates of the centers of the particles (x, y, z), the coordinates of the cube (l, m, n) containing it will be calculated, as shown in the following equation

$$l = \frac{current\ coord\ x - min\ coord\ allowed_x}{dimension\ of\ the\ cube}, \tag{125}$$

filling the vector $volume\_matrix$. The Eq. (125) regards the x direction and an analogous expression can be used to calculate the parameters m and n. In addition, a vector of size equal to the total number of particles will be created and filled, which will store their location, i.e., the number of the cube containing each particle.

As mentioned, the optimization process is applied in the algorithm for contact detection. For this, one must calculate the dimensions of the subdomain for contact search. This subdomain will correspond to the cube containing the particle i under study and the neighboring cubes that contain the particles in possible contact, as shown in Fig. 12. For plane problems, this subdomain is composed by at least 9 squares and for spatial problems by 27 cubes.

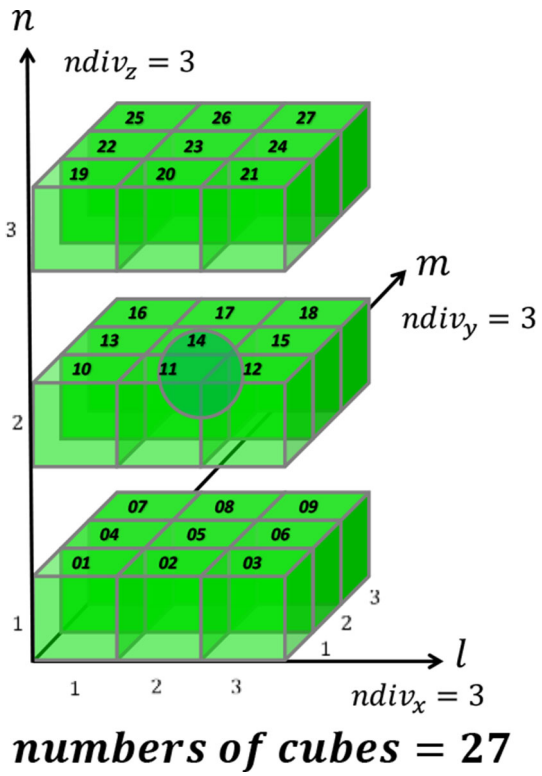

Fig. 11 3D domain's division and the corresponding number of cubes in the domain's discretization

To obtain the dimensions of the subdomain one must calculate a $delta$ value, as shown in equation below

$$delta = \frac{particle's\ diameter\ i + particle's\ highest\ diameter}{2\ *\ dimension\ of\ the\ cube}. \tag{126}$$

Once $delta$ is calculated, the cubes that will compose the subdomain for contact verification are selected. This subdomain contains the cubes with indices comprised by the intervals $[(l - delta), (l + delta)]$, $[(m - delta), (m + delta)]$ and $[(n - delta), (n + delta)]$, as illustrated in Fig. 12.

The general mapping is performed only once, after each time increment (or after a defined time). If there is a position update in any of the particles and it exceeds the limits of the cube that contains it, the particle will be removed from this initial cube and placed in the cube corresponding to the current position, as a consequence, the vector $volume\_matrix$ is updated.

For each particle i, the number of the cube containing it is determined. Then, the neighboring cubes are selected, see Fig. 12 for a graphical interpretation. All particles contained in these cubes are selected to verify the contact with the analyzed particle.

Finally, after the optimization algorithm is finished and all contacts are defined, the calculation of the forces acting on each particle is executed.

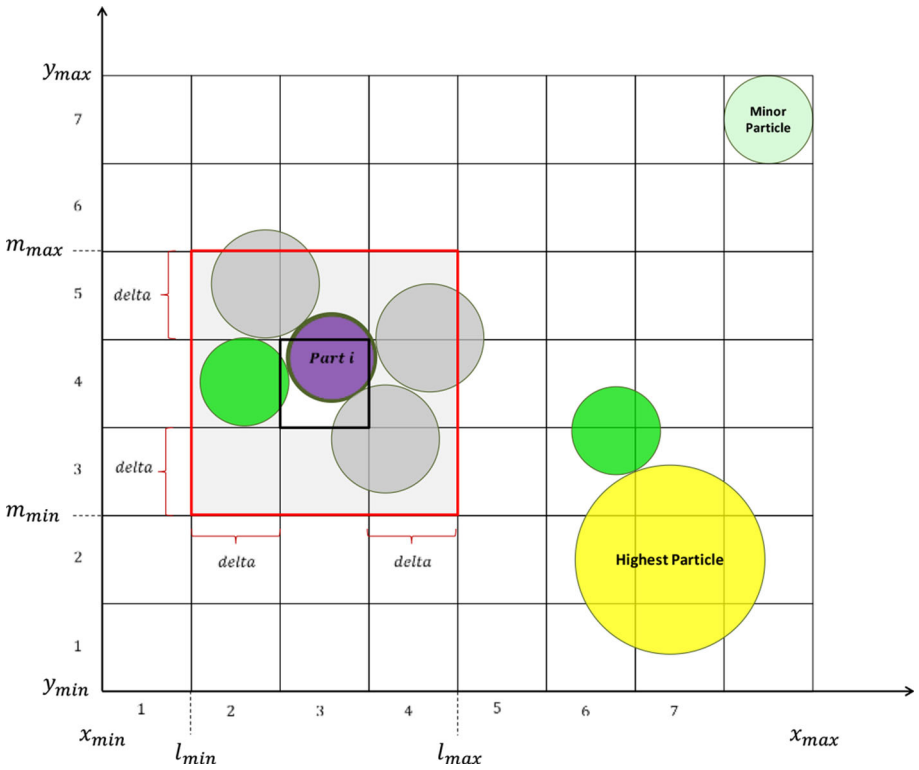

Fig. 12 Subdomain's definition. The subdomain for each particle corresponds to the red square on the figure

The same procedures are made for the contacts between particles and walls. Basically, in each time step, each particle will belong to a specific cube and this will have associated vectors that will store the probable particles and walls that can come in contact with the studied particle. Updating all information per cube is done instantly during the process. The most important procedures are described in the algorithm presented in Table 14 in Appendix D.

Another important fact to be mentioned is the importance of using parallel processing. This can be used both to update the information for the contact search algorithm and for the analysis processing. Parallel processing demonstrated a significant reduction in analysis time.

The contact between a particle and wall can be calculated in two ways. The first is to consider the contact between flat surfaces and the other through smooth surfaces. Contact with flat surfaces requires much knowledge about spatial geometry to find the contact point at the intersection between the wall and the particle's surface. This one was used in all examples in this article. Contact with smooth surfaces requires using the NURBS method. The two ways of calculating the contact point would require a standalone article and therefore will not be presented in this work.

Also, information on parallel processing and spatial geometry will not be presented, since they are not the purpose of this paper. For more information see [8, 9].

6 Validation problems

The basic aim of this section is to apply all theories and algorithms presented in this paper to simulate some known classical physics examples. With this, it is possible to understand the concepts and magnitude of the parameters involved in these formulations and to verify if the proposed algorithm works correctly. In all examples the numerical and analytical solutions will be compared.

In this section, three examples are presented. The first one refers to an oblique impact between a sphere and a flat surface. It allows the validation of the efficiency of Coulomb's friction law and its influence on the angular velocities after impact. The second example refers to the slipping and rolling of a sphere on an inclined plane. And the last example is a specific case of the second one, i.e., the slipping and rolling of a sphere on a horizontal plane. All examples test the Coulomb's friction law and are intended to compare the analytical and numerical results in terms of displacements, velocities and angular velocities.

6.1 Oblique impact of elastoplastic spheres

This section consists of a study of an oblique impact of elastoplastic spheres as shown in Fig. 13. The analytical solution is presented in detail in Appendix A.

For example, consider a solid sphere with radii $R = 0.05$ m with an impact angle $\theta_i = 45°$, the initial impact speed $v_i = \sqrt{2}$ m/s and particle spin $\omega_i = 0$, the normal coef-

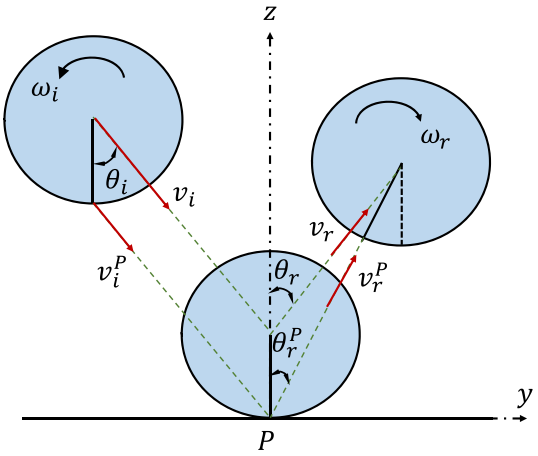

Fig. 13 Diagram of the oblique impact of a sphere with a plane surface (Reproduced with permission from [48])

ficient of restitution $e_n = 1$ and the impulse ratio $f = 0.05$. Here the impulse ratio is considered to be the same as the friction coefficient. The tangential coefficient of restitution is calculated from (146):

$$e_\tau = 1 - 0.05\frac{(1+1.00)}{tan(45°)} = 0.9. \tag{127}$$

The rebound rotational angular velocity is calculated by Eq. (153):

$$\omega_r = 0 - \frac{5 \cdot 0.05 \cdot (1+1) \cdot \sqrt{2} \cdot cos(45°)}{2 \cdot 0.05} = -5\,\text{rad/s}\,. \tag{128}$$

The tangential component of the impact velocity at the contact patch is calculated by

$$v_{i,\tau}^P = v_{i,\tau} + R\omega_i = \sqrt{2} \cdot sin\left(45°\right) + 0.05 \cdot 0 = 1\,\text{m/s}\,. \tag{129}$$

The tangential component of the rebound surface velocity at the contact patch is calculated by Eq. (159):

$$v_{r,\tau}^P = 1 - \frac{7}{2} \cdot 0.05 \cdot (1+1) \cdot \sqrt{2} \cdot cos\left(45°\right) = 0.65\,\text{m/s}\,. \tag{130}$$

The tangential component of the rebound velocity can be calculated by Eq. (154):

$$v_{r,\tau} = v_{r,\tau}^P - R\omega_r = 0.65 - 0.05 \cdot (-5) = 0.9\,\text{m/s}\,. \tag{131}$$

The rebound angle θ_r is calculated by Eq. (164):

$$tan(\theta_r) = -\frac{0.9}{1} tan\left(45°\right) = -0.9 \Rightarrow \theta_r \approx -41.987^\circ. \tag{132}$$

The rebound velocity is calculated by

$$v_r = \frac{v_{r,\tau}}{sin(\theta_r)} = \frac{0.9}{sin\left(41.987^\circ\right)} \approx 1.345\,\text{m/s}\,. \tag{133}$$

And the normal component of the rebound velocity can be calculated by

$$v_{r,n} = v_r cos(\theta_r) = 1.345 \cdot cos\left(41.987^\circ\right) \approx 1.000\,\text{m/s}\,. \tag{134}$$

Basically, in this analytical example, a perfect oblique impact was considered between a solid sphere with radii $R = 0.05\,\text{m}$ with a rigid wall with impact velocity $\boldsymbol{v}_i = (1; -1; 0)\,\text{m/s}$ and impact spin $\boldsymbol{\omega}_i = (0; 0; 0)\,\text{rad/s}$. The analytical solution, as presented before, leads to the rebound velocity $\boldsymbol{v}_r = (0.9; 1; 0)\,\text{m/s}$ and rebound spin $\boldsymbol{\omega}_r = (0; 0; -5)\,\text{rad/s}$.

This problem was also simulated by using the DEM formulation presented in this article despite the contact model being based on the Hertzian formulation. For this purpose, the following values are considered: radii of the sphere $R = 0.05\,\text{m}$, initial velocity $\boldsymbol{v}_i = (1; -1; 0)\,\text{m/s}$, initial spin $\boldsymbol{\omega}_i = (0; 0; 0)\,\text{rad/s}$, specific mass $\rho = 5000\,\text{kg/m}^3$, elasticity modulus of the sphere $E = 10^8\,\text{N/m}^2$, Poisson coefficient $\nu = 0.25$, static friction coefficient $\mu_s = 0.05$, dynamic friction coefficient $\mu_d = 0.05$, friction constant parameter $K_f = 10^{15}$, maximum permissible iterations $K_d = 10$, fully implicit Euler integration scheme ($\varnothing = 1$), tolerances $TOL_r = 10^{-3}$, $TOL_v = 10^{-3}$, $TOL_w = 10^{-3}$ and no contributions of external forces, like gravity, damping, bonding and environment effects (i.e., all respectively parameters were considered to be zero). It is clear that the geometry of this problem does not need to be given, since it can be easily adopted. To develop a quick simulation, the suggestion is that the sphere should be located next to the wall, practically an instant before the impact. The numerical simulation was done for three sizes of time increment, i.e., $\Delta t = 10^{-4}\,\text{s}$, $\Delta t = 10^{-5}\,\text{s}$ and $\Delta t = 10^{-6}\,\text{s}$. After simulation, all numerical results lie to the same analytical results. The maximum iteration in each time increment was $K = 3$. The numerical results for the increment of time $\Delta t = 10^{-4}\,\text{s}$ gives a rebound velocity $\boldsymbol{v}_r = (0.9; 1; 0)\,\text{m/s}$ and rebound spin $\boldsymbol{\omega}_r = (0; 0; -5)\,\text{rad/s}$.

6.2 Slipping and rolling of a sphere on an inclined plane

This section consists of a study of slipping and rolling of a sphere on an inclined plane as shown in Fig. 14. The analytical solution is presented in detail in Appendix B.

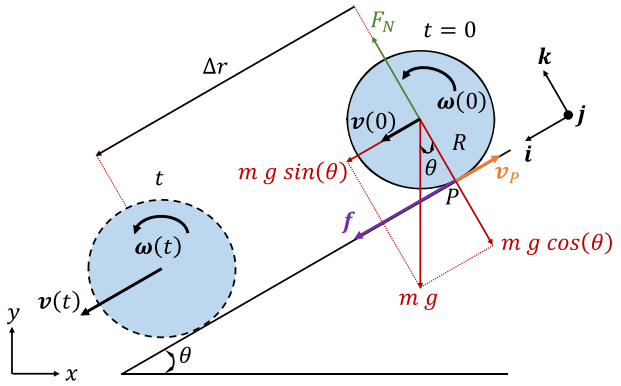

Fig. 14 Diagram of a particle slipping and rolling on an inclined plane

To make a comparison between the analytical and numerical solution, an appropriated example is needed. Consider, for the initial configuration, a solid sphere with radii $R = 0.25$ m placed on an inclined plane with angle $tan(\theta) = 0.75$. At this time, only a point of the sphere is in contact with the wall. The initial velocity is $\boldsymbol{v}(0) = (-6.08; -4.56; 0)$ m/s and initial spin is $\boldsymbol{\omega}(0) = (0; 0; 16)$ rad/s.

For the numerical simulation, consider the following additional values: specific mass $\rho = 5000\,\text{kg/m}^3$, elasticity modulus of the sphere $E = 10^9\,\text{N/m}^2$, Poisson coefficient $\nu = 0.25$, static friction coefficient $\mu_s = 0.20$, dynamic friction coefficient $\mu_d = 0.20$, friction constant parameter $K_f = 10^{15}$, maximum permissible iterations $K_d = 10$, gravity acceleration $\boldsymbol{g} = (0; -10; 0)\,\text{m/s}^2$, time increment $\Delta t = 10^{-3}$ s, fully implicit Euler integration scheme ($\varnothing = 1$), tolerances $TOL_r = 10^{-3}$, $TOL_v = 10^{-3}$ and $TOL_w = 10^{-3}$ and no additional contributions of external forces, like damping, bonding and environment effects (i.e., all respectively parameters were considered to be zero). It is clear that the additional information of geometry is not necessary to be presented. The maximum iteration in each time increment was $K = 3$.

The analysis is performed for 5 s. The numerical and analytical results in terms of displacements, velocities and angular velocities are shown in Fig. 15. These values correspond to the respective norm of the vector in direction parallel to the inclined plane.

For example, at time $t = 3.002$ s, the analytical results lie to displacement $\boldsymbol{r} = (-34.113; -25.585; 0)$ m, velocity $\boldsymbol{v} = (-16.647; -12.485; 0)$ m/s and spin $\boldsymbol{\omega} = (0; 0; 64.032)$ rad/s and the numerical results lie to displacement $\boldsymbol{r} = (-34.119; -25.589; 0)$ m, velocity $\boldsymbol{v} = (-16.628; -12.525; 0)$ m/s and spin $\boldsymbol{\omega} = (0; 0; 63.945)$ rad/s. Comparing the results in terms of displacement, velocity and angular velocity, it is possible to

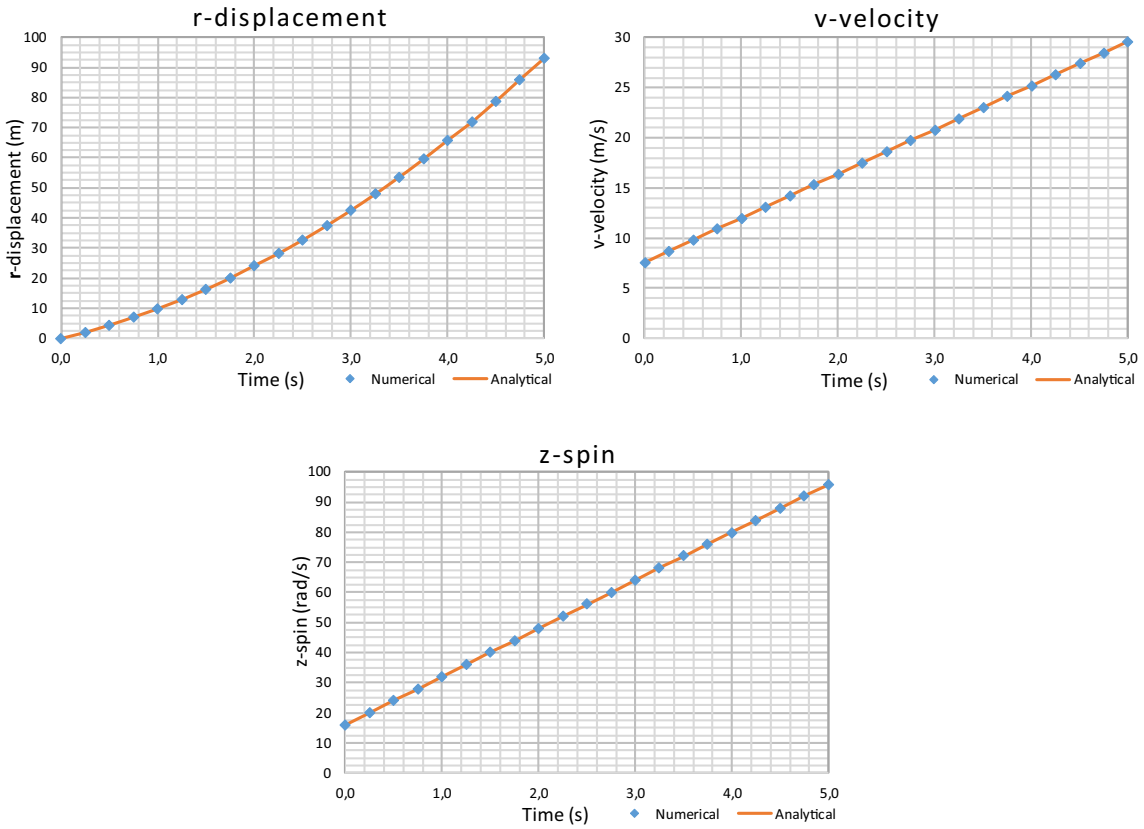

Fig. 15 Time histories of the particle's displacement, velocity and spin

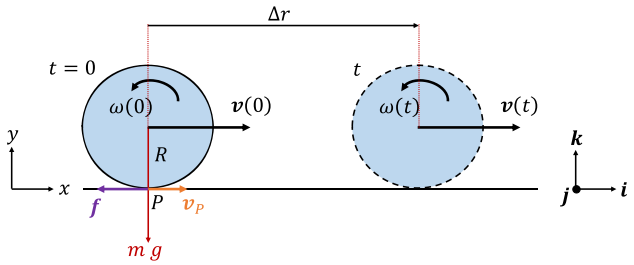

Fig. 16 Diagram of a sphere with a horizontal surface

affirm that the displacement obtained by numerical simulation is 100.02% of the analytical result, the velocity is 100.04% of the analytical one and the angular velocity is 99.86% of the analytical result. It is important to mention that the analytical solution will not be exactly the same as the results obtained by numerical simulations. One reason is that the Coulomb law is a function of the normal force and it is variable during the process, i.e., in Hertz model the normal force is a function of penetration and the stick and slip conditions are changing during the contact. The possibility of alternation between the stick and the slip case is expected from the physical point of view, especially at the contact point. So, always, when the stick case occurs at some moment, the skating will happen. It is inherent to the Coulomb's law. Hence, there will be micro-slips that will dissipate a little more energy than anticipated in analytical models.

6.3 Slipping and rolling of a sphere on a horizontal surface

The analytical solution for slipping and rolling of a sphere on a horizontal plane is a particular case of the previous section. Basically, the angle of the surface must be considered to be zero, i.e., $\theta = 0^{\circ}$. The same example was studied by Campello in [34] and will be presented here to be one more classical problem to validate particles programs (Fig. 16).

Consider, for the initial configuration, a solid sphere with radii $R = 0.20$ m placed on a horizontal plane. At this time, only a point of the sphere is in contact with the wall. The initial velocity is $\boldsymbol{v}(0) = (2.355; 0; 0)$ m/s and initial spin is $\boldsymbol{\omega}(0) = (0; 0; -127.03)$ rad/s.

For the numerical simulation, consider the following additional values: specific mass $\rho = 5000\,\text{kg/m}^3$, elasticity modulus of the sphere $E = 10^{10}\,\text{N/m}^2$, Poisson coefficient $\nu = 0.25$, static friction coefficient $\mu_s = 0.25$, dynamic friction coefficient $\mu_d = 0.25$, friction constant parameter $K_f = 10^{15}$, maximum permissible iterations $K_d = 10$, gravity acceleration $\boldsymbol{g} = (0; -9.81; 0)\,\text{m/s}^2$, time increment $\Delta t = 10^{-4}$ s, fully implicit Euler integration scheme ($\varnothing = 1$), tolerances $TOL_r = 10^{-3}$, $TOL_v = 10^{-3}$ and $TOL_w = 10^{-3}$ and no additional contributions of external forces, like damping, bonding and environment effects (i.e., all respectively parameters were considered to be zero). Again, additional information of geometry is not needed. The maximum iteration in each time increment was $K = 3$.

The analysis is performed for 5 s. The numerical and analytical results in terms of displacements, velocities and angular velocities are shown in Fig. 17. These values correspond to the respective norm of the vector in direction parallel to the inclined plane.

For example, at time $t = 3$ s, the analytical results lie to displacement $\boldsymbol{r} = (17.939; 0; 0)$ m, velocity $\boldsymbol{v} = (8.941; 0; 0)$ m/s and spin $\boldsymbol{\omega} = (0; 0; -44.705)$ rad/s and the numerical results lie to displacement $\boldsymbol{r} = (17.982; ; 0)$ m, velocity $\boldsymbol{v} = (8.941; 0; 0)$ m/s and spin $\boldsymbol{\omega} = (0; 0; -44.705)$ rad/s. Comparing the results in terms of displacement, velocity and angular velocity, is possible to affirm that the displacement obtained by numerical simulation is 100.24% of the analytical result, the velocity is 100.00% of the analytical one and the angular velocity is 100.00% of the analytical result.

Observing the velocity and spin in Fig. 17, it is possible to conclude that the horizontal line corresponds to the stick case. So, in that time the relative velocity at the contact point goes to zero and as consequence, the friction force also goes to zero, see Eq. (181). The corresponding time of the beginning of stick case can be determined substituting the equations from (178) to (182) into (168). Considering that this problem has the motion in only one direction, the Eq. (178) can be rewritten as

$$v_0 + \frac{1}{m}\Delta t f + \omega_0 R + \frac{R^2}{I}\Delta t f = 0. \tag{135}$$

From above equation the corresponding time to start the stick case is calculated by

$$\begin{aligned}\Delta t &= -\frac{(v_0 + \omega_0 R)}{f\left(\frac{1}{m} + \frac{R^2}{I}\right)} \\ &= -\frac{2\,(v_0 + \omega_0 R)}{7\,\mu g} \\ &= -\frac{2\,[2.355 + (-127.03)\cdot 0.2]}{7 \cdot 0.25 \cdot 9.81} \\ &= 2.685\,\text{s}.\end{aligned} \tag{136}$$

At $t = 0$ s the velocity at contact point is $v_P = 2.355 + (-127.03)\cdot 0.2 = -23.051$ m/s. Since the friction force is opposed to the direction of this velocity, the magnitude of v_P will decrease progressively until it reaches zero. When this occurs, the relative motion between the contact point P and the flat surface stops, meaning that sliding no longer occurs and the particle starts to have pure rolling.

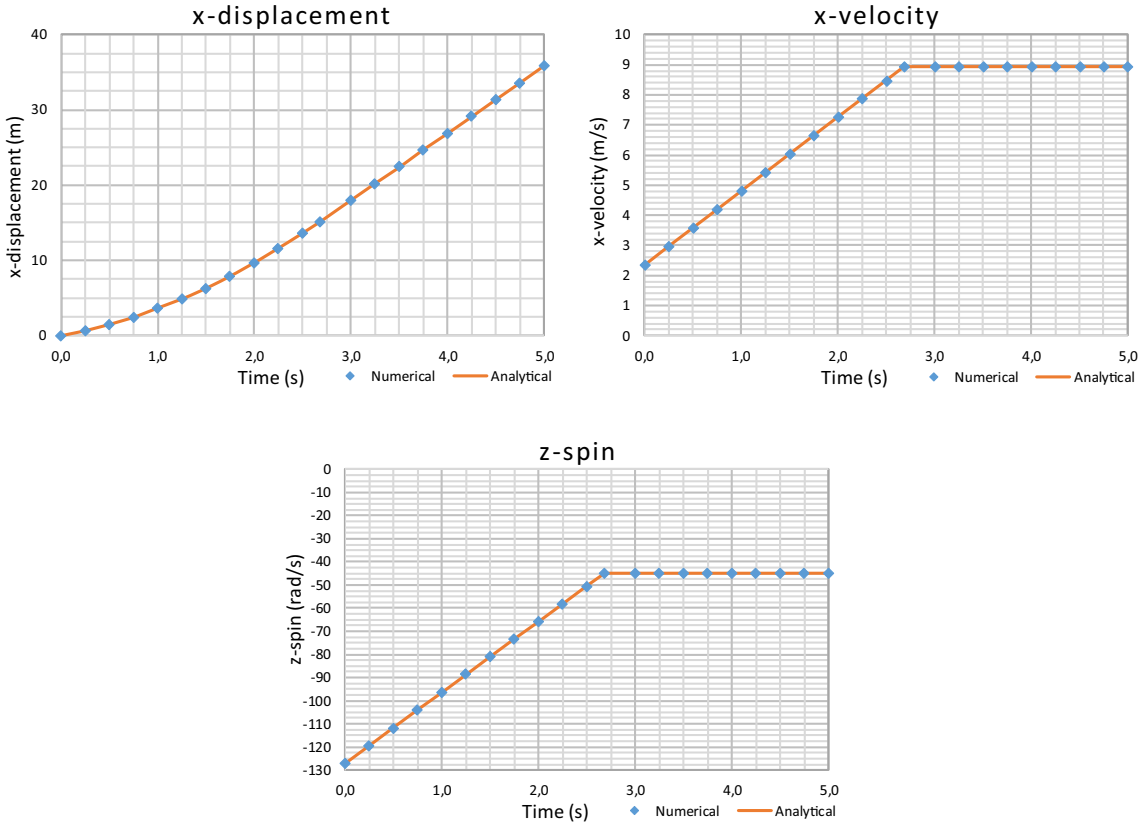

Fig. 17 Time histories of the particle's displacement, velocity and spin

7 Numerical simulation

The main objective of this section is to present three numerical examples of granular materials to apply the algorithm studied in this work. The first example consists of studying the drop of 180 particles in a container. The second and third examples consist of a simulation of an unloading of granular materials from one upper container to the other lower. The difference between these two examples lies in the geometry of the upper container and the number of particles used to discretize the granular material. The second and third examples have 40 and 3100 particles, respectively.

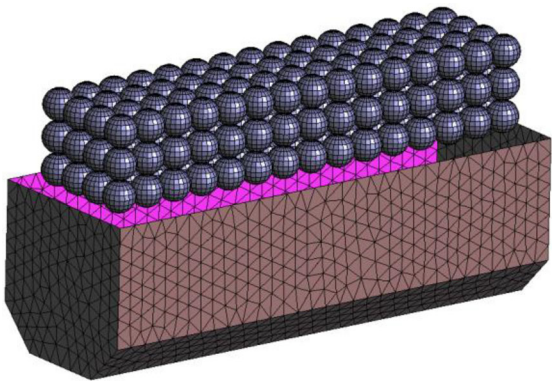

Fig. 18 Example 1: problem definition

7.1 Example 1: Free falling granular material

The basic aim of this section is to analyze the efficiency of the numerical algorithm to solve particles problems. This specific example consists to model the mechanical behavior of granular materials when they are thrown into a dumpster, see Fig. 18. In this model, the walls are assumed to be rigid. The geometry of this problem is presented in Fig. 19.

This model consists of 180 particles placed as shown in Fig. 19. All particle parameters are presented in Table 2. The materials properties of the walls are the same as the particles.

This example was simulated for three different values for the parameter $\varnothing$, i.e., referring to the explicit ($\varnothing \approx 0$), semi-implicit ($\varnothing = 0.5$) and fully implicit Euler integration scheme ($\varnothing = 1$). After the numerical simulation some equilibrium configurations are shown in Fig. 20. All particles are completely stopped at time $t = 1.52$ s.

In this specific example, all particles are located very close to each other, so there aren't much free spaces for mobility. The numerical analysis demonstrated that the final results obtained for each integration parameter $\varnothing$ are exactly

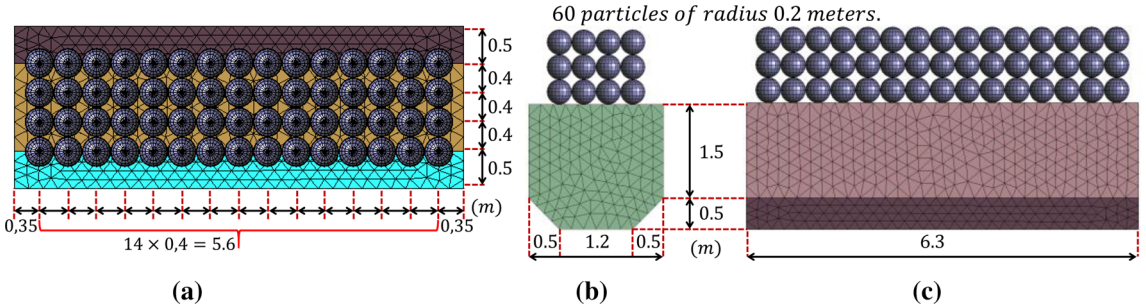

Fig. 19 Geometrical dimensions of the problem definition

Table 2 Numerical parameters of example 1

Particles
Particles radii $R = 0.2$ m
Specific mass $\rho = 7850\,\text{kg/m}^3$
Elasticity modulus of the spheres $E = 10^9\,\text{N/m}^2$
Poisson coefficient $\nu = 0.25$
Static friction coefficient $\mu_s = 0.20$
Dynamic friction coefficient $\mu_d = 0.20$
Friction constant parameter $K_f = 10^{15}$
Damping coefficient $\xi = 0.90$
Normalized deformation $\mathcal{E}^* = 0.04$
Bonding constant $K_{ij}^{nb} = 10^6$
Rotational bonding constant $K_{ij}^{rb} = 10^3$
Material parameter $P_p = 2.0$.
Analysis parameters
Maximum permissible iterations $K_d = 8$
Gravity acceleration $\boldsymbol{g} = (0; 0; -9.81)\,\text{m/s}^2$
Time increment $\Delta t = 5 \cdot 10^{-6}$ s
Euler integration scheme $\varnothing \approx 0$; $\varnothing = 0.5$ and $\varnothing = 1$
Tolerances $TOL_r = 10^{-3}$, $TOL_v = 10^{-3}$, $TOL_w = 10^{-3}$
Dynamic viscosity of the air $c^e = 0.00265$
Local average velocity of the external interstitial medium is $\boldsymbol{v}^e = 0$

the same. Regarding the numerical computing time, it is noticed that the explicit method is considerably faster than the implicit one. It was verified that the explicit method solved the problem with an analysis time approximately 40% smaller than the implicit one and 17% smaller than the semi-implicit method. In this case, it is better to use the explicit method because it is faster and the results are basically the same. The numerical results (regarding positions, velocities and angular velocities) of two selected particles are presented in Tables 5, 6 and 7, respectively, in the Appendix C.1.

7.2 Example 2: Unloading granular material discretized by 40 particles

The interesting issue of this section is to provide a simple 3D example to make a comparison of an implicit and explicit time integration scheme and see what is most efficient and if the results are the same. For this purpose, a simple example of forty particles is presented as shown in Fig. 21. The particle distribution is shown in Fig. 22.

This example, unlike the previous one, allows the particles to move with greater freedom, being able to actually verify if there is a difference between the integration schemes. To make this comparison, the numerical analysis is performed for 8 s of simulation equivalent to the real time. The particles and analysis parameters are presented in Table 3. The materials properties of the walls are the same as the particles.

Three different values for integration parameters are used to simulate this problem, i.e., referring to the explicit ($\varnothing \approx 0$), semi-implicit ($\varnothing = 0.5$) and fully implicit Euler integration scheme ($\varnothing = 1$).

First, the obtained results will be analyzed to verify if they are the same when different values for the parameter $\varnothing$ are used. The numerical results are compared for three different times (2, 4, 8 s). The particle configurations for each integration parameter are illustrated in Fig. 23.

For each defined time and for each integration parameter ($\varnothing$) the current configuration is given, see Fig. 23. Notice that three particles are selected and highlighted with different colors to compare their position at each time. Observing the configurations of the particles, it is noticed that the results are not the same when different values of $\varnothing$ are used. By observing the kinematic of the particles in the upper container, one notices that its movement is restricted by the sidewalls. In this way, the movement of these particles are practically the same when they are inside the upper container. However, when they are practically outside the upper container, there are small variations in the values of displacements, velocities and angular velocities for different values of $\varnothing$, which significantly modify the forces acting on the particles when they are located outside the upper container, since there is freedom of movement. So, it is possible to conclude that, in general, the results can be changed when different values are used for the parameter $\varnothing$, especially in tridimensional problems.

Analyzing the numerical computing time, it is noticed that the explicit method is considerably faster than the implicit one. It was verified that the explicit method solved the prob-

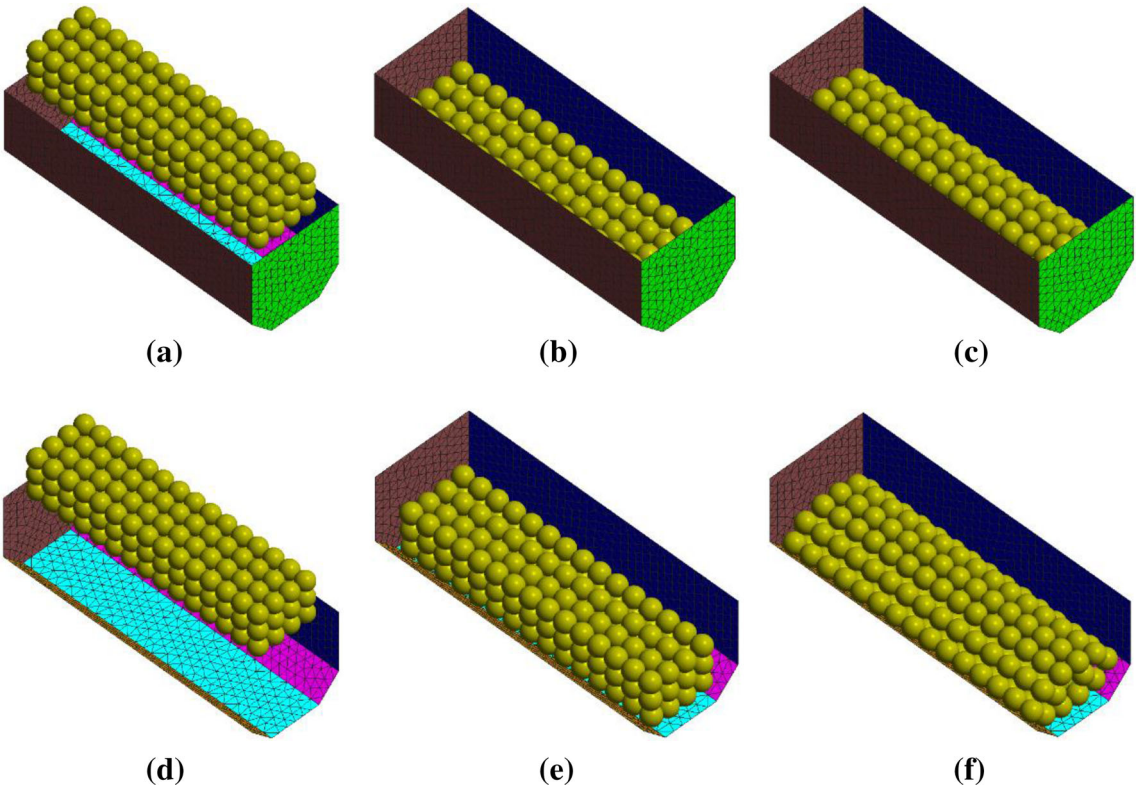

Fig. 20 Equilibrium configuration during the numerical simulation. **a** Time $t = 0$ s, **b** time $t = 0.64$ s, **c** time $t = 0.1.52$ s, **d** time $t = 0$ s, **e** time $t = 0.64$ s, **f** time $t = 1.52$ s

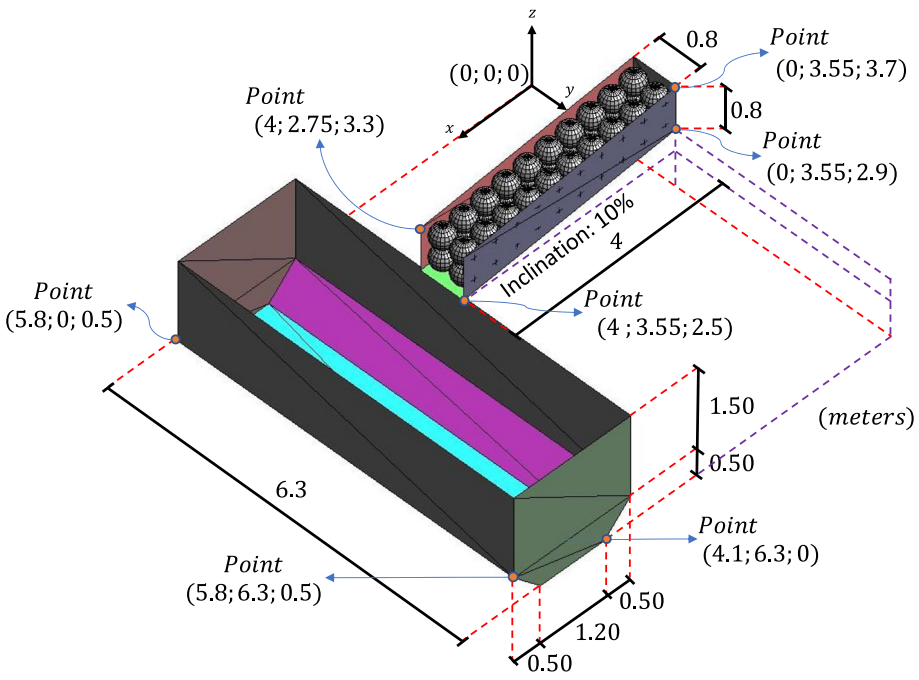

Fig. 21 Example 2: problem definition

lem with an analysis time approximately 41% smaller than the implicit one and 25% smaller than the semi-implicit method. However, it is difficult to say which method results in values closer to the real phenomenon, since all results obtained correspond to behaviors consistent with physical reality.

The numerical results (regarding positions, velocities and angular velocities) of the three selected particles are pre-

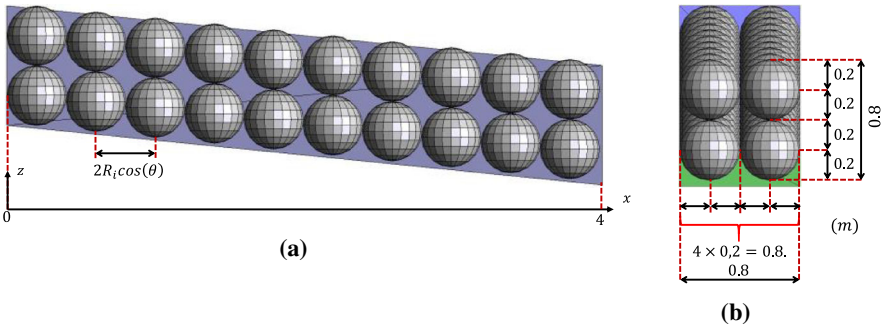

Fig. 22 Example 2: particles distribution

Table 3 Numerical parameters of example 2

Particles
Particles radii $R = 0.2$ m
Specific mass $\rho = 2500\,\text{kg/m}^3$
Elasticity modulus of the spheres $E = 10^9\,\text{N/m}^2$
Poisson coefficient $\nu = 0.25$
Static friction coefficient $\mu_s = 0.20$
Dynamic friction coefficient $\mu_d = 0.20$
Friction constant parameter $K_f = 10^{15}$
Damping coefficient $\xi = 0.90$
Normalized deformation $\mathcal{E}^* = 0.04$
Bonding constant $K_{ij}^{nb} = 10^6$
Rotational bonding constant $K_{ij}^{rb} = 10^3$
Material parameter $P_p = 2.0$.
Analysis parameters
Maximum permissible iterations $K_d = 10$
Gravity acceleration $\boldsymbol{g} = (0; 0; -9.81)\,\text{m/s}^2$
Time increment $\Delta t = 5 \cdot 10^{-6}$ s
Euler integration scheme ($\varnothing \approx 0; \varnothing = 0.5$ and $\varnothing = 1$)
Tolerances $TOL_r = 10^{-3}$, $TOL_v = 10^{-3}$, $TOL_w = 10^{-3}$
Dynamic viscosity of the air $c^e = 0.00265$
Local average velocity of the external interstitial medium is $\boldsymbol{v}^e = 0$

sented in Tables 8, 9 and 10, respectively, in the Appendix C.2. All velocities and angular velocities vectors have zero value components at time $t = 0$ s.

7.3 Example 3: unloading granular material discretized by 3100 particles

This example represents a discharge of a granular material from a dump bucket of a truck into another dump bucket (lower one), see Fig. 24 for geometrical representation. In this model, the walls are assumed to be rigid. This example contains 3100 particles in the upper container.

The geometry of the lower bucket corresponds to $2.20\,\text{m}(width) \times 6.30(length) \times 2.00(height)$ and the upper bucket corresponds to $2.10\,\text{m}(width) \times 6.00\,\text{m}(length) \times 1.76\,\text{m}(height)$. The discretized granular material is sand. The sand was discretized by 3100 particles. The particle distribution in the yz-plane is shown in Fig. 25.

The particle distribution in the xz-plane is shown in Fig. 26.

The particles and analysis parameters are presented in Table 4. The material properties of the walls are the same as the particles.

In this example a fully implicit Euler integration scheme is used. The authors opted to use the implicit method, since it finds a solution by solving an equation involving both the current state of the system and the later one and thus, is more stable than the explicit method, see [49]. Some equilibrium configurations are shown in Fig. 27.

It is important to mention that the analysis time for this problem was initially very high. The analysis resulted in a processing time greater than 6 months of analysis if any treatment of optimization is done. To avoid this problem, it was verified that the contact search algorithm must be optimized, and consequently, the process would not consume much computational time in the search for algorithms to verify the contact suffered by the particles. Then a complex study of search solutions for these multiscale problems was started. A basic notion of the contact search optimization was presented in Sect. 5. Currently, the numerical analysis for a time of 15 s is done in an acceptable time and can finish this analysis in less than 1 week using a standard computer, depending on the velocities of the particles and the increment of time used. In our case, the time increment is of around 10^{-6} s.

Figure 28 illustrates some equilibrium configurations in the side view.

Figure 29 illustrates some equilibrium configurations in the front view.

The numerical results (regarding positions, velocities and angular velocities) of two selected particles are presented in Tables 11, 12 and 13, respectively, in the Appendix C.3.

8 Conclusions

The main purpose of this paper was to review the formulations of the Discrete Element Method (DEM) and apply it to

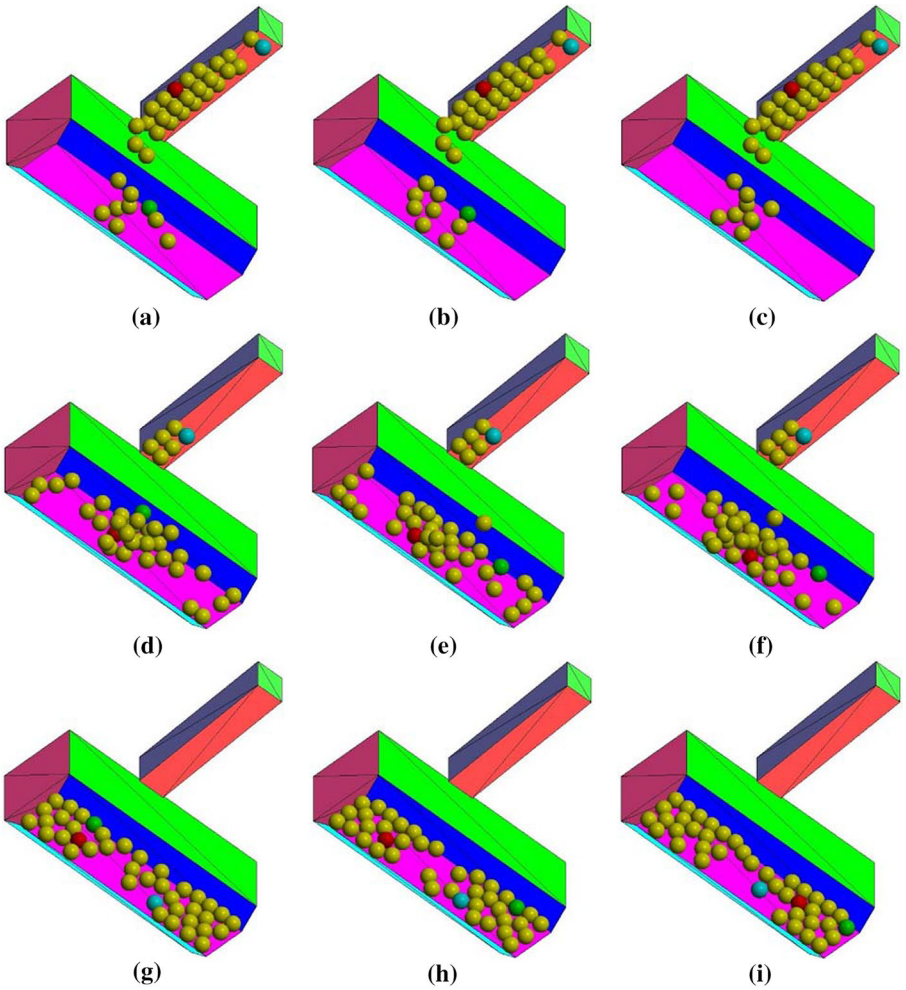

Fig. 23 Example 2: problem definition. **a** $t = 2$ s and $\varnothing \cong 0$, **b** $t = 2$ s and $\varnothing \cong 0.5$, **c** $t = 2$ s and $\varnothing \cong 1$, **d** $t = 4$ s and $\varnothing \cong 0$, **e** $t = 4$ s and $\varnothing \cong 0.5$, **f** $t = 4$ s and $\varnothing \cong 1$, **g** $t = 8$ s and $\varnothing \cong 0$, **h** $t = 8$ s and $\varnothing \cong 0.5$, **i** $t = 8$ s and $\varnothing \cong 1$

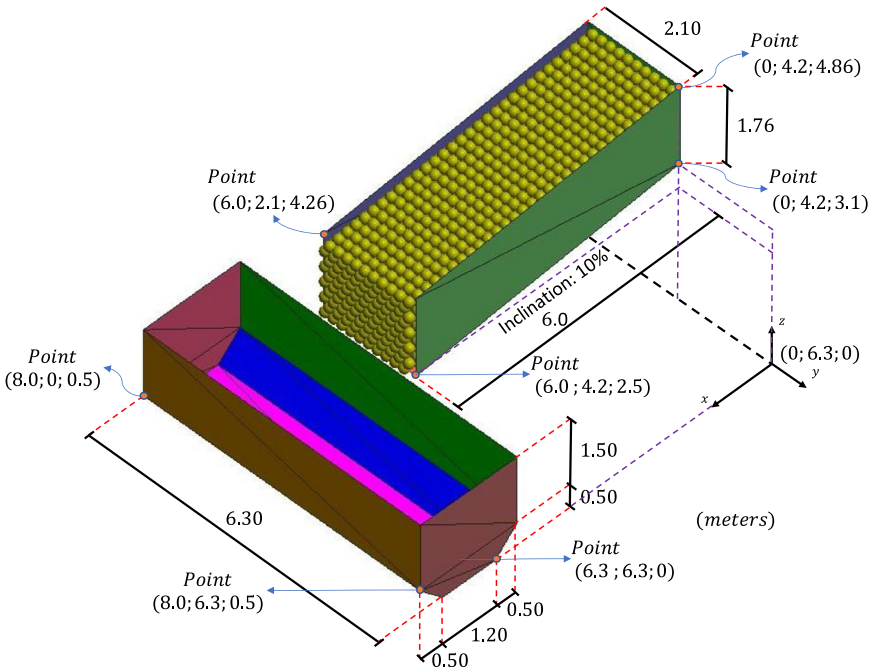

Fig. 24 Example 3: problem definition

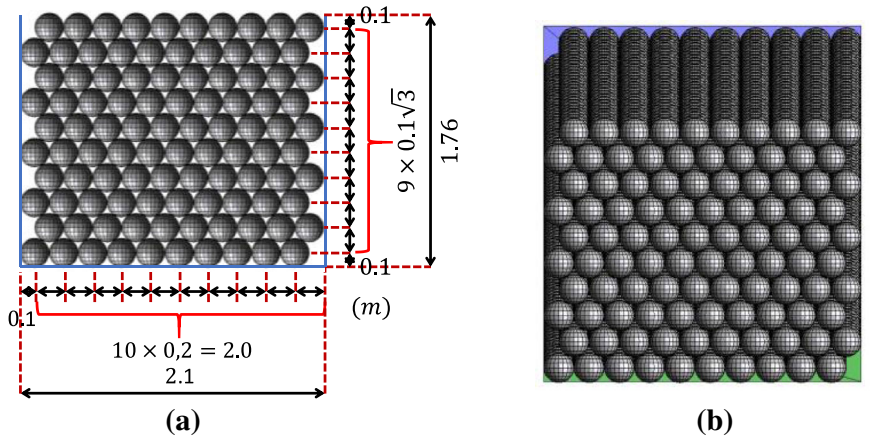

Fig. 25 Example 3: yz-plane view. **a** Particles on plane yz. **b** View plane yz

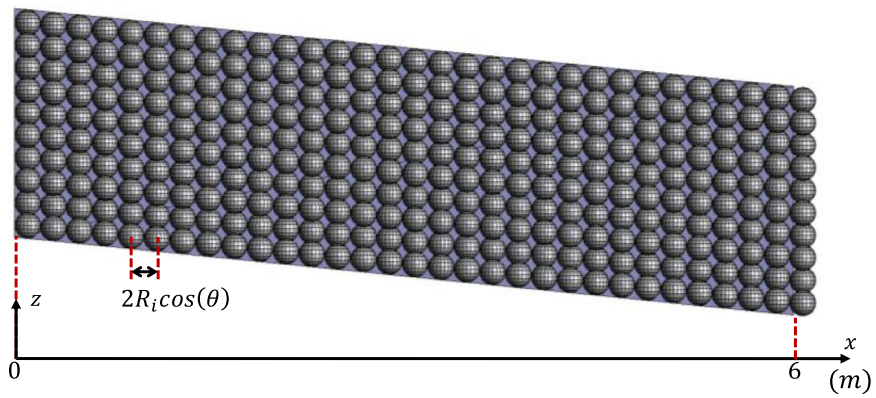

Fig. 26 Example 3: xz-plane view

Table 4 Numerical parameters of example 3

Particles
Particles radii $R = 0.1$ m
Specific mass $\rho = 2500\,\text{kg/m}^3$
Elasticity modulus of the spheres $E = 10^9\,\text{N/m}^2$
Poisson coefficient $\nu = 0.25$
Static friction coefficient $\mu_s = 0.20$
Dynamic friction coefficient $\mu_d = 0.20$
Friction constant parameter $K_f = 10^{15}$
Damping coefficient $\xi = 0.90$
Normalized deformation $\mathcal{E}^* = 0.04$
Bonding constant $K_{ij}^{nb} = 10^6$
Rotational bonding constant $K_{ij}^{rb} = 10^3$
Material parameter $P_p = 2.0$.
Analysis parameters
Maximum permissible iterations $K_d = 8$
Gravity acceleration $\boldsymbol{g} = (0; 0; -9.81)\,\text{m/s}^2$
Time increment $\Delta t = 5 \cdot 10^{-6}$ s
Fully implicit Euler integration scheme ($\varnothing = 1$)
Tolerances $TOL_r = 10^{-3}$, $TOL_v = 10^{-3}$, $TOL_w = 10^{-3}$
Dynamic viscosity of the air $c^e = 0.00265$
Local average velocity of the external interstitial medium is $\boldsymbol{v}^e = 0$

model granular materials. This work reviewed the researches developed in the DEM field and explained the rolling phenomena using the Coulomb's friction law, the forces acting on a particle (normal contact, friction, damping, adhesive bonding, environmental and gravity), the time integration scheme to solve DEM and the contact search algorithm. These topics were important to be explained because they are the fundamentals of the method. So, it is important to make a brief discussion about them.

The influence of the rotation is also included in the physical phenomena studied. The rotation is important to describe correctly the motion of the particles. Without the rotation, only the translation is not able to describe some physical phenomena.

Many forces in the procedures are investigated and included in the numerical model. Concerning the friction law presented in this paper, the authors concluded that the friction law works perfectly for higher values of the friction constant parameter K_f. The friction is also very important to calculate the angular velocities, as verified during the study made in the validation problems.

The strongly multiphysics models are solved iteratively within each time-step using a staggering scheme, proposed by Zohdi in [35], which employs temporal adaptation to control the error. A comparative study was carried out between

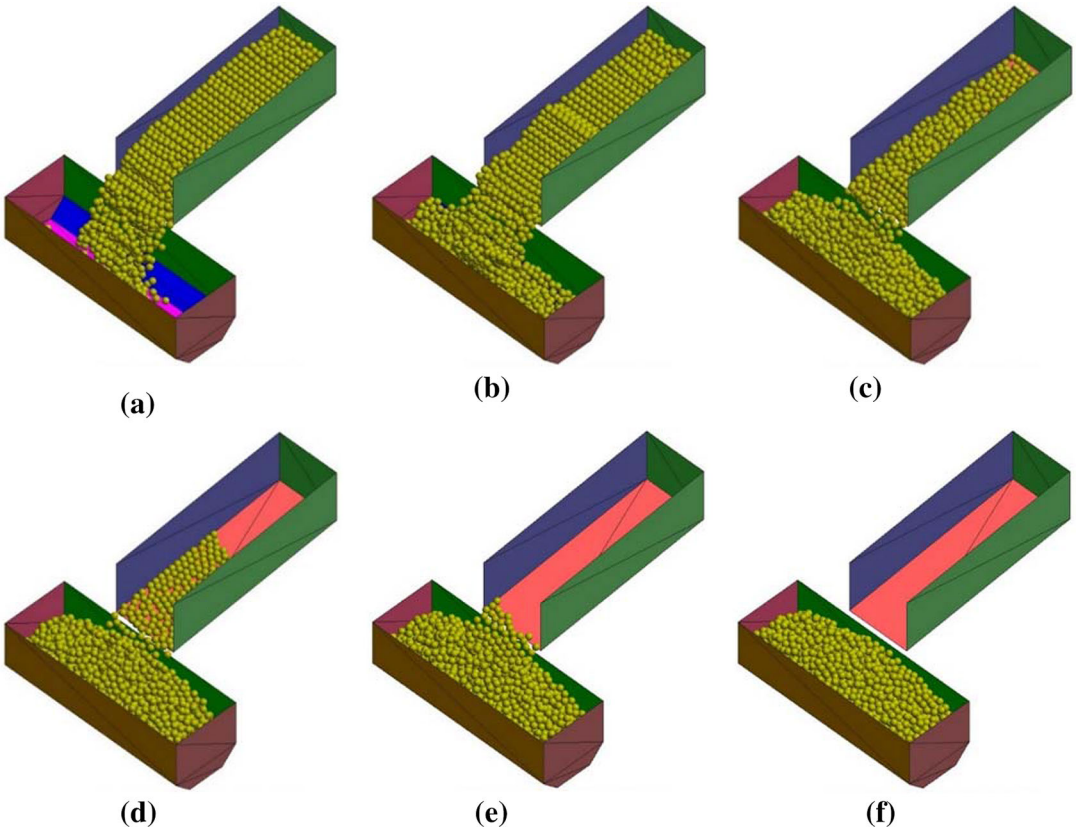

Fig. 27 Equilibrium configuration during the numerical simulation. **a** $t = 1.28$ s, **b** $t = 2.52$ s, **c** $t = 7.64$ s, **d** $t = 10.40$ s, **e** $t = 11.96$ s, **f** $t = 15.00$ s

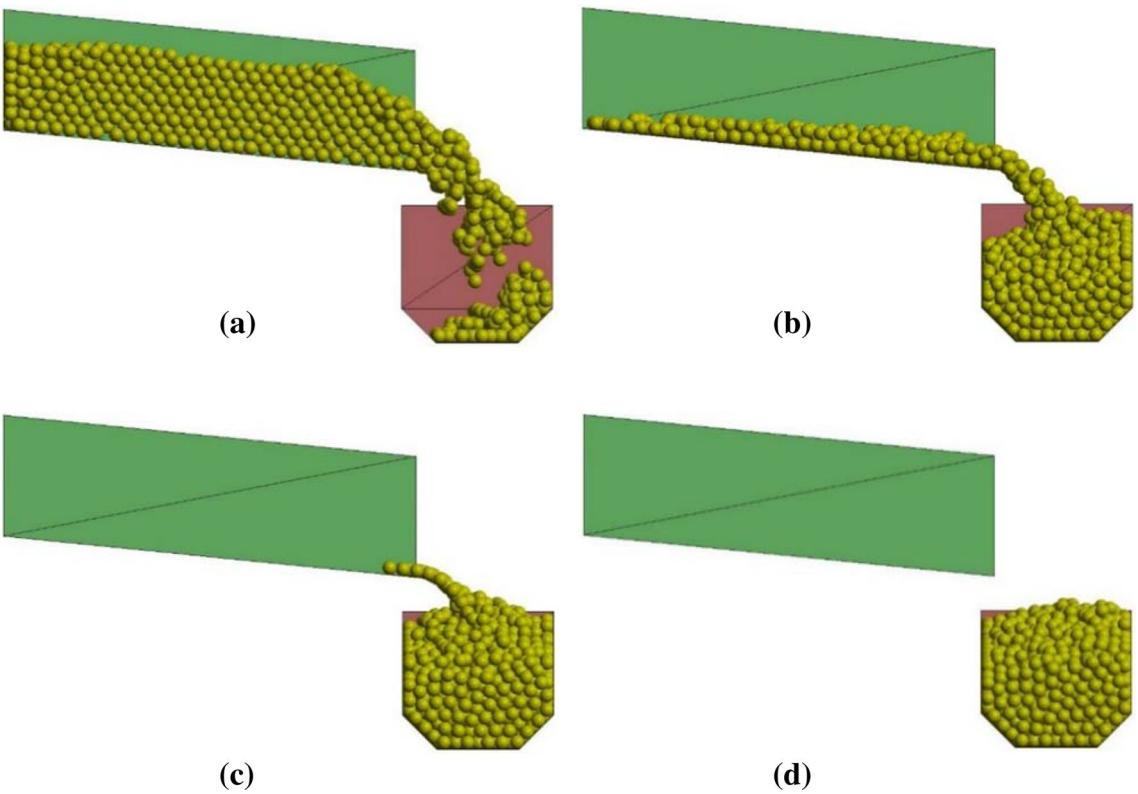

Fig. 28 Equilibrium configuration (side view). **a** $t = 1.28$ s, **b** $t = 7.64$ s, **c** $t = 11.96$ s, **d** $t = 15.00$ s

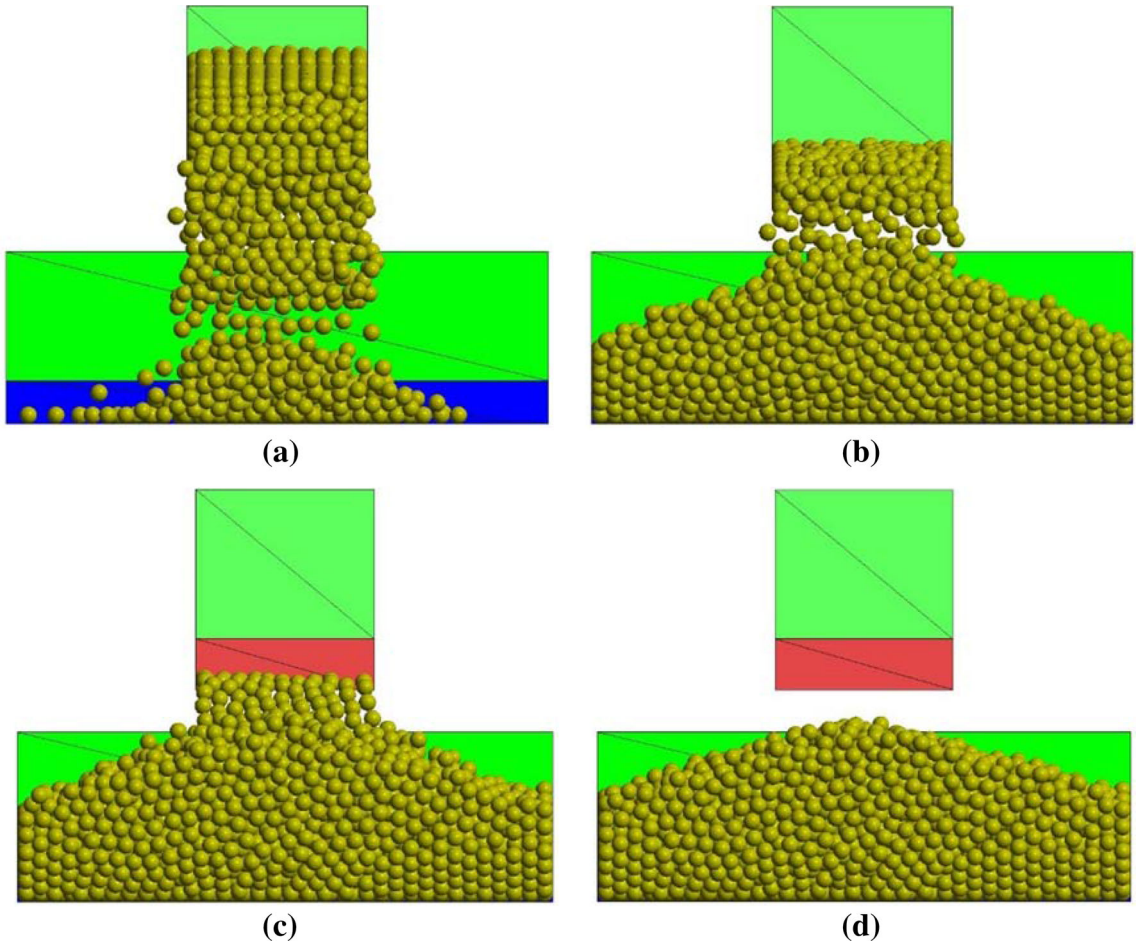

Fig. 29 Equilibrium configuration (front view). **a** $t = 1.28$ s, **b** $t = 7.64$ s, **c** $t = 11.96$ s, **d** $t = 15.00$ s

the explicit and implicit method and it was verified that the explicit method is faster than the implicit one, when the same time increments are used. It was also verified that the numerical results can be changed when different values of ϕ are used, especially in three-dimensional problems.

During these investigations, this paper also presented some standard examples of classical mechanics to validate all theories shown and consequently, the numerical program by comparing the numerical results with the analytical one.

The authors concluded that all theories and algorithms presented in this paper, work numerically perfectly and can correctly simulate the phenomena of multi-contact between particles, representing in a real form the physical phenomena.

Basically, the new contributions of this work, besides reviewing all theories, were to make a validation of the method and present 3D numerical examples to show the capability of the algorithm.

Acknowledgements The authors wish to express sincere appreciation to the independent public foundation Capes (Coordenação de Aperfeiçoamento de Pessoal de Nível Superior, Ministry of Education of Brazil, Brasília-DF, Brazil), which mission is to foster research and the scientific and technological development. This work was supported by Capes, under the Grants BEX2565/15-3. The authors would like to thank the CRML (Computational Materials Research Laboratory, University of California at Berkeley, USA).

Funding This study was funded by the independent public foundation Capes ("Coordenação de Aperfeiçoamento de Pessoal de Nível Superior", Ministry of Education of Brazil, Brasília-DF, Brazil) (Grant Number BEX 2565/15-3).

Compliance with ethical standards

Conflict of interest Regarding the conflict of interest, the author Alex Alves Bandeira has received research grants from Capes to stay one year in University of California, at Berkeley, to developed his post-doc. The author Tarek Ismail Zohdi, coordinator of the CRML (Computational Materials Research Laboratory, University of California, at Berkeley, USA), was his supervisor in this research and kindly welcomed the first author in his Laboratory. The authors declare that they have no conflict of interest. The only requirement of the Capes foundation is to mention its collaboration in the acknowledgments in the publication, as shown in Acknowledgements.

Appendix A: Analytical solution for oblique impacts of elastoplastic spheres

This example considers an oblique impact of a sphere with a target wall in the $y-z$ plane, see Fig. 13. The current formulation presented here was developed by Wu et al. in [48] and will be explained here in more details. The spins around the y and z axes and its corresponding moment impulses are ignored. Is supposed that the sphere approaches the wall with an initial translational velocity v_i and angular velocity ω_i at an impact angle θ_i. After interaction with the wall, the sphere rebounds with a rebound translational velocity v_r and rebound angular velocity ω_r. Note that v_i and v_r are the velocities of the sphere center. The corresponding translational velocities at the contact patch are denoted by v_i^P and v_r^P. Consider the normal and tangential coefficients of restitution defined by

$$e_n = -\frac{v_{r,n}}{v_{i,n}} \tag{137}$$

$$e_\tau = \frac{v_{r,\tau}}{v_{i,\tau}}. \tag{138}$$

where $v_{i,n}$ and $v_{r,n}$ are the normal components of the impact speed and rebound speed, respectively, and $v_{i,\tau}$ and $v_{r,\tau}$ are the corresponding tangential velocity components. It should be noted that it is necessary to introduce the negative sign in Eq. (137) since the normal component of the velocity reverses its direction after the impact, i.e., $v_{r,n}$ has the opposite direction of $v_{r,n}$ and the normal coefficient of restitution is usually quoted as a positive value. The tangential coefficient of restitution can be negative because, with initial spin, under certain conditions the sphere can bounce backwards, see [50, 51]. The coefficients e_n and e_τ can be used to represent the recovery of translational kinetic energy in the normal and tangential directions, respectively.

The correlation between the tangential and normal interactions during the impact can be characterized by an impulse ratio, which is defined as

$$f = \frac{P_\tau}{P_n} = \frac{\int F_\tau dt}{\int F_n dt}, \tag{139}$$

where P_n and P_τ are the normal and tangential impulses, respectively, and F_n and F_τ are the normal and tangential components of the contact force. It is clear that the impulse ratio f is different to the interface friction coefficient μ. It may or may not be equal to μ, see [52].

According to Newton's second law, P_n and P_τ can be expressed in terms of the incident and rebound velocities as

$$P_n = m\left(v_{r,n} - v_{i,n}\right) \tag{140}$$

$$P_\tau = m\left(v_{r,\tau} - v_{i,\tau}\right), \tag{141}$$

where m is the mass of the particle. Substituting (140) and (141) into Eq. (139) leads to

$$f = \frac{\left(v_{r,\tau} - v_{i,\tau}\right)}{\left(v_{r,n} - v_{i,n}\right)}. \tag{142}$$

This equation can be rewritten as

$$f\, v_{i,n}\left(\frac{v_{r,n}}{v_{i,n}} - 1\right) = v_{i,\tau}\left(\frac{v_{r,\tau}}{v_{i,\tau}} - 1\right). \tag{143}$$

Using (137) and (138) in Eq. (143):

$$f\, v_{i,n}(-e_n - 1) = v_{i,\tau}(e_\tau - 1). \tag{144}$$

Simplifying:

$$f\, \frac{v_{i,n}}{v_{i,\tau}}(-e_n - 1) = e_\tau - 1. \tag{145}$$

Rewriting (145) and considering ${}^{v_{i,n}}\!/_{v_{i,\tau}} = {}^{1}\!/_{tan(\theta_i)}$, results in

$$e_\tau = 1 - f\frac{(1+e_n)}{tan(\theta_i)}. \tag{146}$$

Similarly, a rotational impulse P_ω can be defined by

$$P_\omega = I(\omega_r - \omega_i), \tag{147}$$

where I is the moment of inertia of the sphere, and ω_i and ω_r are the initial and rebound rotational angular velocities, respectively. According to the conservation of angular momentum about point P as shown in Fig. 13, is correct to write

$$H_\omega = R P_\tau, \tag{148}$$

where R is the radius of the sphere.

Substituting (141) and (147) in (148):

$$I(\omega_r - \omega_i) = Rm\left(v_{r,\tau} - v_{i,\tau}\right). \tag{149}$$

The Eq. (149) can be rewritten as

$$\omega_r = \omega_i - \frac{Rm}{I}\left(v_{i,\tau} - v_{r,\tau}\right). \tag{150}$$

For a solid sphere, $I = {}^{2mR^2}\!/_{5}$. Hence,

$$\begin{aligned}\omega_r &= \omega_i - \frac{5}{2R}\left(v_{i,\tau} - v_{r,\tau}\right)\\ &= \omega_i - \frac{5v_{i,\tau}}{2R}\left(1 - \frac{v_{r,\tau}}{v_{i,\tau}}\right)\\ &= \omega_i - \frac{5v_{i,\tau}}{2R}\left(1 - e_\tau\right).\end{aligned} \tag{151}$$

Substituting (146) into (151):

$$\omega_r = \omega_i - \frac{5f(1+e_n)v_{i,\tau}}{2R\,tan(\theta_i)}. \tag{152}$$

Considering $v_{i,n} = {}^{v_{i,\tau}}/_{tan(\theta_i)}$, the Eq. (152) can be rewritten as

$$\omega_r = \omega_i - \frac{5f(1+e_n)v_{i,n}}{2R}. \tag{153}$$

The tangential component of the rebound surface velocity at the contact patch, $v^P_{r,\tau}$, can be expressed as

$$v^P_{r,\tau} = v_{r,\tau} + R\omega_r. \tag{154}$$

Substituting (153) into (154)

$$v^P_{r,\tau} = v_{r,\tau} + R\omega_i - \frac{5}{2}f(1+e_n)v_{i,n}. \tag{155}$$

Substituting (138) into (155), results in

$$v^P_{r,\tau} = e_\tau v_{i,\tau} + R\omega_i - \frac{5}{2}f(1+e_n)v_{i,n}. \tag{156}$$

Substituting (146) into (156), gives

$$v^P_{r,\tau} = \left[1 - f(1+e_n)\frac{v_{i,n}}{v_{i,\tau}}\right]v_{i,\tau} + R\omega_i - \frac{5}{2}f(1+e_n)v_{i,n} \tag{157}$$

Simplifying,

$$v^P_{r,\tau} = v_{i,\tau} + R\omega_i - f(1+e_n)v_{i,n} - \frac{5}{2}f(1+e_n)v_{i,n}. \tag{158}$$

Considering $v^P_{i,\tau} = v_{i,\tau} + R\omega_i$, the Eq. (158) can be written as

$$v^P_{r,\tau} = v^P_{i,\tau} - \frac{7}{2}f(1+e_n)v_{i,n} \tag{159}$$

From Eq. (146) is clear that $(1-e_\tau)v_{i,\tau} = f(1+e_n)v_{i,n}$. Hence, Eq. (159) can be rewritten as

$$v^P_{r,\tau} = v^P_{i,\tau} - \frac{7}{2}(1-e_\tau)v_{i,\tau}. \tag{160}$$

The Eq. (160) can be rewritten as

$$e_\tau = 1 - \frac{2v^P_{i,\tau}}{7v_{i,\tau}} + \frac{2v^P_{r,\tau}}{7v_{i,\tau}}. \tag{161}$$

Considering $v^P_{i,\tau} = v_{i,\tau} + R\omega_i$, the Eq. (161) can be rewritten as

$$e_\tau = 1 - \frac{2v_{i,\tau}}{7v_{i,\tau}} - \frac{2R\omega_i}{7v_{i,\tau}} + \frac{2v^P_{r,\tau}}{7v_{i,\tau}}. \tag{162}$$

Hence,

$$e_\tau = \frac{5}{7} + \frac{2v^P_{r,\tau}}{7v_{i,\tau}} - \frac{2R\omega_i}{7v_{i,\tau}}. \tag{163}$$

From Fig. 13, the rebound angle θ_r can be obtained from

$$tan(\theta_r) = \frac{v_{r,\tau}}{v_{r,n}} = \frac{e_\tau v_{i,\tau}}{-e_n v_{i,n}} = -\frac{e_\tau}{e_n}tan(\theta_i). \tag{164}$$

It can be seen from (146), (153), (159) and (160) that all the kinematics of the rebounding sphere depend upon the impact angle θ_i, the initial impact speed v_i and particle spin ω_i, the normal coefficient of restitution e_n and the impulse ratio f. In other words, for a given impact angle and impact speed, the rebounding kinematics of the sphere can be determined once e_n and f are known (see [52, 53]). Many studies have been carried out to investigate the normal coefficient of restitution e_n during elastoplastic impacts, and the rebound behavior of elastoplastic spheres during normal impacts is well established in [37, 48, 54, 55]. The impulse ratio can be determined by measuring the initial and rebound velocities at the sphere center (see [52, 53, 56]). For more details see [48].

Appendix B: Analytical solution for slipping and rolling of a sphere on an inclined plane

This problem consists of a particle with radii R and mass m slipping and rolling on an inclined surface with angle θ, see Fig. 14. In the initial time, a particle is placed on the surface with velocity $v(0)$ and spin $\omega(0)$. Depending on friction coefficient, initial velocity and angular velocity the sphere may roll or slide on the inclined plane. The full original formulation was developed by Aghamohammadia and Aghamohammadib in [57] and will be shortly presented here. It is important to mention that the formulation presented in this article is adapted and simplified to consider that the velocity of the sphere has the same direction as the unit vector $\boldsymbol{i}$.

The Newton's equilibrium equation of motion for the sphere is

$$m\ddot{\boldsymbol{r}} = mg\,sin(\theta)\boldsymbol{i} + \boldsymbol{f}, \tag{165}$$

where g is the gravity acceleration and $\boldsymbol{f}$ is the friction force. The local coordinate system is defined by

$\boldsymbol{i} = (-cos(\theta), -sin(\theta), 0)$, $\boldsymbol{j} = (0, 0, 1)$ and $\boldsymbol{k} = (-sin(\theta), cos(\theta), 0)$. Observing Eqs. (9) and (10), is easy to demonstrate the following relation

$$\boldsymbol{M} = I\dot{\boldsymbol{\omega}}, \tag{166}$$

where M is the momentum, I is the inertial momentum and $\boldsymbol{\omega}$ is the angular velocity. The moment of inertia of the sphere with respect to its center is defined in (11). Looking at Fig. 14, the momentum can be calculated by

$$\boldsymbol{M} = I\dot{\boldsymbol{\omega}} = (-R\boldsymbol{k}) \times \boldsymbol{f}. \tag{167}$$

Now, it is important to study the phenomena in two parts, i.e., one considering the rolling of sphere and other considering the sliding of sphere.

Appendix B.1.: Rolling a sphere on an inclined plane

Rolling constraint demands the velocity of the sphere at the contact point P to be zero. Then,

$$\boldsymbol{v}_P = \boldsymbol{v} + \boldsymbol{\omega} \times (-R\boldsymbol{k}) = 0. \tag{168}$$

Differentiating the above equation with respect to time, obtains

$$\ddot{\boldsymbol{r}} + \dot{\boldsymbol{\omega}} \times (-R\boldsymbol{k}) = 0. \tag{169}$$

Using (167) in the above equation, leads to

$$\ddot{\boldsymbol{r}} + \left[\frac{(-R\boldsymbol{k}) \times \boldsymbol{f}}{\frac{2}{5}mR^2}\right] \times (-R\boldsymbol{k}) = 0. \tag{170}$$

Simplifying (170), results in

$$\ddot{\boldsymbol{r}} + \frac{5}{2m}\boldsymbol{f} = 0 \rightarrow \boldsymbol{f} = -\frac{2m}{5}\ddot{\boldsymbol{r}}. \tag{171}$$

Substituting (171) in (165), one obtains

$$m\ddot{\boldsymbol{r}} = mg\, sin(\theta)\boldsymbol{i} - \frac{2m}{5}\ddot{\boldsymbol{r}}. \tag{172}$$

The above equation can be rewritten as

$$\ddot{\boldsymbol{r}} = \frac{5}{7}g\, sin(\theta)\boldsymbol{i}. \tag{173}$$

Substituting (173) in (171), gives

$$\boldsymbol{f} = -\frac{2}{7}mg\, sin(\theta)\boldsymbol{i}. \tag{174}$$

The sphere rolls on the inclined plane if $f \leq \mu mg\, cos(\theta)$. Then, the rolling occurs if

$$\mu \geq \frac{2}{7}tan(\theta). \tag{175}$$

Appendix B.2.: Sliding a sphere on an inclined plane

If the sphere slips, then the velocity at the contact point P is not zero and the friction is

$$\boldsymbol{f} = -\mu mg\, cos(\theta)\boldsymbol{e}_P, \tag{176}$$

where $\boldsymbol{e}_P = \frac{\boldsymbol{v}_P}{v_P}$ is the unit vector along velocity at contact point P. Using (165), the time evolution equation of $\boldsymbol{v}_P$ is

$$m\dot{\boldsymbol{v}}_P = mg\, sin(\theta)[\boldsymbol{i} - \mu\, cot(\theta)\boldsymbol{e}_P]. \tag{177}$$

Appendix B.3.: Exact solution

Let's solve exactly the Newton's equation. Integrating (165) and (167) gives

$$\boldsymbol{r} = \boldsymbol{r}_0 + \int_0^t \boldsymbol{v}dt \tag{178}$$

$$\boldsymbol{v} = \boldsymbol{v}_0 + g\, sin(\theta)\Delta t\, \boldsymbol{i} + \frac{1}{m}\int_0^t dt\, \boldsymbol{f} \tag{179}$$

$$\boldsymbol{\omega} = \boldsymbol{\omega}_0 + \left(-\frac{R}{I}\boldsymbol{k}\right) \times \int_0^t dt\, \boldsymbol{f}, \tag{180}$$

where

$$\boldsymbol{f} = \begin{cases} -\frac{2}{7}mg\, sin(\theta)\boldsymbol{i}, & if\ \boldsymbol{v}_P = 0 \\ -\mu mg\, cos(\theta)\boldsymbol{e}_P, & if\ \boldsymbol{v}_P \neq 0 \end{cases}, \tag{181}$$

and

$$\ddot{\boldsymbol{r}} = \begin{cases} \frac{5}{7}g\, sin(\theta)\boldsymbol{i}, & if\ \boldsymbol{v}_P = 0 \\ g\, sin(\theta)[\boldsymbol{i} - \mu\, cot(\theta)\boldsymbol{e}_P], & if\ \boldsymbol{v}_P \neq 0 \end{cases}. \tag{182}$$

Note that the velocity at the contact point $\boldsymbol{v}_P$ is defined in (168).

Appendix C.: Numerical results

Appendix C.1. Numerical results of example 1

See Tables 5, 6 and 7.

Table 5 Position vectors of two selected particles through time ($\varnothing = 1.0$)

Particle	$t = 0\,\mathrm{s}$	$t = 0.4\,\mathrm{s}$	$t = 0.8\,\mathrm{s}$	$t = 1.2\,\mathrm{s}$	$t = 1.52\,\mathrm{s}$
1	$\begin{bmatrix}1.700\\5.950\\2.100\end{bmatrix}$	$\begin{bmatrix}1.700\\5.950\\1.315\end{bmatrix}$	$\begin{bmatrix}1.746\\5.950\\0.328\end{bmatrix}$	$\begin{bmatrix}1.691\\5.950\\0.273\end{bmatrix}$	$\begin{bmatrix}1.692\\5.950\\0.273\end{bmatrix}$
2	$\begin{bmatrix}0.500\\2.750\\2.900\end{bmatrix}$	$\begin{bmatrix}0.500\\2.750\\2.115\end{bmatrix}$	$\begin{bmatrix}0.452\\2.750\\1.239\end{bmatrix}$	$\begin{bmatrix}0.450\\2.750\\0.886\end{bmatrix}$	$\begin{bmatrix}0.487\\2.750\\0.859\end{bmatrix}$

Table 6 Velocities vectors of two selected particles through time ($\varnothing = 1.0$)

Particle	$t = 0\,\mathrm{s}$	$t = 0.4\,\mathrm{s}$	$t = 0.8\,\mathrm{s}$	$t = 1.2\,\mathrm{s}$	$t = 1.52\,\mathrm{s}$
1	$\begin{bmatrix}0.000\\0.000\\0.000\end{bmatrix}$	$\begin{bmatrix}0.000\\0.000\\-3.924\end{bmatrix}$	$\begin{bmatrix}-0.011\\0.000\\-0.011\end{bmatrix}$	$\begin{bmatrix}-0.003\\0.000\\0.006\end{bmatrix}$	$\begin{bmatrix}0.000\\0.000\\0.000\end{bmatrix}$
2	$\begin{bmatrix}0.000\\0.000\\0.000\end{bmatrix}$	$\begin{bmatrix}0.000\\0.000\\-3.924\end{bmatrix}$	$\begin{bmatrix}-0.256\\0.000\\0.393\end{bmatrix}$	$\begin{bmatrix}0.884\\0.000\\-0.569\end{bmatrix}$	$\begin{bmatrix}0.000\\0.000\\0.000\end{bmatrix}$

Table 7 Angular velocities vectors of two selected particles through time ($\varnothing = 1.0$)

Particle	$t = 0\,\mathrm{s}$	$t = 0.4\,\mathrm{s}$	$t = 0.8\,\mathrm{s}$	$t = 1.2\,\mathrm{s}$	$t = 1.52\,\mathrm{s}$
1	$\begin{bmatrix}0.000\\0.000\\0.000\end{bmatrix}$	$\begin{bmatrix}0.000\\0.000\\0.000\end{bmatrix}$	$\begin{bmatrix}0.000\\0.253\\0.000\end{bmatrix}$	$\begin{bmatrix}0.000\\0.008\\0.000\end{bmatrix}$	$\begin{bmatrix}0.000\\0.000\\0.000\end{bmatrix}$
2	$\begin{bmatrix}0.000\\0.000\\0.000\end{bmatrix}$	$\begin{bmatrix}0.000\\0.000\\0.000\end{bmatrix}$	$\begin{bmatrix}0.000\\2.099\\0.000\end{bmatrix}$	$\begin{bmatrix}0.000\\3.265\\0.000\end{bmatrix}$	$\begin{bmatrix}0.000\\0.000\\0.000\end{bmatrix}$

Appendix C.2.: Numerical results of example 2

See Tables 8, 9 and 10.

Table 8 Position vectors of three selected particles through time

Particle	ϕ	$t = 0\,\mathrm{s}$	$t = 1\,\mathrm{s}$	$t = 2\,\mathrm{s}$	$t = 3\,\mathrm{s}$	$t = 4\,\mathrm{s}$	$t = 5\,\mathrm{s}$	$t = 6\,\mathrm{s}$	$t = 7\,\mathrm{s}$	$t = 8\,\mathrm{s}$
1	0.0	$\begin{bmatrix}3.782\\3.35\\2.741\end{bmatrix}$	$\begin{bmatrix}4.492\\3.342\\0.200\end{bmatrix}$	$\begin{bmatrix}4.219\\3.260\\0.200\end{bmatrix}$	$\begin{bmatrix}4.427\\2.995\\0.200\end{bmatrix}$	$\begin{bmatrix}3.933\\2.778\\0.450\end{bmatrix}$	$\begin{bmatrix}4.045\\2.359\\0.338\end{bmatrix}$	$\begin{bmatrix}4.228\\1.843\\0.200\end{bmatrix}$	$\begin{bmatrix}4.194\\1.482\\0.200\end{bmatrix}$	$\begin{bmatrix}4.183\\1.397\\0.200\end{bmatrix}$
	0.5	$\begin{bmatrix}3.782\\3.350\\2.741\end{bmatrix}$	$\begin{bmatrix}4.986\\3.340\\0.200\end{bmatrix}$	$\begin{bmatrix}4.183\\3.585\\0.200\end{bmatrix}$	$\begin{bmatrix}4.183\\3.915\\0.200\end{bmatrix}$	$\begin{bmatrix}4.206\\4.768\\0.200\end{bmatrix}$	$\begin{bmatrix}4.367\\5.309\\0.200\end{bmatrix}$	$\begin{bmatrix}4.360\\5.336\\0.200\end{bmatrix}$	$\begin{bmatrix}4.289\\5.281\\0.200\end{bmatrix}$	$\begin{bmatrix}4.239\\5.273\\0.200\end{bmatrix}$
	1.0	$\begin{bmatrix}3.782\\3.350\\2.741\end{bmatrix}$	$\begin{bmatrix}4.510\\3.342\\0.503\end{bmatrix}$	$\begin{bmatrix}4.764\\3.351\\0.200\end{bmatrix}$	$\begin{bmatrix}4.512\\3.860\\0.200\end{bmatrix}$	$\begin{bmatrix}4.216\\5.049\\0.200\end{bmatrix}$	$\begin{bmatrix}4.190\\6.100\\0.200\end{bmatrix}$	$\begin{bmatrix}4.235\\6.098\\0.200\end{bmatrix}$	$\begin{bmatrix}4.287\\6.099\\0.200\end{bmatrix}$	$\begin{bmatrix}4.345\\6.096\\0.200\end{bmatrix}$
2	0.0	$\begin{bmatrix}1.792\\2.950\\3.340\end{bmatrix}$	$\begin{bmatrix}2.007\\2.950\\3.250\end{bmatrix}$	$\begin{bmatrix}3.023\\2.950\\3.146\end{bmatrix}$	$\begin{bmatrix}4.932\\2.950\\2.435\end{bmatrix}$	$\begin{bmatrix}4.737\\2.648\\0.200\end{bmatrix}$	$\begin{bmatrix}4.415\\1.852\\0.200\end{bmatrix}$	$\begin{bmatrix}4.566\\1.624\\0.200\end{bmatrix}$	$\begin{bmatrix}4.766\\1.532\\0.200\end{bmatrix}$	$\begin{bmatrix}4.818\\1.523\\0.200\end{bmatrix}$
	0.5	$\begin{bmatrix}1.792\\2.950\\3.340\end{bmatrix}$	$\begin{bmatrix}2.005\\2.950\\3.251\end{bmatrix}$	$\begin{bmatrix}3.010\\2.950\\3.148\end{bmatrix}$	$\begin{bmatrix}4.895\\2.950\\2.456\end{bmatrix}$	$\begin{bmatrix}4.911\\2.573\\0.200\end{bmatrix}$	$\begin{bmatrix}4.579\\1.728\\0.200\end{bmatrix}$	$\begin{bmatrix}4.698\\1.486\\0.200\end{bmatrix}$	$\begin{bmatrix}4.820\\1.511\\0.200\end{bmatrix}$	$\begin{bmatrix}4.826\\1.456\\0.200\end{bmatrix}$
	1.0	$\begin{bmatrix}1.792\\2.950\\3.340\end{bmatrix}$	$\begin{bmatrix}2.007\\2.950\\3.249\end{bmatrix}$	$\begin{bmatrix}3.030\\2.950\\3.146\end{bmatrix}$	$\begin{bmatrix}4.947\\2.950\\2.415\end{bmatrix}$	$\begin{bmatrix}4.990\\3.505\\0.200\end{bmatrix}$	$\begin{bmatrix}4.764\\4.129\\0.200\end{bmatrix}$	$\begin{bmatrix}4.560\\4.627\\0.200\end{bmatrix}$	$\begin{bmatrix}4.570\\4.740\\0.200\end{bmatrix}$	$\begin{bmatrix}4.564\\4.723\\0.200\end{bmatrix}$

Table 8 continued

Particle	ϕ	$t = 0\,\mathrm{s}$	$t = 1\,\mathrm{s}$	$t = 2\,\mathrm{s}$	$t = 3\,\mathrm{s}$	$t = 4\,\mathrm{s}$	$t = 5\,\mathrm{s}$	$t = 6\,\mathrm{s}$	$t = 7\,\mathrm{s}$	$t = 8\,\mathrm{s}$
3	0.0	$\begin{bmatrix}0.200\\3.350\\3.499\end{bmatrix}$	$\begin{bmatrix}0.200\\3.350\\3.186\end{bmatrix}$	$\begin{bmatrix}0.455\\3.350\\3.055\end{bmatrix}$	$\begin{bmatrix}1.395\\3.350\\2.961\end{bmatrix}$	$\begin{bmatrix}3.028\\3.350\\2.798\end{bmatrix}$	$\begin{bmatrix}5.255\\3.350\\1.163\end{bmatrix}$	$\begin{bmatrix}5.162\\3.858\\0.200\end{bmatrix}$	$\begin{bmatrix}5.080\\4.188\\0.200\end{bmatrix}$	$\begin{bmatrix}5.033\\4.300\\0.200\end{bmatrix}$
	0.5	$\begin{bmatrix}0.200\\3.350\\3.499\end{bmatrix}$	$\begin{bmatrix}0.200\\3.350\\3.186\end{bmatrix}$	$\begin{bmatrix}0.460\\3.350\\3.055\end{bmatrix}$	$\begin{bmatrix}1.405\\3.350\\2.960\end{bmatrix}$	$\begin{bmatrix}3.043\\3.350\\2.796\end{bmatrix}$	$\begin{bmatrix}5.247\\3.350\\1.134\end{bmatrix}$	$\begin{bmatrix}5.063\\3.754\\0.200\end{bmatrix}$	$\begin{bmatrix}4.955\\4.109\\0.200\end{bmatrix}$	$\begin{bmatrix}5.012\\4.170\\0.200\end{bmatrix}$
	1.0	$\begin{bmatrix}0.200\\3.350\\3.499\end{bmatrix}$	$\begin{bmatrix}0.200\\3.350\\3.186\end{bmatrix}$	$\begin{bmatrix}0.453\\3.350\\3.056\end{bmatrix}$	$\begin{bmatrix}1.391\\3.350\\2.962\end{bmatrix}$	$\begin{bmatrix}3.023\\3.350\\2.798\end{bmatrix}$	$\begin{bmatrix}5.249\\3.349\\1.176\end{bmatrix}$	$\begin{bmatrix}5.295\\3.600\\0.277\end{bmatrix}$	$\begin{bmatrix}4.931\\3.766\\0.200\end{bmatrix}$	$\begin{bmatrix}4.901\\3.734\\0.200\end{bmatrix}$

Table 9 Velocities vectors of three selected particles through time

Particle	ϕ	$t = 1\,\mathrm{s}$	$t = 2\,\mathrm{s}$	$t = 3\,\mathrm{s}$	$t = 4\,\mathrm{s}$	$t = 5\,\mathrm{s}$	$t = 6\,\mathrm{s}$	$t = 7\,\mathrm{s}$	$t = 8\,\mathrm{s}$
1	0.0	$\begin{bmatrix}-3.050\\-0.018\\0.000\end{bmatrix}$	$\begin{bmatrix}0.645\\-0.262\\0.000\end{bmatrix}$	$\begin{bmatrix}-0.784\\-0.060\\0.000\end{bmatrix}$	$\begin{bmatrix}-0.088\\-0.423\\0.0860\end{bmatrix}$	$\begin{bmatrix}0.184\\-0.481\\-0.194\end{bmatrix}$	$\begin{bmatrix}0.006\\-0.404\\0.000\end{bmatrix}$	$\begin{bmatrix}-0.083\\-0.334\\0.000\end{bmatrix}$	$\begin{bmatrix}0.001\\0.028\\0.000\end{bmatrix}$
	0.5	$\begin{bmatrix}-1.943\\-0.041\\0.0209\end{bmatrix}$	$\begin{bmatrix}-0.003\\0.414\\0.000\end{bmatrix}$	$\begin{bmatrix}-0.004\\0.311\\0.000\end{bmatrix}$	$\begin{bmatrix}0.107\\1.206\\0.000\end{bmatrix}$	$\begin{bmatrix}0.401\\0.393\\0.000\end{bmatrix}$	$\begin{bmatrix}-0.072\\-0.064\\0.000\end{bmatrix}$	$\begin{bmatrix}-0.063\\-0.013\\0.000\end{bmatrix}$	$\begin{bmatrix}-0.036\\-0.001\\0.000\end{bmatrix}$
	1.0	$\begin{bmatrix}0.740\\-0.010\\-6.564\end{bmatrix}$	$\begin{bmatrix}-0.281\\0.061\\0.000\end{bmatrix}$	$\begin{bmatrix}-0.353\\0.984\\0.000\end{bmatrix}$	$\begin{bmatrix}-0.276\\1.219\\0.000\end{bmatrix}$	$\begin{bmatrix}0.062\\-0.007\\-0.044\end{bmatrix}$	$\begin{bmatrix}0.040\\-0.012\\0.000\end{bmatrix}$	$\begin{bmatrix}0.058\\-0.003\\0.000\end{bmatrix}$	$\begin{bmatrix}0.058\\-0.003\\0.000\end{bmatrix}$
2	0.0	$\begin{bmatrix}0.675\\0.000\\-0.077\end{bmatrix}$	$\begin{bmatrix}1.379\\-0.000\\-0.138\end{bmatrix}$	$\begin{bmatrix}2.503\\-0.001\\-3.330\end{bmatrix}$	$\begin{bmatrix}-1.358\\-0.738\\0.000\end{bmatrix}$	$\begin{bmatrix}-0.088\\-0.691\\0.000\end{bmatrix}$	$\begin{bmatrix}0.256\\-0.101\\0.000\end{bmatrix}$	$\begin{bmatrix}0.040\\-0.022\\0.000\end{bmatrix}$	$\begin{bmatrix}0.044\\-0.003\\0.000\end{bmatrix}$
	0.5	$\begin{bmatrix}0.651\\0.000\\-0.080\end{bmatrix}$	$\begin{bmatrix}1.369\\0.000\\-0.137\end{bmatrix}$	$\begin{bmatrix}2.461\\0.001\\-3.282\end{bmatrix}$	$\begin{bmatrix}-0.665\\-1.022\\0.000\end{bmatrix}$	$\begin{bmatrix}-0.158\\-1.007\\0.000\end{bmatrix}$	$\begin{bmatrix}0.138\\0.050\\0.000\end{bmatrix}$	$\begin{bmatrix}0.001\\-0.106\\0.000\end{bmatrix}$	$\begin{bmatrix}0.003\\-0.039\\0.000\end{bmatrix}$
	1.0	$\begin{bmatrix}0.680\\-0.000\\-0.091\end{bmatrix}$	$\begin{bmatrix}1.385\\0.000\\-0.139\end{bmatrix}$	$\begin{bmatrix}2.505\\0.000\\-3.389\end{bmatrix}$	$\begin{bmatrix}-0.867\\0.855\\0.000\end{bmatrix}$	$\begin{bmatrix}-0.207\\0.587\\0.000\end{bmatrix}$	$\begin{bmatrix}-0.086\\0.280\\-0.001\end{bmatrix}$	$\begin{bmatrix}0.033\\-0.034\\0.000\end{bmatrix}$	$\begin{bmatrix}-0.026\\-0.020\\0.000\end{bmatrix}$
3	0.0	$\begin{bmatrix}0.003\\-0.001\\-1.560\end{bmatrix}$	$\begin{bmatrix}0.593\\0.000\\-0.059\end{bmatrix}$	$\begin{bmatrix}1.286\\-0.000\\-0.129\end{bmatrix}$	$\begin{bmatrix}1.980\\0.000\\-0.198\end{bmatrix}$	$\begin{bmatrix}2.301\\-0.000\\-5.494\end{bmatrix}$	$\begin{bmatrix}-0.153\\0.395\\0.000\end{bmatrix}$	$\begin{bmatrix}0.008\\0.248\\0.000\end{bmatrix}$	$\begin{bmatrix}-0.075\\0.041\\0.000\end{bmatrix}$
	0.5	$\begin{bmatrix}0.003\\-0.001\\-1.557\end{bmatrix}$	$\begin{bmatrix}0.598\\0.000\\-0.060\end{bmatrix}$	$\begin{bmatrix}1.291\\0.000\\-0.129\end{bmatrix}$	$\begin{bmatrix}1.985\\0.000\\-0.199\end{bmatrix}$	$\begin{bmatrix}2.262\\-0.000\\-5.546\end{bmatrix}$	$\begin{bmatrix}-0.336\\0.449\\0.000\end{bmatrix}$	$\begin{bmatrix}-0.006\\0.065\\0.000\end{bmatrix}$	$\begin{bmatrix}0.082\\0.053\\0.000\end{bmatrix}$
	1.0	$\begin{bmatrix}0.003\\0.000\\-1.556\end{bmatrix}$	$\begin{bmatrix}0.591\\-0.000\\-0.059\end{bmatrix}$	$\begin{bmatrix}1.285\\0.000\\-0.129\end{bmatrix}$	$\begin{bmatrix}1.979\\0.000\\-0.198\end{bmatrix}$	$\begin{bmatrix}2.301\\-0.001\\-5.471\end{bmatrix}$	$\begin{bmatrix}-0.242\\0.224\\-0.242\end{bmatrix}$	$\begin{bmatrix}-0.068\\-0.004\\0.000\end{bmatrix}$	$\begin{bmatrix}-0.027\\-0.034\\0.000\end{bmatrix}$

Table 10 Angular velocities vectors of three selected particles through time

Particle	ϕ	$t = 1\,\mathrm{s}$	$t = 2\,\mathrm{s}$	$t = 3\,\mathrm{s}$	$t = 4\,\mathrm{s}$	$t = 5\,\mathrm{s}$	$t = 6\,\mathrm{s}$	$t = 7\,\mathrm{s}$	$t = 8\,\mathrm{s}$
1	0.0	$\begin{bmatrix}0.092\\-15.249\\0.177\end{bmatrix}$	$\begin{bmatrix}1.310\\3.223\\0.636\end{bmatrix}$	$\begin{bmatrix}1.076\\-2.019\\0.214\end{bmatrix}$	$\begin{bmatrix}3.025\\-0.595\\0.034\end{bmatrix}$	$\begin{bmatrix}2.817\\1.489\\-0.559\end{bmatrix}$	$\begin{bmatrix}2.021\\0.032\\0.285\end{bmatrix}$	$\begin{bmatrix}1.668\\-0.417\\0.836\end{bmatrix}$	$\begin{bmatrix}-0.103\\0.005\\0.232\end{bmatrix}$
	0.5	$\begin{bmatrix}-0.003\\5.510\\0.586\end{bmatrix}$	$\begin{bmatrix}-2.068\\-0.013\\0.904\end{bmatrix}$	$\begin{bmatrix}-1.613\\-0.019\\0.514\end{bmatrix}$	$\begin{bmatrix}-6.031\\0.535\\2.192\end{bmatrix}$	$\begin{bmatrix}-0.648\\1.442\\0.770\end{bmatrix}$	$\begin{bmatrix}0.318\\-0.361\\0.712\end{bmatrix}$	$\begin{bmatrix}0.067\\-0.315\\0.607\end{bmatrix}$	$\begin{bmatrix}0.007\\-0.182\\0.323\end{bmatrix}$
	1.0	$\begin{bmatrix}0.102\\3.712\\0.453\end{bmatrix}$	$\begin{bmatrix}-0.306\\-1.405\\1.331\end{bmatrix}$	$\begin{bmatrix}-4.547\\-1.898\\1.155\end{bmatrix}$	$\begin{bmatrix}-6.095\\-1.378\\0.345\end{bmatrix}$	$\begin{bmatrix}-1.084\\0.080\\0.355\end{bmatrix}$	$\begin{bmatrix}0.061\\0.198\\-0.188\end{bmatrix}$	$\begin{bmatrix}0.016\\0.289\\-0.332\end{bmatrix}$	$\begin{bmatrix}0.016\\0.289\\-0.332\end{bmatrix}$

Table 10 continued

Particle	ϕ	$t = 1\,\mathrm{s}$	$t = 2\,\mathrm{s}$	$t = 3\,\mathrm{s}$	$t = 4\,\mathrm{s}$	$t = 5\,\mathrm{s}$	$t = 6\,\mathrm{s}$	$t = 7\,\mathrm{s}$	$t = 8\,\mathrm{s}$
2	0.0	$\begin{bmatrix} 0.001 \\ -3.262 \\ -0.001 \end{bmatrix}$	$\begin{bmatrix} 0.003 \\ -6.929 \\ -0.004 \end{bmatrix}$	$\begin{bmatrix} 0.020 \\ -4.942 \\ -0.009 \end{bmatrix}$	$\begin{bmatrix} 3.691 \\ -6.792 \\ 1.388 \end{bmatrix}$	$\begin{bmatrix} 3.455 \\ -0.438 \\ 0.329 \end{bmatrix}$	$\begin{bmatrix} 0.507 \\ 1.279 \\ 0.291 \end{bmatrix}$	$\begin{bmatrix} 0.112 \\ 0.201 \\ 0.778 \end{bmatrix}$	$\begin{bmatrix} 0.016 \\ 0.219 \\ 0.895 \end{bmatrix}$
	0.5	$\begin{bmatrix} 0.001 \\ -3.181 \\ 0.000 \end{bmatrix}$	$\begin{bmatrix} 0.005 \\ -6.877 \\ 0.001 \end{bmatrix}$	$\begin{bmatrix} 0.033 \\ -5.124 \\ -0.006 \end{bmatrix}$	$\begin{bmatrix} 5.110 \\ -3.326 \\ 2.946 \end{bmatrix}$	$\begin{bmatrix} 4.223 \\ 0.691 \\ 1.838 \end{bmatrix}$	$\begin{bmatrix} -0.248 \\ 0.688 \\ 0.520 \end{bmatrix}$	$\begin{bmatrix} 0.532 \\ 0.005 \\ 0.406 \end{bmatrix}$	$\begin{bmatrix} 0.196 \\ 0.017 \\ 0.156 \end{bmatrix}$
	1.0	$\begin{bmatrix} 0.000 \\ -3.149 \\ -0.001 \end{bmatrix}$	$\begin{bmatrix} 0.000 \\ -6.960 \\ -0.002 \end{bmatrix}$	$\begin{bmatrix} -0.001 \\ -4.956 \\ -0.001 \end{bmatrix}$	$\begin{bmatrix} -4.273 \\ -4.338 \\ 1.105 \end{bmatrix}$	$\begin{bmatrix} -2.934 \\ -1.037 \\ 1.772 \end{bmatrix}$	$\begin{bmatrix} -1.402 \\ -0.428 \\ 0.550 \end{bmatrix}$	$\begin{bmatrix} 0.171 \\ 0.166 \\ 0.052 \end{bmatrix}$	$\begin{bmatrix} 0.101 \\ -0.132 \\ 0.260 \end{bmatrix}$
3	0.0	$\begin{bmatrix} 0.035 \\ -7.104 \\ -0.006 \end{bmatrix}$	$\begin{bmatrix} 0.016 \\ 2.978 \\ 0.159 \end{bmatrix}$	$\begin{bmatrix} 0.016 \\ 6.464 \\ 0.159 \end{bmatrix}$	$\begin{bmatrix} 0.016 \\ 9.950 \\ 0.159 \end{bmatrix}$	$\begin{bmatrix} 0.017 \\ 11.564 \\ 0.158 \end{bmatrix}$	$\begin{bmatrix} -1.975 \\ -0.766 \\ -0.772 \end{bmatrix}$	$\begin{bmatrix} -1.238 \\ 0.039 \\ -0.113 \end{bmatrix}$	$\begin{bmatrix} -0.206 \\ -0.373 \\ 0.023 \end{bmatrix}$
	0.5	$\begin{bmatrix} 0.003 \\ -7.108 \\ 0.000 \end{bmatrix}$	$\begin{bmatrix} 0.014 \\ 3.004 \\ 0.145 \end{bmatrix}$	$\begin{bmatrix} 0.014 \\ 6.489 \\ 0.145 \end{bmatrix}$	$\begin{bmatrix} 0.014 \\ 9.975 \\ 0.145 \end{bmatrix}$	$\begin{bmatrix} 0.015 \\ 11.367 \\ 0.144 \end{bmatrix}$	$\begin{bmatrix} -2.246 \\ -1.681 \\ -0.671 \end{bmatrix}$	$\begin{bmatrix} -0.334 \\ -0.032 \\ 0.497 \end{bmatrix}$	$\begin{bmatrix} -0.265 \\ 0.408 \\ 0.744 \end{bmatrix}$
	1.0	$\begin{bmatrix} 0.001 \\ -7.106 \\ 0.000 \end{bmatrix}$	$\begin{bmatrix} 0.009 \\ 2.971 \\ 0.086 \end{bmatrix}$	$\begin{bmatrix} 0.009 \\ 6.457 \\ 0.086 \end{bmatrix}$	$\begin{bmatrix} 0.009 \\ 9.943 \\ 0.086 \end{bmatrix}$	$\begin{bmatrix} 0.015 \\ 11.563 \\ 0.079 \end{bmatrix}$	$\begin{bmatrix} 1.836 \\ -1.653 \\ -3.423 \end{bmatrix}$	$\begin{bmatrix} 0.022 \\ -0.339 \\ -2.354 \end{bmatrix}$	$\begin{bmatrix} 0.171 \\ -0.136 \\ -2.190 \end{bmatrix}$

Appendix C.3.: Numerical results of example 3

See Tables 11, 12 and 13.

Table 11 Position vectors of two selected particles through time ($\varnothing = 1.0$)

Particle	$t = 0\,\mathrm{s}$	$t = 1.28\,\mathrm{s}$	$t = 2.52\,\mathrm{s}$	$t = 7.64\,\mathrm{s}$	$t = 10.40\,\mathrm{s}$	$t = 15\,\mathrm{s}$
1	$\begin{bmatrix} 0.299 \\ 2.200 \\ 4.210 \end{bmatrix}$	$\begin{bmatrix} 0.263 \\ 2.200 \\ 3.802 \end{bmatrix}$	$\begin{bmatrix} 0.279 \\ 2.200 \\ 3.621 \end{bmatrix}$	$\begin{bmatrix} 1.055 \\ 2.200 \\ 3.095 \end{bmatrix}$	$\begin{bmatrix} 3.651 \\ 2.202 \\ 2.835 \end{bmatrix}$	$\begin{bmatrix} 7.096 \\ 1.333 \\ 1.637 \end{bmatrix}$
2	$\begin{bmatrix} 0.498 \\ 3.000 \\ 4.190 \end{bmatrix}$	$\begin{bmatrix} 0.474 \\ 3.004 \\ 3.789 \end{bmatrix}$	$\begin{bmatrix} 0.475 \\ 3.014 \\ 3.670 \end{bmatrix}$	$\begin{bmatrix} 2.095 \\ 3.038 \\ 2.991 \end{bmatrix}$	$\begin{bmatrix} 5.258 \\ 3.064 \\ 2.675 \end{bmatrix}$	$\begin{bmatrix} 7.116 \\ 3.183 \\ 1.931 \end{bmatrix}$

Table 12 Velocities vectors of two selected particles through time ($\varnothing = 1.0$)

Particle	$t = 0\,\mathrm{s}$	$t = 1.28\,\mathrm{s}$	$t = 2.52\,\mathrm{s}$	$t = 7.64\,\mathrm{s}$	$t = 10.40\,\mathrm{s}$	$t = 15\,\mathrm{s}$
1	$\begin{bmatrix} 0.000 \\ 0.000 \\ 0.000 \end{bmatrix}$	$\begin{bmatrix} 0.043 \\ -0.001 \\ -0.192 \end{bmatrix}$	$\begin{bmatrix} 0.035 \\ 0.000 \\ -0.065 \end{bmatrix}$	$\begin{bmatrix} 0.336 \\ 0.009 \\ -0.034 \end{bmatrix}$	$\begin{bmatrix} 1.452 \\ -0.036 \\ -0.145 \end{bmatrix}$	$\begin{bmatrix} -0.018 \\ -0.018 \\ 0.006 \end{bmatrix}$
2	$\begin{bmatrix} 0.000 \\ 0.000 \\ 0.000 \end{bmatrix}$	$\begin{bmatrix} -0.075 \\ 0.048 \\ -0.060 \end{bmatrix}$	$\begin{bmatrix} 0.023 \\ -0.076 \\ -0.041 \end{bmatrix}$	$\begin{bmatrix} 0.651 \\ -0.022 \\ -0.065 \end{bmatrix}$	$\begin{bmatrix} 1.449 \\ 0.020 \\ -0.145 \end{bmatrix}$	$\begin{bmatrix} 0.000 \\ 0.000 \\ 0.000 \end{bmatrix}$

Table 13 Angular velocities vectors of two selected particles through time ($\varnothing = 1.0$)

Particle	$t = 0\,\mathrm{s}$	$t = 1.28\,\mathrm{s}$	$t = 2.52\,\mathrm{s}$	$t = 7.64\,\mathrm{s}$	$t = 10.40\,\mathrm{s}$	$t = 15\,\mathrm{s}$
1	$\begin{bmatrix} 0.000 \\ 0.000 \\ 0.000 \end{bmatrix}$	$\begin{bmatrix} -1.896 \\ -1.298 \\ -0.280 \end{bmatrix}$	$\begin{bmatrix} -0.648 \\ 0.616 \\ -0.346 \end{bmatrix}$	$\begin{bmatrix} -0.258 \\ 3.375 \\ -1.714 \end{bmatrix}$	$\begin{bmatrix} 0.131 \\ 14.593 \\ -2.295 \end{bmatrix}$	$\begin{bmatrix} 0.206 \\ -0.088 \\ -0.001 \end{bmatrix}$
2	$\begin{bmatrix} 0.000 \\ 0.000 \\ 0.000 \end{bmatrix}$	$\begin{bmatrix} -0.696 \\ -1.140 \\ 0.334 \end{bmatrix}$	$\begin{bmatrix} 1.065 \\ 0.385 \\ 1.206 \end{bmatrix}$	$\begin{bmatrix} 0.213 \\ 6.545 \\ -0.105 \end{bmatrix}$	$\begin{bmatrix} -0.180 \\ 14.561 \\ 0.220 \end{bmatrix}$	$\begin{bmatrix} 0.002 \\ 0.005 \\ -0.001 \end{bmatrix}$

Appendix D.: Contact search algorithm

See Table 14.

Table 14 Optimization algorithm for tridimensional contact search

Optimization algorithm for tridimensional contact search	
Step 1	IF $t = t_0$, where t_0 is the starting time of the analysis THEN Go to step 2 to initialize the variables before starting the analysis ELSE Go to step 6 for the contact search procedures to be performed during the analysis
Step 2	Define the values of each global variable of the problem: (1) identify the smallest particle diameter (d_{min}); (2) establish the minimum and maximum admissible coordinates to define a hexahedron to limit the position (x, y, z) of particles and walls during the analysis, i.e., $x_{min} \leq x \leq x_{max}$, $y_{min} \leq y \leq y_{max}$, and $z_{min} \leq z \leq z_{max}$. Adjust the limits coordinates so that each dimension of the hexahedron becomes a multiple of d_{min}; (3) divide the hexahedron in several cubes with size equal to d_{min}, i.e., $dim_{cube} = d_{min}$; (4) establish the maximum number of particles allowed per cube ($npc_{max} = 8$).
Step 3	Calculate the number of cubes in each direction of the hexahedron $\left(ndiv_x, ndiv_y, ndiv_z\right)$ and calculate the total number of cubes $\left(n_{cube} = ndiv_x \cdot ndiv_y \cdot ndiv_z\right)$, see Fig. 11
Step 4	Define and initialize a vector called $volume\_matrix$ with dimension equal to $dim_{vol.matrix} = n_{cube} \cdot npc_{max}$. It will store all particles number assigned to each cube
Step 5	Define a vector called $particle_{cube}$, with dimension equal to N_p, to inform in which cube each particle belongs ($cube_i$). For this, calculate the cube position (l, m, n), using the Eq. (125). The number of the cube is given by $cube_i = l + ndiv_x \cdot (m-1) + ndiv_x \cdot ndiv_y \cdot (n-1)$. Do the same for the walls
Step 6	IF $K = 0$ (beginning of the first step of each time increment) THEN Actualize the vectors $volume\_matrix$ and $particle_{cube}$, once the particle positions have been updated, and go to step 7. (Obs.: Other possibility, is to update these vectors after some predefined time) ELSE Go to step 7
Step 7	Perform the contact search of each particle i : (1) identify the number of the cube that this particle belongs, stored in the vector $particle_{cube}$; (2) select the cubes that compose the domain defined by the parameter $delta$ (see Eq. (126) and Fig. 12); (3) finally, check the contact between the particle i with the others belonging to the selected cubes Suggestion: to reduce the analysis time, check the contact only in the first step ($K = 0$) and make it constant during the time increment ($1 \leq K \leq K_d$)

References

1. Cundall PA (1971) A computer model for simulating progressive large-scale movements in Blocky rock system. In: Proceedings of international symposium on rock fractures, Nancy, France, vol 2, pp 128–132
2. Cundall PA, Strack O (1979) A discrete numerical mode for granular assemblies. Geotechnique 29(1):47–65
3. Deresiewicz H (1958) Mechanics of granular matter. Adv Appl Mech 5:233–306
4. Wakabayashi T (1950) Photo-elastic method for determination of stress in powered mass. J Phys Soc Jpn 5:383–385
5. Dantu P (1957) Contribuition à l'étude mécanique et géométrique des milieux pul-vérulents. In: Proceedings of the 4th international conference on soil mechanics and foundation engineering, London, vol 1, pp 144–148
6. Josseling De, de Jong G, Verruijt A (1969) Etude photo-élastique d'un empilement de disques. Cashiers du Groupe Français de Rheologie 2:73–86
7. Serrano AA, Rodríguez Ortiz JM (1973) A contribution to the mechanics of heterogeneous granular media. In: Symposium on plasticity and soil mechanics, Cambridge, England, pp 215–228
8. Schwartz SR, Richardson DC, Michel P (2012) An implementation of the soft-sphere discrete element method in a high-performance parallel gravity tree-code. Granul Matter 14:363–380
9. Sànchez D (2015) Asteroid evolution: role of geotechnical properties. In: International Astronomical Union, Cambridge University Press, Cambridge, pp 111–121
10. Hong DC, McLennan JA (1992) Molecular dynamics simulations of hard sphere granular particles. Phys A 187:159–171
11. Huilin L, Yunhua Z, Ding J, Gidaspow D, Wei L (2007) Investigation of mixing/segregation of mixture particles in gas-solid fluidized beds. Chem Eng Sci 62:301–317

12. Kosinski P, Hoffmann AC (2009) Extension of the hard-sphere particle-wall collision model to account for particle deposition. Phys Rev 79(6):061302: 1–061302: 11
13. Mitarai N, Nakanishi H (2003) Hard-sphere limit of soft-sphere model for granular materials: stiffness dependence of steady granular flow. Phys Rev 67(2):021301: 1–021301: 8
14. Cleary PW, Sawley ML (2002) DEM modelling of industrial granular flows: 3D case studies and the effect of particle shape on hopper discharge. Appl Math Model 26:89–111
15. Tsuji Y, Tanaka T, Ishida T (1992) Lagrangian numerical simulation of plug flow of cohesionless particles in a horizontal pipe. Powder Technol 71:239–250
16. Sànchez DPSDJ (2011) Simulating asteroid rubble piles with a self-gravitating soft-sphere distinct element method model. Astrophys J 727:120–134
17. Tancredi G, Maciel A, Heredia L, Richeri P, Nesmachnow S (2011) Granular physics in low-gravity environments using DEM. In: MNRAS, pp 3368–3380
18. Mehta AJ (2011) Granular physics. Cambridge University Press, Cambridge. ISBN 9780511535314
19. Vu-Quoc L, Zhang X, Walton OR (2000) A 3-D discrete-element method for dry granular flows of ellipsoidal particles. Comput Methods Appl Mech Eng 187:483–528
20. Martin CL, Bouvard D (2003) Study of the cold compaction of composite powders by the discrete element method. Acta Mater 51:373–386
21. Oñate E, Labra C, Zarate F, Rojek J, Miquel J (2005) Avances en el Desarrollo de los Métodos de Elementos Discretos y de Elementos Finitos para el Análisis de Problemas de Fractura. Anales de Mecánica de la Fractura 22:27–34
22. Zohdi TI, Wriggers P (2001) Modeling and simulation of the decohesion of particulate aggregates in a binding matrix. Eng Comput 18:79–95. ISSN 0264-4401
23. Zohdi TI (2013) Rapid simulation of laser processing of discrete particulate materials. Arch Comput Methods Eng 20(4):309–325
24. Ghaboussi J, Barbosa R (1990) Tree-dimensional discrete element method for granular material. Int J Numer Anal Meth Geomech 14:451–472
25. Donzé FV, Richefeu V, Magnier SA (2009) Advances in discrete element method applied to soil, rock and concrete. Mech Electron J Geotech Eng 8:1–44
26. Fortin J, Millet O, De Saxce G (2005) Numerical simulation of granular materials by an improved discrete element method. Int J Numer Meth Eng 62:639–663
27. Kruggel-Emden H, Simsek E, Rickelt S, Wirtz S, Scherer V (2007) Review and extension of normal force models for the discrete element method. Powder Technol 171:157–173
28. Obermayr M, Dressler K, Vrettos C, Eberhard P (2011) Prediction of draft force in cohesionless soil with the discrete element method. J Terrramech 48:347–358
29. El Shamy U, Aldebhamid Y (2014) Modeling granular soils liquefaction using coupled lattice Boltzmann method and discrete element method. Soil Dyn Earthq Eng 67:119–132
30. Casas G, Mukjerjee D, Celigueta MA, Zohdi TI, Eugenio O (2017) A modular, partitioned, discrete element framework for industrial grain distribution systems with rotating machinery. J Comput Part Mech 4:181–198
31. Kacianauskas R, Maknickas A, Kaceniauskas A, Markauskas D, Balevicius R (2010) Parallel discrete element simulation of poly-dispersed granular material. Adv Eng Softw 41:52–63
32. Elaskar SA, Godoy LA, Gray DD, Stiles JM (2000) A viscoplastic approach to model the flow of granular solids. Int J Solids Struct 37:2185–2214
33. Wada K, Senshu H, Matsui T (2006) Numerical simulation of impact cratering on granular material. Icarus 180(2):528–545
34. Campello EDMB (2015) A description of rotations for DEM models of particle system. Comput Part Mech 2:109–125
35. Zohdi TI (2014) Additive particle deposition and selective laser processing—a computational manufacturing framework. Comput Mech 54(1):171–191
36. Zohdi TI (2014) A direct particle-based computational framework for electrically-enhanced thermo-mechanical sintering of powdered materials. Math Mech Solids 19(1):1–21
37. Johnson KL (2003) Contact mechanics, 9th edn. Cambridge University Press, Cambridge
38. Bandeira AA, Wriggers P, Pimenta PM (2001) Homogenization methods leading to interface laws of contact mechanics—a finite element approach for large 3D deformation using augmented lagrangian method. Int J Numer Method Eng
39. Wriggers P (2006) Computational contact mechanics, 2nd edn. Springer, Berlin
40. Zohdi TI (2007) Computation of strongly coupled multifield interaction in particle-fluid systems. Comput Methods Appl Mech Eng 196(37):3927–3950
41. Avci B, Wriggers P (2012) A DEM-FEM coupling approach for the direct numerical simulation of 3D particulate flows. J Appl Mech 79:010901: 1–010901: 7
42. Zohdi TI (2012) Dynamics of charged particulate systems. Springer, Berlin
43. LeVeque RJ (2007) Finite difference methods for ordinary and partial differential equations: stead-state and time-dependent problems. SIAM (Society for Industrial and Applied Mathematics), Philadelphia
44. Zohdi TI (2005) Charge-induced clustering in multifield particulate flow. Int J Numer Meth Eng 62(7):870–898
45. Zohdi TI (2013) Numerical simulation of the impact and deposition of charged particulate droplets. J Comput Phys 233(1):509–526
46. Zohdi TI (2002) An adaptive–recursive staggering strategy for simulating multifield coupled processes in microheterogeneous solids. Int J Numer Meth Eng 53(7):1511–1532
47. Zohdi TI (2010) On the dynamics of charged electromagnetic particulate jets. Arch Comput Methods Eng 17:109–135
48. Wu C-Y, Thornton C, Li L-Y (2009) A semi-analytical model for oblique impacts of elastoplastic spheres. R Soc A 465(2103):937–960
49. Moin P (2010) Fundamentals of engineering numerical analysis, 2nd edn. Cambridge University Press, New York
50. Batlle JA, Cardona S (1998) The jamb (self-locking) process in three-dimensional rough collisions. Trans ASME J Appl Mech 65(2):417–423
51. Batlle JA (1993) On Newton's and Poisson's rules of percussive dynamics. J Appl Mech 60(2):376–381
52. Brach RM (1988) Impact dynamics with applications to solid particle erosion. Int J Impact Eng 7(1):37–53
53. Brach RM (1991) Mechanical impact dynamics: rigid body collisions. NY Wiley Interscience, New York
54. Thornton C (1997) Coefficient of restitution for collinear collisions of elastic-perfectly plastic spheres. Trans ASME J Appl Mech 64(2):383–386
55. Wu CY, Li LY, Thornton C (2003) Rebound behaviour of spheres for plastic impacts. Int J Impact Eng 28(9):929–946
56. Cheng W, Brach RM, Dunn PF (2002) Three-dimensional modeling of microsphere contact/impact with smooth, flat surfaces. Aerosol Sci Technol 36(11):1045–1060
57. Aghamohammadia C, Aghamohammadib A (2011) Slipping and rolling on an inclined plane. Eur J Phys 32:1049–1057